



UNIVERSIDAD NACIONAL AUTÓNOMA DE MÉXICO
POSGRADO EN CIENCIAS DE LA TIERRA
INSTITUTO DE GEOLOGÍA

**Variabilidad climática en el Desierto de Chihuahua en escala orbital y
milenaria durante el último ciclo interglacial-glacial-interglacial**

TESIS

Que para optar por el grado de:

Doctor en Ciencias de la Tierra

PRESENTA:

Jesús David Quiroz Jiménez

COMITÉ TUTOR

Dr. Priyadarsi Debajyoti Roy (Director) Instituto de Geología, UNAM

Dra. María del Socorro Lozano García, Instituto de Geología UNAM

Dr. Lorenzo Vázquez Selem, Instituto de Geografía, UNAM

Ciudad de México, Junio 2017



UNAM – Dirección General de Bibliotecas

Tesis Digitales
Restricciones de uso

DERECHOS RESERVADOS ©
PROHIBIDA SU REPRODUCCIÓN TOTAL O PARCIAL

Todo el material contenido en esta tesis está protegido por la Ley Federal del Derecho de Autor (LFDA) de los Estados Unidos Mexicanos (Méjico).

El uso de imágenes, fragmentos de videos, y demás material que sea objeto de protección de los derechos de autor, será exclusivamente para fines educativos e informativos y deberá citar la fuente donde la obtuvo mencionando el autor o autores. Cualquier uso distinto como el lucro, reproducción, edición o modificación, será perseguido y sancionado por el respectivo titular de los Derechos de Autor.

Agradecimientos académicos

Mi profundo agradecimiento al Dr. Priyadarsi Debajyoti Roy por su paciencia y asesoramiento incondicional.

A mi comité tutor, la Dra. María del Socorro Lozano García y el Dr. Lorenzo Vázquez Selem por sus consejos y apoyo en cada etapa de este posgrado.

A mi comité Sinodal, Dr. Priyadarsi Debajyoti Roy, Dra. María del Socorro Lozano García, Dra. Laura Beramendi Orosco, Dra. Isabel Israde Alcántara, Dr. Gabriel Vázquez Castro por su apoyo y consejos para la mejora del trabajo de tesis.

A los revisores de los artículos publicados por las observaciones realizadas.

A los químicos Patricia Girón García, Rufino Lozano Santacruz, Fabiola Vega e Inés Ramos (Instituto de Geología, UNAM), Nayeli López Balbiaux y Víctor Lemus Neri (USAI, UNAM) por el apoyo en la obtención de información mineralógica y elemental.

Al Dr. José Luis Sánchez Zavala por los consejos y apoyo brindado en el trabajo de campo.

A la Dra. Laura Beramendi Orosco por su amistad y apoyo en la realización del modelo cronológico de la investigación.

Mi más sincero agradecimiento a Carolina Castelán Hernández por su apoyo en la utilización de Sistemas de Información Geográfica para realizar los mapas de ubicación del presente trabajo.

Al Posgrado en Ciencias de la Tierra y al Instituto de Geología por permitirme ser parte de esta gran institución académica que es la UNAM.

Al Consejo Nacional de Ciencia y Tecnología por el otorgamiento de la beca doctoral 235509 y el financiamiento del proyecto CONACYT CB-237579, con el cual se realizó la investigación.

Agradecimientos personales

...Y ahora que termina este ciclo agradezco a muchas personas que conocí en cada escalón. Me enseñaron, me inspiraron y sin siquiera saberlo me hicieron crecer.

Es en parte gracias a mi asesor que hoy llego al final de este ciclo y quiero iniciar otro. Me has ayudado a crecer en todos los aspectos, a desarrollarme y aprender. Siempre impulsándome, retándome, aconsejándome, siempre detrás o frente de mí. Gracias Roy.

A ti Caro que estuviste en las buenas y en las malas, impulsándome a cada paso. Aportando esa dosis de ligereza que a menudo hace falta. Por cada regaño, cada reto, cada espaldarazo, por cada empujón y apoyo, por cada sonrisa. Le has dado la locura y cordura a esta etapa de mi vida. Te has convertido en una razón para mí. Gracias.

A mis padres porque, aunque suene trillado, a ellos les debo todo. Ellos son siempre parte de mis razones e inspiración. Ellos son mi mayor ejemplo para caminar.

A mis hermanos porque gracias a ustedes dos, cada paso lo trato de dar bien y de la mejor manera. Siempre los tuve y los tengo presentes.

A mis amigos, a esos del café, de las chelas, de los viajes, de las pláticas, de los consejos. Con ellos compartí ideas, puntos de vista, corajes, vida. Bere, Gabo, Fanis, Vale, Tapia, Ida, Ana, Gina, Axel, Johanna, Ramón Cocopech, Lulú, Pera, Clau, Manuel, Felipe, Javi, Memo. Gracias.

Este trabajo, no sería posible sin el apoyo de todos ustedes, es en parte suyo.
Gracias!

. . . we are of the Earth,

to her we do return,

future is inside us,

it's not somewhere else. . .

(R.H.)

	Contenido	Página
Resumen		I
Abstract		III
Capítulo I	Introducción	1
	I.1.1 Variabilidad Climática durante el Cuaternario Tardío	3
Capítulo II	Objetivos y Justificación	
	II.1 Objetivo general	9
	II.1.1 Objetivos específicos	9
	II.2 Justificación	10
Capítulo III	Marco Geográfico	
	III.1 Ubicación geográfica	12
	III.2 Geología	12
	III.3 Climatología	13
Capítulo IV	Metodología	
	IV.1 Trabajo de campo y muestreo	17
	IV.2 Trabajo de Laboratorio	17
	IV.2.1 <u>Mineralogía</u>	18
	IV.2.2 <u>Susceptibilidad magnética</u>	18
	IV.2.3 <u>Control cronológico</u>	19
	IV.2.4 <u>Concentraciones multielementales (FRX)</u>	20
	IV.2.5 <u>Abundancia de carbono inorgánico (IC), carbono orgánico (OC) y nitrógeno total (TN)</u>	23
	IV.2.6 <u>Isotopía de oxígeno ($\delta^{18}\text{O}$) y carbono ($\delta^{13}\text{C}$)</u>	25
	IV.2.7 <u>Ánálisis estadísticos</u>	25
Referencias		28
Capítulo V	Paleohydrology of the Santiaguillo Basin (Mexico) since late last glacial and climate variation in southern part of western subtropical North America	
Capítulo VI	Orbital-scale droughts in the central-northern Mexico during the late Quaternary and comparison with other subtropical and tropical records	
Capítulo VII	Hydrological responses of the Chihuahua Desert of Mexico to possible Heinrich Stadials	
Conclusiones		73

Figuras y Tabla

	Descripción	Página
Fig. 1	a) Ubicación de la cuenca del lago Santiaguillo y diferentes estudios paleoambientales en el trópico y subtrópico de Norteamérica. b) Geología de la cuenca de Santiaguillo, ubicación del sitio de muestreo y estaciones meteorológicas cercanas. c) Histogramas de precipitación-temperatura de las estaciones meteorológicas. La temperatura sigue la misma tendencia que la insolación de 30 °N para los últimos 1000 años (Berger y Loutre, 1991).	14
Fig. 2	a) Equipo de perforación de núcleos sedimentarios en la cuenca del lago Santiaguillo. b) Procesamiento y corte transversal de los núcleos en el laboratorio.	17
Fig. 3	Equipos de Fluorescencia de rayos X para medir las concentraciones de elementos mayores y traza de los sedimentos. a) Niton XL3t y b) Niton FXL 950 de la marca Thermo Scietific. c) Equipo convencional de FRX SRS 3000 marca Siemens.	22
Fig. 4	a) Equipo HiperTOC de la marca Thermo Scientific para medir la abundancia de carbono inorgánico (IC) y carbono total. La resta de IC al carbono total da como resultado la abundancia de carbono orgánico (OC). b) Equipo Perkin Elmer Series II CHNS/O que mide la abundancia de Nitrógeno total (TN) en la muestra.	24
Tabla 1	Métodos analíticos empleados y número de muestras analizadas para generar los datos de los diferentes capítulos (artículos científicos).	27

Resumen

El desierto de Chihuahua se localiza en la región subtropical de Norteamérica y los sedimentos depositados en las diferentes cuencas lacustres que alberga, han documentado las condiciones ambientales del Cuaternario tardío. La cuenca de Santiagillo (~25 °N, 105°O) se ubica en el margen occidental del desierto (centro-norte de México) y tiene un régimen hidrológico dominado por lluvias de verano-otoño con intervalos áridos en invierno-primavera. Este trabajo presenta registros proxy que permiten inferir la variabilidad hidrológica y climática durante el último ciclo interglacial-glacial-interglacial. La investigación se compone del estudio de los sedimentos colectados en dos sitios diferentes, el primero en una trinchera de 3 m de profundidad en la parte marginal de la cuenca y el segundo comprende una secuencia de núcleos de c.10 m de profundidad en la parte central. Los resultados e interpretaciones fueron publicados en tres revistas indexadas y arbitradas, *Quaternary Research*, *Geological Journal* y *Journal of South American Earth Sciences*.

Los modelos cronológicos se construyeron a partir de dataciones por ^{14}C AMS y la comparación entre la abundancia de carbonato y la insolación de primavera. Las secuencias sedimentarias fueron depositadas durante los últimos cinco Estadios Isotópicos Marinos (MIS). La mineralogía, susceptibilidad magnética, concentraciones de elementos mayores y traza, abundancia de carbono inorgánico (IC), carbono orgánico (OC), nitrógeno total (TN) y también las relaciones isotópicas de oxígeno ($\delta^{18}\text{O}$) y carbono ($\delta^{13}\text{C}$) en los carbonatos permitieron reconstruir la variabilidad climática en escala orbital y milenaria. El registro indica ausencia de sequías en el MIS 2, y su comparación regional sugiere que los ciclones tropicales (TC) del Norpacífico aportaron mayor precipitación de otoño en el último glacial tardío, cuando el monzón de Norteamérica (NAM) tenía mínima influencia en la precipitación. El MIS 1 presentó dos intervalos de aridez (~13.5 ka y 7 ka), donde la sequía de 13.5 ka ocurrió en una etapa de mayor actividad de El Niño Oscilación del Sur (ENSO) y temperaturas cálidas globales. Este periodo fue sincrónico con un

intervalo/evento árido documentado en otros registros del trópico y subtrópico de México. El Holoceno temprano se caracterizó por condiciones húmedas relacionadas con el fortalecimiento del NAM y los TC que a su vez, llevaron mayor humedad en verano-otoño desde el Golfo de California y Norpacífico a una región comprendida entre el centro-norte de México y el interior del suroeste de EUA.

En relación con la variabilidad de escala milenaria, los Estadiales Heinrich H6, H4, H2 y H1 presentaron escorrentía inferior al promedio y los Estadiales H5 y H3 tuvieron escorrentía superior al promedio. La comparación regional sugiere ausencia de sincronicidad de los regímenes de escorrentía en Santiaguillo y el aumento de la precipitación invernal en el suroeste de EUA durante los Estadiales Heinrich. Esto indica la falta de concurrencia entre los forzamientos que controlaron la precipitación de verano-otoño y las tormentas invernales. Las similitudes entre el registro de Santiaguillo y la Cueva Hulu (China) sugieren un posible vínculo hemisférico entre el hidroclima del desierto de Chihuahua en México y el Monzón del Este Asiático.

Abstract

The Chihuahua Desert is located in the subtropical region of North America. Sediments deposited in lacustrine basin of this desert have documented the environmental conditions of the late Quaternary. Santiagillo Basin (~25°N, 105°W) is located in the western margin of the desert (central-northern Mexico) and is characterized by a hydrological regime dominated by rainfall during the summer-autumn and dry winter-spring. This thesis presents proxy records that infer hydrological and climate variability occurred during the last interglacial-glacial-interglacial cycle. This research comprised the study of sediments collected from two different sampling sites; first sedimentary sequence is a pit of 3 m of depth in the marginal part of the basin and the second sequence is c.10 m long sediment core extracted in profundal-central part of the basin. The results and interpretations were published in three indexed and arbitrated journals like, *Quaternary Research*, *Geological Journal* and *Journal of South American Earth Sciences*.

Chronological models were constructed using ^{14}C AMS dates and comparing trends of variations in CO₃ with spring insolation. The sedimentary sequences were deposited during the last five Marine Isotope Stages (MIS). Mineralogy, magnetic susceptibility, concentrations of major and trace elements, abundance of inorganic carbon (IC), organic carbon (OC), total nitrogen (TN) and also isotopic relations of oxygen ($\delta^{18}\text{O}$) and carbon ($\delta^{13}\text{C}$) in carbonates were useful to reconstruct orbital and millennial scale climate variability. The record indicates absence of droughts during MIS 2 and regional comparison suggests that North Pacific tropical cyclones provided more autumn precipitation during the late last glacial. During this interval, the basin had minimal influence of the North American Monsoon (NAM). MIS 1 presented two intervals of aridity (~13.5 and 7 ka) and the drought at 13.5 ka occurred during an interval of stronger ENSO activity and warmer global temperatures. This arid event was contemporary to an arid interval/event documented in other proxy records from the tropical and subtropical Mexico. The wetter early Holocene was

related to enhanced NAM and tropical cyclones bringing more summer and autumn precipitation from the Gulf of California and North Pacific to a broader region extending from the central-northern Mexico up to continental interiors of the southwestern US.

In relation to millennial scale variability, Heinrich Stadials of H6, H4, H2 and H1 had less than average runoff and runoff was more than average during H5 and H3. Regional comparison suggest lack of synchronicity in runoff dynamics into Santiaguillo basin and enhanced winter precipitation in the southwest US during the Heinrich Stadials. It was possibly related to lack of concurrency in the forcings that control the summer-autumn precipitation as well as winter storms. Similarities between proxy records from the Santiaguillo basin and Hulu Cave (China) suggest a possible hemispheric link between hydroclimate of the Chihuahua desert of Mexico and East Asian Monsoon.

CAPÍTULO I

Introducción



La paleoclimatología es el estudio del clima en el periodo previo a los registros instrumentales que abarcan sólo una pequeña parte de la historia de la Tierra y por lo tanto no ofrecen una perspectiva adecuada de las variaciones y evolución climática en escala geológica. En cambio, el estudio de los fenómenos naturales dependientes del clima, que exhiben evidencia de esta dependencia, pueden ser útiles para ampliar nuestra perspectiva de la variabilidad climática. Tales fenómenos son la fuente de registros que guardan indicadores climáticos, y su estudio es el fundamento de la paleoclimatología. Tanto más detallados y confiables sean los estudios de las fluctuaciones climáticas, será mayor la posibilidad de identificar las causas y los mecanismos de dichas variaciones (Bradley, 1999). El creciente número de investigaciones paleoambientales sienta las bases para poner a prueba las hipótesis acerca del cambio climático, y sólo cuando se entiendan las razones de estos cambios, estaremos en posibilidad de anticipar o pronosticar las variaciones climáticas futuras (Bradley y Eddy, 1991).

Los registros paleoclimáticos guardan indicadores ambientales (proxies) que pueden abordarse mediante diferentes enfoques disciplinarios (ej. química, biología, geología). Entre los registros más estudiados podemos citar los núcleos de hielo glaciar, las espeleotemas, los sedimentos marinos y los sedimentos lacustres que preservan proxies biológicos, magnéticos, estratigráficos, geoquímicos, etc., (ej. Dansgaard *et al.*, 1993; NGRIP Project members, 2004; Asmeron *et al.*, 2007; Wang *et al.*, 2001; Mitchell *et al.*, 2002; Barron *et al.*, 2005; Grimm *et al.*, 2006; Roy *et al.*, 2010, 2012). Entre los mencionados, los sedimentos lacustres reflejan de manera fiel las condiciones ambientales que los originaron y depositaron, que aunado con la gran resolución temporal y continuidad que suelen presentar, son ideales para reconstruir la paleoclimatología del Pleistoceno y el Holoceno (ej. Bradley, 1999; Cohen, 2003).

I.1 Variabilidad Climática durante el Cuaternario tardío

En los últimos 130 ka de la historia de la Tierra han tenido lugar el Último Periodo Interglacial (LIG) (130-115 ka), el Último Periodo Glacial (~73.5-14.7 ka) y el Actual Periodo Interglacial que coincide temporalmente con el Holoceno (<11.7 ka) (Sánchez-Goñi y Harrison, 2010; NEEM community members, 2013; Cohen *et al.*, 2013). De acuerdo con los cambios globales de temperatura a largo plazo, dichos intervalos constituyen el último ciclo interglacial-glacial-interglacial, y se relacionan con la configuración astronómica de la Tierra (ciclos de Milankovitch). El LIG se caracterizó por mayores temperaturas globales y es el precedente inmediato de una época interglacial previa al Holoceno (ej. NEEM community members, 2013). El Último Periodo Glacial constituye un intervalo de bajas temperaturas globales (aunque con grandes oscilaciones) en que crecieron los glaciares de montaña y los casquetes de hielo polar en Norteamérica y Eurasia (ej. COHMAP, 1988; Cronin, 1999). Dentro de este intervalo frío, se identifica el Último Máximo Glacial (LGM = 23-19 ka) que representa el periodo más reciente en la historia de la tierra en que los casquetes de hielo alcanzaron su máximo volumen y el nivel del mar descendió considerablemente (Mix *et al.*, 2001; Peltier y Fairbanks, 2006). El Holoceno constituye el Actual Periodo Interglacial, y se caracteriza por un incremento de temperaturas y el reordenamiento del clima global después del último glacial (ej. COHMAP, 1988, Mayewski *et al.*, 2004). Cabe mencionar que a la transición entre el último glacial y el actual interglacial se denomina Última Deglaciación o Terminación, y representa el retroceso y derretimiento de los glaciares del Hemisferio Norte ocurrido entre ~20 y 7 ka (ej. Broecker y Donk, 1970; Denton *et al.*, 2010).

Los periodos glaciares e interglaciares también presentaron variabilidad climática. Los intervalos que muestran una tendencia específica de $\delta^{18}\text{O}$ en los sedimentos oceánicos permiten dividir el Cuaternario en diferentes Estadios Isotópicos Marinos (MIS, por sus siglas en inglés) que hacen referencia a intervalos con diferentes climas y temperaturas en la tierra. Los MIS se asocian

con la interacción entre los distintos parámetros orbitales y representan fluctuaciones del volumen de los casquetes glaciares y cambios de temperatura del agua oceánica profunda (Skinner y Shackleton, 2005). Por convención, los MIS de número par (ej. MIS 2) indican intervalos fríos y los de número impar intervalos cálidos (ej. MIS 1) (Emiliani, 1955; Shackleton, 1967).

Desde el último periodo glacial se han identificado 5 estadios isotópicos marinos (MIS 1-MIS 5). El MIS 5 (130-73.5 ka) se subdivide en cinco subestadios (5a-5e) de acuerdo con las variaciones de menor duración de $\delta^{18}\text{O}$, y el 5e corresponde con el LIG (Shackleton, 1969). El MIS 4 (73.5-59.4 ka) representó la generación de casquetes de hielo continentales; el MIS 3 (59.4-27.8 ka) se caracterizó por una gran inestabilidad climática y fluctuaciones de temperatura de gran amplitud; el MIS 2 (27.8-14.7 ka) evidenció el punto máximo crecimiento glaciar de la última glaciación (LGM) y el MIS 1 (<14.7 ka) ha sido un periodo de relativamente mayor estabilidad que abarca el término del Pleistoceno y todo el Holoceno (Lisieky y Raymo, 2005; Sánchez-Goñi y Harrison, 2010).

Durante los Estadios Isotópicos Marinos, específicamente en los que abarcaron el último periodo glacial (MIS 5d – MIS 1), ocurrieron eventos milenarios únicos que representaron rápidos cambios en el estado climático terrestre durante un régimen glacial. A estos intervalos se les conoce como estadiales (fríos) e interestadiales (cálidos); su inicio ocurrió en un intervalo de entre 10 y 200 años, y se prolongaron por cientos o miles de años (Steffensen *et al.*, 2008; Cronin, 2010). El MIS 3 fue el estadio con mayor variabilidad de escala milenaria, con 14 interestadiales (GI-4 – GI-17) y 14 estadiales (GS-4 – GS-17) identificados en los núcleos de hielo de Groenlandia (Björck *et al.*, 1998). Dicha variabilidad climática no puede ser explicada por procesos orbitales (aunque los cambios en la insolación pudieron estar involucrados); en cambio, pueden relacionarse con la dinámica interna del casquete Laurentino (Alley y MacAyeal, 1994), la interacción océano-atmósfera-criósfera en el Noratlántico o la modificación en

la circulación atmosférica por los glaciares continentales, entre otros mecanismos (Cronin, 1999).

En el Último Periodo Glacial, se identificaron dos tipos de eventos climáticos abruptos: los eventos Dansgaard-Oeschger (D-O) y los Estadiales Heinrich (H). Los eventos D-O fueron intervalos cálidos identificados por las variaciones isotópicas de los núcleos de hielo de Groenlandia. Estos interestadiales iniciaron con un incremento abrupto de la temperatura seguido de un enfriamiento gradual. Tales oscilaciones interestadial-estadial se conocen como ciclos D-O, y el interestadial por sí solo, se denomina evento D-O (Dansgaard *et al.*, 1984; Benson *et al.*, 2003; Sánchez-Goñi y Harrison, 2010). Se han identificado 24 ciclos D-O con una periodicidad promedio de 1470 años (Björck *et al.*, 1998; Rahmstorf, 2003) y en los sedimentos del Noratlántico, justo antes de estos eventos, se puede distinguir la depositación de capas sedimentarias de origen glaciar (Ice Rafted Debris, IRD).

Los Estadiales Heinrich (H) son fenómenos resultantes de la interacción hielo-océano-sedimento, que fueron identificados por primera vez por Helmut Heinrich (1988), y son un ejemplo claro de la forma en que la interacción de los componentes del sistema climático puede ser un control dominante del clima de la Tierra (Broecker, 1994). Los H se caracterizaron por la producción masiva de icebergs del casquete de hielo Laurentino que depositaron cantidades superiores de detritos glaciares (IRD) durante $\sim 500 \pm 250$ años (Bond *et al.*, 1992; Andrews *et al.*, 1993; Hemming, 2004). Las armadas de icebergs, liberaron grandes cantidades de agua dulce y fría en el Noratlántico, disminuyendo la temperatura y salinidad oceánica, lo que afectó directamente la circulación termohalina y el clima global (Maslin y Shackleton, 1995; Vidal *et al.*, 1997).

Durante la última glaciación existieron al menos 6 episodios paleoclimáticos de gran deposición de IRD en el Noratlántico que duraron entre 1.4 y 3.1 ka y caracterizaron a los Estadiales Heinrich (H6-H1), además de un posible Estadial

Heinrich 0 durante el Younger Dryas (YD: 12.8-11.6 ka) (Broecker *et al.*, 1992; Bond *et al.*, 1992; Bond y Lotti, 1995; Andrews *et al.*, 1995; Rasmussen *et al.*, 2006; Sánchez-Goñi y Harrison, 2010). Si bien los Estadios Heinrich ocurrieron en el Atlántico norte, su señal ha sido identificada en los sistemas marinos y terrestres de diversas latitudes y longitudes, lo que muestra el efecto global de estos intervalos fríos en el clima global (ej. Wang *et al.*, 2001; Zic *et al.*, 2002; Jennerjahn *et al.*, 2004; Roy *et al.*, 2015).

Este trabajo de tesis presenta los resultados estratigráficos, mineralógicos y geoquímicos de los sedimentos depositados en el lago Santiaguillo (centro-norte de México) para inferir las condiciones de la variabilidad hidrológica y climática que ocurrieron en el desierto de Chihuahua durante el último ciclo interglacial-glacial-interglacial. La parte medular está constituida por tres artículos publicados en las siguientes revistas científicas: *Quaternary Research*, *Geological Journal* y *Journal of South American Earth Sciences*. Adicionalmente, para complementar esta investigación, se realizó Introducción, Marco Geográfico, Metodología y Conclusiones generales de los tres artículos.

El Capítulo V está formado por el artículo “*Paleohydrology of the Santiaguillo Basin (Mexico) since late last glacial and climate variation in southern part of western subtropical North America*” publicado en *Quaternary Research*. Éste artículo reconstruye la dinámica hidrológica de escala milenaria de los últimos 27 ka de la parte suroeste del subtrópico de Norteamérica, a partir de la caracterización geoquímica, magnética y estratigráfica de los sedimentos de la cuenca del lago Santiaguillo. Además, presenta una comparación con otros registros regionales e identifica la influencia de la dinámica del Monzón de Norteamérica y las tormentas tropicales en la variabilidad climática, durante la parte terminal del Último Periodo Glacial y el Holoceno temprano.

El Capítulo VI está constituido por el artículo “*Orbital-scale droughts in the central-northern Mexico during the late Quaternary and comparison with other*

subtropical and tropical records" publicado en *Geological Journal*. Este artículo reconstruye las condiciones paleohidrológicas del lago Santiaguillo durante diferentes Estadios Isotópicos Marinos, a partir de la geoquímica elemental, mineralogía y estratigrafía de los sedimentos del lago. Además, evalúa el papel de los forzamientos de El Niño Oscilación del Sur (ENSO, por sus siglas en inglés) y la temperatura global en la distribución temporal de las sequías en la región tropical y subtropical de México.

El Capítulo VII está conformado por el artículo "*Hydrological responses of the Chihuahua Desert of Mexico to possible Heinrich Stadials*" publicado en *Journal of South American Earth Sciences*. Este artículo reconstruye la variabilidad paleohidrológica de escala milenaria que representaron los seis diferentes Estadiales Heinrich (H1-H6) a partir de las concentraciones de Al y Ca, además del fraccionamiento de los isótopos de carbono y oxígeno en los carbonatos de los sedimentos del lago Santiaguillo.

CAPÍTULO II

Objetivos y Justificación

II.1 Objetivo general

Reconstruir la respuesta hidrológica de la parte mexicana del desierto de Chihuahua a la variabilidad climática de escala orbital y milenaria durante el último ciclo interglacial-glacial-interglacial, mediante el estudio geoquímico de los sedimentos depositados en la cuenca del lago Santiaguillo ubicado en el centro-norte de México.

II.1.1 Objetivos específicos

- Identificar los diferentes intervalos de cambio climático registrados en los sedimentos de la cuenca del lago Santiaguillo.
- Determinar la respuesta del desierto de Chihuahua (Méjico) a la variabilidad climática de escala orbital y milenaria que representan los Estadios Isotópicos Marinos y Estadiales Heinrich, respectivamente.
- Generar un registro de aridez y compararlo con distintos registros paleoambientales de la región tropical y subtropical de Norteamérica.
- Establecer la respuesta paleohidrológica de la parte mexicana del desierto de Chihuahua a los Estadiales Heinrich.
- Inferir los forzamientos climáticos involucrados en la variabilidad hidrológica del desierto de Chihuahua.

II.2 Justificación

Trabajos recientes de diferentes autores (ej. Lyle *et al.*, 2012; Barron *et al.*, 2012; Roy *et al.*, 2013; Kirby *et al.*, 2013; Metcalfe *et al.*, 2015) aportan evidencias que han permitido generar nuevas y diferentes hipótesis a la propuesta por los miembros del COHMAP en 1988 para explicar el cambio climático ocurrido en el Cuaternario tardío en el subtrópico de Norteamérica. Sin embargo, la escasez de registros continuos, de extensa temporalidad y alta resolución, en el centro y centro-norte de México ha sido una gran limitante para poner a prueba dichas hipótesis y entender mejor la variabilidad climática.

En este estudio se presentan registros proxy que reconstruyen las condiciones paleohidrológicas del centro-norte de México en escala orbital (Estadios Isotópicos Marinos) y milenaria (Estadiales Heinrich) durante el último ciclo interglacial-glacial-interglacial. De esta manera, se infiere la respuesta hidrológica de la parte mexicana del desierto de Chihuahua a la variabilidad climática e identifica los posibles forzamientos que la afectaron.

CAPÍTULO III

Marco Geográfico

III.1 Ubicación Geográfica

El desierto de Chihuahua en México se ubica en al menos 6 diferentes estados del norte del país (Chihuahua, Durango, Zacatecas, Coahuila, Nuevo León y San Luis Potosí). El lago Santiaguillo ($24^{\circ}39'N$, $104^{\circ}57'W$, 1960 msnm) se asienta en una cuenca endorreica de origen tectónico orientada NW-SE, en el subtrópico mexicano, en el margen oeste del desierto de Chihuahua y a las faldas de la Sierra Madre Occidental, en el estado de Durango (Fig. 1a). La cuenca cubre un área aproximada de 2000 km^2 y es alimentada por arroyos efímeros activos durante la época de lluvias (Fig. 1b). Santiaguillo es un sistema lacustre dividido en dos porciones por un dique artificial, la porción norte sirve como una represa de almacenaje de agua con fines de riego, mientras que la porción sur conforma un lago natural sin perturbaciones antropogénicas considerables. Este lago efímero al sur, guarda un tirante de agua máximo de c.1 m durante los meses lluviosos (verano-otoño) y disminuye considerablemente su nivel, e incluso puede permanecer seco durante la época de estiaje (invierno-primavera).

III.2 Geología

La geología de la región en que se ubica el lago Santiaguillo está compuesta por rocas ígneas y sedimentarias del Paleógeno, Neógeno y Cuaternario, pequeños afloramientos de areniscas-lutitas del Jurásico superior y rocas metamórficas del Pérmico (Servicio Geológico Mexicano., 1998; Nieto Samaniego *et al.*, 2012). La tectónica regional dio como resultado un sistema de fallas normales, laterales e inversas, con una orientación preferencial NW-SE, que modelaron el graben de Santiaguillo en el Eoceno tardío - Oligoceno temprano ($\sim 39\text{-}32\text{ Ma}$), y condicionaron la geología de la cuenca (Nieto Samaniego *et al.*, 2012). Las rocas predominantes son ignimbritas y riolitas que constituyen las montañas circundantes tanto al este como al oeste del lago y tienen una elevación entre c.2500-3000 msnm. Además, se pueden observar conglomerados polimíticos en el borde este del sistema lacustre, al igual que en el oeste y sur de la cuenca. En menor proporción, afloran andesitas al este y oeste, y materiales piroclásticos al

norte. Esparcidos por la región, existen numerosos afloramientos de basaltos del Neógeno y Cuaternario y en las partes circundantes al lago se presentan sedimentos aluviales y lacustres recientes (Fig. 1b).

III.3 Climatología

A partir de tres estaciones meteorológicas distribuidas a una distancia entre *c.1* y 13 km del lago Santiaguillo (Guatimapé, El Pino y Canatlán), se determinaron el clima, el régimen de precipitación y la temperatura de la cuenca. Estas estaciones comprenden un periodo máximo de medición de 42 años (1964 y 2006) (Fuente: Servicio Meteorológico Nacional). Tomando en cuenta estas estaciones, el lago presenta un clima árido templado con un régimen de lluvias de verano tipo BS1kw (García, 1973). La temperatura media anual oscila entre 16 y 18 °C, con máximos en verano (junio) que superan los 38 °C y mínimos en invierno (diciembre-enero) inferiores a 0 °C. Las variaciones anuales de temperatura son similares a las de la insolación a 30 °N, con máximos en verano (475 W/m^2) y mínimos en invierno (227 W/m^2) (Berger y Loutre, 1991) (Fig. 1c). La precipitación media anual varía entre 430 y 554 mm, de la cual *c.90 %* ocurre entre junio y octubre en función de las lluvias del Monzón de Norteamérica en verano y los ciclones tropicales en otoño. El restante *c.10 %* de la precipitación anual tiene lugar entre noviembre y mayo, siendo la primavera la época del año más seca, contribuyendo únicamente con <4 % de la precipitación anual.

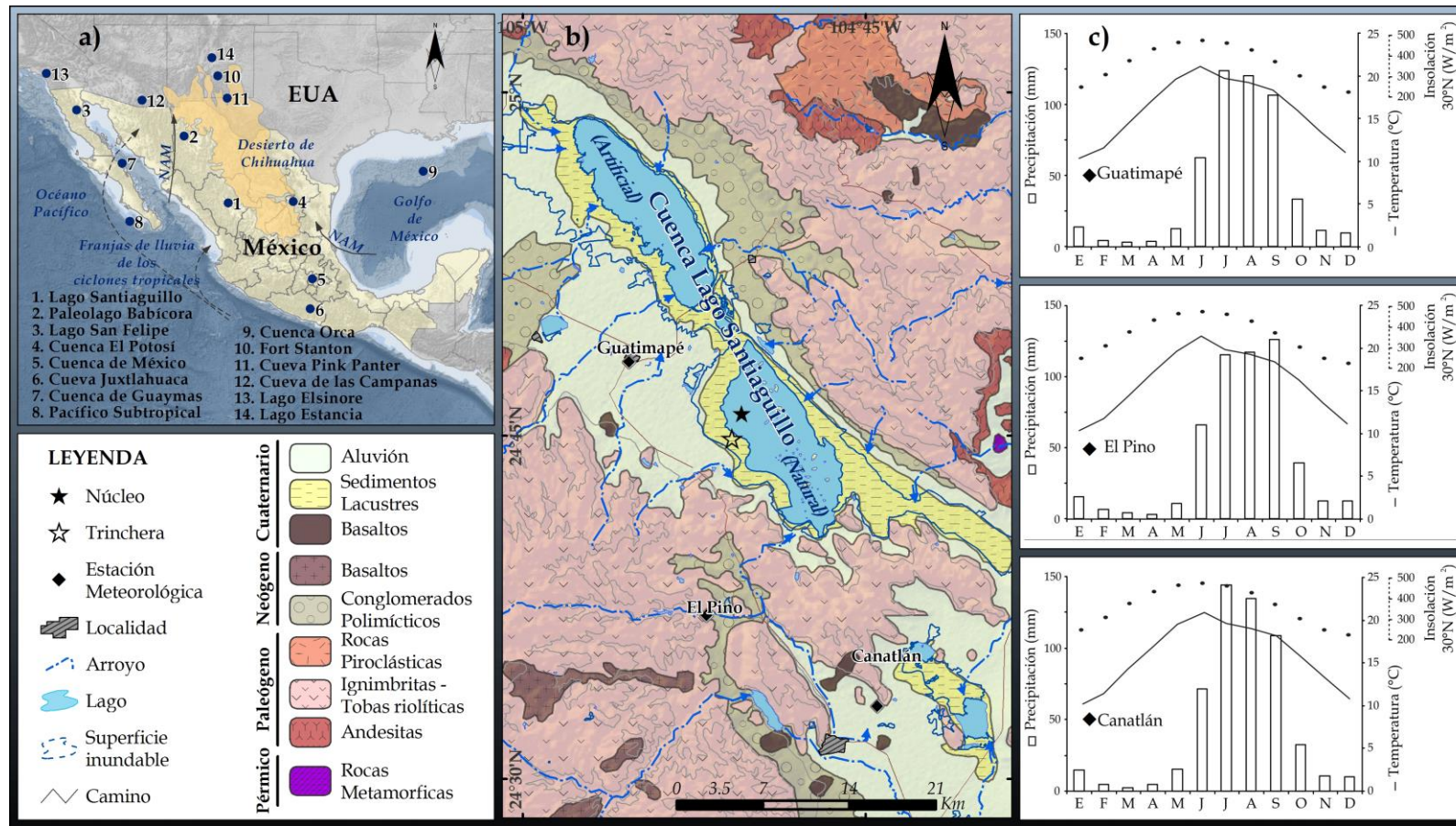


Fig. 1. a) Ubicación de la cuenca del lago Santiago y diferentes estudios paleoambientales en el trópico y subtrópico de Norteamérica. b) Geología de la cuenca de Santiago, ubicación del sitio de muestreo y estaciones meteorológicas cercanas. c) Histogramas de precipitación-temperatura de las estaciones meteorológicas. La temperatura sigue la misma tendencia que la insolación de 30 °N para los últimos 1000 años (Berger y Loutre, 1991).

Los registros históricos, así como los registros de anillos de árboles, que reconstruyen las condiciones paleohidrológicas del norte de México para los últimos 600 años, indican una conexión directa entre las variaciones de precipitación y la temperatura superficial del mar (SST) del océano Pacífico y Atlántico, en respuesta a El Niño Oscilación del Sur (ENSO), la Oscilación Decadal del Pacífico (PDO) y la Oscilación Multidecadal del Atlántico (AMO) (Magaña *et al.*, 2003; Cleveland *et al.*, 2003; González-Elizondo *et al.*, 2005; Sutton y Hodson, 2005; Versteegh, 2005; Cerano-Paredes *et al.*, 2010; Villanueva-Díaz *et al.*, 2014). Las fases positivas (cálidas) de ENSO y PDO, y las fases negativas (frías) de la AMO, reducen la cantidad de precipitación anual en la región desencadenando sequías. Esto se debe a la disminución de la precipitación de verano durante los intervalos de mayores temperaturas en el Pacífico tropical en respuesta a la migración de la Zona Intertropical de Convergencia (ZITC) hacia menores latitudes (Castro *et al.*, 2001; Magaña *et al.*, 2003).

CAPÍTULO IV

Metodología



IV.1 Trabajo de campo y muestreo

Con el objetivo de reconstruir la variabilidad climática del desierto de Chihuahua en el Pleistoceno tardío, se recolectaron sedimentos depositados en la cuenca del lago Santiaguillo (estado de Durango, México) en diferentes sitios, a partir de una trinchera (3 m de profundidad) y dos secuencias de núcleos (c.10 m de profundidad) (Fig. 2a). Se realizó una descripción estratigráfica de la secuencia sedimentaria de la trinchera y se extrajeron muestras cada 2 cm para posteriores análisis en laboratorio. Las secuencias de núcleos fueron colectadas en dos sitios, con una separación de 5 m, utilizando una perforadora de percusión y operación automática en la parte central del lago. Adicionalmente, se recolectaron 8 muestras de las principales rocas que afloran en los alrededores de la cuenca.

IV.2 Trabajo de laboratorio

Los núcleos fueron cortados transversalmente y se realizó una descripción textural con base en inspección macroscópica y microscópica (ej. Schnurrenberger *et al.*, 2003) (Fig. 2b). De esta forma, la distribución del tamaño de grano arrojó información de la energía deposicional en la cuenca.

Uno de los núcleos se guardó como testigo y el otro se submuestreó en un intervalo de 1 cm para realizar diferentes análisis en laboratorio.



Fig. 2. a) Equipo de perforación de núcleos sedimentarios en la cuenca del lago Santiaguillo. b) procesamiento y corte transversal de los núcleos en el laboratorio.

Tanto las muestras de trinchera como de los núcleos fueron secadas en un horno a 40°C, homogenizadas y molidas en un mortero de ágata hasta alcanzar una textura similar a limo. Dichas muestras fueron analizadas por distintas metodologías para determinar mineralogía, susceptibilidad magnética, abundancia de carbono inorgánico (IC), carbono orgánico (OC) y nitrógeno total (TN), concentraciones de elementos mayores y traza de los sedimentos y relaciones isotópicas de oxígeno ($\delta^{18}\text{O}$) y carbono ($\delta^{13}\text{C}$) en los carbonatos.

IV.2.1 Mineralogía

Se analizó la mineralogía de la fracción clástica y no-clástica de los sedimentos en 22 muestras con textura variable, distribuidas a lo largo de la secuencia de núcleos. Estos análisis se hicieron con un difractómetro de rayos X (DRX) Shimadzu 6000 en el Laboratorio de Fluorescencia de Rayos X del Instituto de Geología (IGL) de la Universidad Nacional Autónoma de México (UNAM). Con ayuda del programa *Traces V6*, la distancia interplanar y el ángulo 2θ en los difractogramas resultantes se identificó la mineralogía de los sedimentos. Los resultados fueron empleados en los Capítulos VI y VII.

IV.2.2 Susceptibilidad Magnética (SM)

Con el objetivo de estimar la concentración de los minerales magnéticos en la secuencia de trinchera, se midió la susceptibilidad magnética (SM) de los sedimentos (ej. Thomson y Oldfield, 1986; Urrutia-Fucugauchi *et al.*, 1997; Blanchet *et al.*, 2007). El equipo utilizado fue un susceptibilímetro con un sensor de barrido de superficie de alta resolución (2×10^{-6}) MS2E a 2kHz de la marca Bartington, directamente sobre bolsas de plástico con los sedimentos molidos, en el Laboratorio de Paleoambientes del IGL de la UNAM. La SM es controlada por la mineralogía de los sedimentos; la presencia de minerales ferromagnéticos (ej. magnetita, hematita) y paramagnéticos (ej. anfíbol, piroxeno) contribuyen con valores positivos de susceptibilidad mientras que los minerales diamagnéticos (ej. yeso, calcita) con valores negativos (Thomson y Oldfield, 1986; Roy *et al.*, 2014).

IV.2.3 Control Cronológico

El control cronológico se realizó con base en análisis ^{14}C AMS de diferentes muestras de materia orgánica en el sedimento total en laboratorios comerciales (*Beta Analytic e International Chemical Analysis Inc. (ICA)*) de EUA. Las muestras fechadas fueron seleccionadas en función de los cambios significativos de la textura sedimentaria de las secuencias. Con el propósito de evitar contaminación por carbono reciente, éstas fueron descostradas y empacadas en papel aluminio antes de enviar a analizar. El control cronológico de las secuencias sedimentarias se llevó a cabo mediante modelos Bayesianos “edad vs profundidad” calibrando las edades ^{14}C con la curva IntCal 13 (Reimer *et al.*, 2013) en la versión en línea OxCal 4.2 (Bronk Ramsey, 2009). Dichos modelos fueron evaluados en función del Índice de Acuerdo (A), donde valores superiores a 60 % indican alta correspondencia entre el modelo y las observaciones, lo que sugiere la ausencia de datos anómalos (*outliers*) en las edades radiocarbono.

La cronología de los sedimentos de la trinchera hace uso de 6 dataciones por ^{14}C AMS en muestras de las profundidades 49, 73, 111, 167, 205 y 279 cm. El modelo creado consideró una secuencia P y una flexibilidad $k=1$ (Bronk Ramsey, 2008). La asignación de edades a los sedimentos de toda la secuencia tomó en cuenta la interpolación de diferentes tasas de sedimentación entre dataciones consecutivas.

El control cronológico de la secuencia del núcleo se llevó a cabo a partir de 13 dataciones por ^{14}C AMS en muestras colectadas a diferentes profundidades (25, 49, 78, 89, 110, 136, 174, 266, 291, 319, 355, 385 y 410 cm). Sin embargo, con base en su posición estratigráfica, sólo 8 tuvieron resultados exitosos (25, 49, 78, 89, 110, 136, 174 y 266 cm) y fueron utilizadas para crear un modelo “edad vs profundidad” considerando una secuencia P y una flexibilidad de $k=0.3$. La asignación de edades a los sedimentos depositados los 266 cm superficiales de la secuencia tomó en cuenta la interpolación de las diferentes tasas de

sedimentación calculadas entre edades consecutivas, mientras que las edades de los sedimentos depositados en la parte basal de la secuencia (1026 – 266 cm) se asignaron extrapolando una tasa de sedimentación promediada calculada entre 266 y 25 cm de profundidad. El modelo cronológico del Capítulo VII consideró 6 de las dataciones exitosas (78, 89, 110, 136, 174 y 266 cm), utilizó los mismos parámetros del modelo Bayesiano (secuencia P y k=0.3) y comparó las tendencias de variación del registro de CO₃ con respecto a la insolación de primavera a 30° latitud norte y las variaciones de los isótopos de oxígeno con respecto a la edad.

IV.2.4 Concentraciones multielementales (FRX)

Con el propósito de caracterizar los minerales clásticos y evaporíticos autigénicos, se midieron las concentraciones de elementos mayores y traza en muestras homogenizadas y molidas con Fluorescencia de rayos X (FRX) portátil. Los equipos utilizados fueron Thermo Scientific Niton XL3t y FXL 950 de los Laboratorios de Geoquímica Ambiental y Paleoambientes del IGL de la UNAM. El control de calidad de ambos equipos se estimó midiendo por duplicado distintas muestras, además del cálculo de parámetros de precisión y exactitud en estándares certificados (ej. SRM-2702 (NIST, 2016)).

Como los equipos portátiles sobreestiman o subestiman las concentraciones de los elementos (ej. Roy *et al.*, 2012), un total de 107 muestras colectadas de las secuencias sedimentarias fueron medidas en un equipo de FRX convencional SRS 3000 de la marca Siemens en el Laboratorio de Fluorescencia de rayos X del IGL de la UNAM. Dichos resultados sirvieron como referencia para comparar metodologías y generar ecuaciones para la corrección de las concentraciones obtenidas por los equipos portátiles.

El equipo Niton XL3t es un espectrómetro de Fluorescencia de rayos X de dispersión de energía (EDXRF) que cuenta con un tubo emisor de rayos X de 50 kv de oro (Au) y un detector semiconductor de alto rendimiento. El equipo

estimó las concentraciones de Ti, Fe, K, Ca, Sr y Zr a partir de un método de medición no destructivo, directamente sobre una bolsa de plástico con muestra pulverizada y seca, usando el modo de medición “Soil” (sensible a los elementos deseados) y un tiempo de medición total por muestra de ~90 s.

El equipo Niton FXL 950 (también EDXRF), cuenta con un tubo emisor de Rayos X de 50 kv de plata (Ag) y un detector Geométricamente Optimizado de Gran Área Flotante (GOLDD, por sus siglas en inglés) (Fig. 3). Este equipo midió las concentraciones de Si, Al, Fe, K, Ti y Ca mediante un método no destructivo, donde c.5 g de sedimento, pulverizado y seco, se colocaron dentro de una cápsula de plástico complementada con una película delgada para rayos X de polipropileno de 4 μm de espesor. La muestra fue cubierta con papel filtro y el espacio restante fue rellenado con fibra de algodón. El modo de medición del equipo utilizado fue “Mining Cu/Zn” y el tiempo de análisis total por muestra fue de ~4 minutos.

El espectrómetro secuencial de fluorescencia de rayos-X de dispersión de longitud de onda (WDXRF) SRS 3000 de marca Siemens utiliza una metodología destructiva y cuenta con un tubo emisor de rayos X de Rh y una ventana de Berilio (Be) de 125 μm . Para el análisis de elementos mayores (Si, Ti, Al, Fe, Mn, Mg, Ca, K y P), 0.8 g de muestra de sedimento fueron fundidos junto con 7.2 g de LiBO₂ y Li₂B₄O₇ (1:1) granular ultrapuro en crisoles de Pt/Au (95:5) bajo un procedimiento programado de calentamiento en un periodo de c.10 minutos (Lozano Santacruz *et al.*, 1995). Para los análisis de elementos traza (Sr y Zr), 4 g de muestra y 0.4 g de aglutinante fueron mezclados y prensados (Lozano Santacruz *et al.*, 1995; Verma *et al.*, 1996).



Fig. 3. Equipos de Fluorescencia de rayos X para medir las concentraciones de elementos mayores y traza de los sedimentos. a) Niton XL3t y b) Niton FXL 950 de la marca Thermo Scietific. c) equipo convencional de FRX SRS 3000 marca Siemens.

A continuación se describen los análisis realizados de acuerdo con el número de muestras medidas y las variables obtenidas.

Se midieron las concentraciones de Ti, Fe, K, Ca, Sr y Zr en 150 muestras de la secuencia de trinchera, mediante el equipo Niton XL3t. Adicionalmente, 61 de estas muestras y 8 más de roca se analizaron en el equipo de FRX convencional (SRS 3000) para determinar las concentraciones de los elementos mencionados, además de Si, Al, Na, K, Ca y P. Con dichos resultados, se corrigieron las concentraciones del equipo portátil y se estimó el grado de intemperismo y procedencia de los sedimentos clásticos mediante el Índice de Alteración Química CIA=[Al₂O₃/(Al₂O₃+CaO+Na₂O+K₂O)] × 100 (Nesbitt y Young, 1984, 1989).

Se midieron las concentraciones de Ti, Fe, K, Ca y Sr en 102 muestras de la secuencia de núcleos en un intervalo de 10 cm mediante el equipo Niton XL3t y, 38 de estas muestras, también fueron analizadas en el equipo convencional para obtener las concentraciones de Ti, Fe, K, Ca, Sr, Si, Al, Na, K, Ca y P. Comparando los resultados de las diferentes metodologías analíticas, se corrigieron los resultados del equipo de FRX portátil. Así mismo, se calculó el grado de alteración de los sedimentos clásticos (CIA) en las 38 muestras medidas por FRX convencional.

En la misma secuencia de núcleos, se midieron las concentraciones de Si, Al, Fe, K, Ti y Ca en 183 muestras entre las profundidades de 78 y 560 cm, en intervalos <5 cm, mediante el equipo Niton FXL 950. Cabe mencionar que la resolución del muestreo fue mayor (cada 1-2 cm) en los sedimentos que se depositaron probablemente durante los Estadios Heinrich, y fue menor (cada 5 cm) en el resto de la secuencia. Las concentraciones del equipo portátil fueron corregidas usando los resultados del análisis de las 38 muestras medidas en el equipo convencional.

IV.2.5 Abundancia de carbono inorgánico (IC), carbono orgánico (OC) y nitrógeno total (TN)

Se analizaron las concentraciones de carbono inorgánico (IC) y carbono orgánico (OC) y carbono total (IC+OC) con la finalidad de estimar la abundancia de carbonatos autigénicos e identificar variaciones de productividad orgánica. Las muestras fueron analizadas en el Laboratorio de Paleoambientes del IGL de la UNAM mediante un equipo HiperTOC de la marca Thermo Scientific. De igual forma, se analizó el contenido de nitrógeno total (TN) para, en conjunto con el carbono orgánico, obtener información de las variaciones de productividad orgánica en el lago. Los análisis de TN se realizaron en un equipo Perkin Elmer Series II CHNS/O de la Facultad de Química de la UNAM.

El equipo que determina la abundancia de carbono inorgánico y carbono total de los sedimentos, cuantifica el CO₂ liberado de las muestras (c.10 g) al agregarles ácido fosfórico (H₃PO₄) al 10 % (abundancia de IC) y calcinarlas a c.1000 °C (abundancia de carbono total) (Fig. 4). El carbono orgánico (OC) se obtiene de restar el carbono inorgánico al carbono total.

El equipo de análisis elemental utilizado para cuantificar el nitrógeno total, mide el contenido de nitrógeno, carbono, hidrógeno y oxígeno en muestras sólidas y líquidas. La metodología empleada fue la de Dumas que consiste en

oxidar la muestra total a través de una combustión instantánea que transforma los elementos en óxidos. Estos gases son conducidos a través de un tubo de reducción que quita el exceso de oxígeno, obteniendo una mezcla de elementos que son separados por un cromatógrafo y medidos con un detector de conductividad térmica (CIMA, 2002).

En los sedimentos de trinchera la abundancia de IC y OC se midió en un total de 61 muestras (en intervalos de 4-6 cm) y la cantidad de TN en 31 muestras (en intervalos de c.10 cm). La abundancia de carbono inorgánico es expresada como carbonato ($\text{CO}_3 = \text{IC} \times 4.998$).

En los sedimentos de núcleos, la abundancia de IC, OC y TN se estimó en 237, 102 y 48 muestras, respectivamente. El Capítulo VI considera la abundancia de IC y OC en 102 muestras separadas en intervalos de c.10 cm y el carbono inorgánico se expresa como la abundancia de calcita ($\text{CaCO}_3 = \text{IC} \times 8.33$). El Capítulo VII toma en cuenta la abundancia de IC en 183 muestras, separadas entre si por intervalos <5 cm, depositadas entre 78 y 560 cm de profundidad y expresa la abundancia de IC como carbonato ($\text{CO}_3 = \text{IC} \times 4.998$). Además considera el OC y TN de 48 muestras medidas en intervalos de cada 10 cm.



Fig. 4. a) Equipo HiperTOC de la marca Thermo Scientific para medir la abundancia de carbono inorgánico (IC) y carbono total. La resta de IC al carbono total da como resultado la abundancia de carbono orgánico (OC). b) Equipo Perkin Elmer Series II CHNS/O que mide la abundancia de Nitrógeno total (TN) en la muestra.

IV.2.6 Isotopía de oxígeno ($\delta^{18}\text{O}$) y carbono ($\delta^{13}\text{C}$)

Con el propósito de determinar las variaciones de los isótopos estables de oxígeno y carbono en los sedimentos de la cuenca de Santiaguillo, e identificar cambios paleoambientales relacionados con la temperatura del cuerpo de agua y la fuente de bicarbonato, se estimaron las relaciones isotópicas de $\delta^{18}\text{O}$ y $\delta^{13}\text{C}$. A continuación se describe la metodología empleada para medir la abundancia de los isótopos de oxígeno y carbono en la fracción carbonatada de los sedimentos.

Tomando en cuenta la mineralogía uniforme de los sedimentos carbonatados y el modelo cronológico establecido para la secuencia de núcleos, se seleccionaron 33 muestras depositadas durante posibles Estadios Heinrich y en ausencia de estos eventos. Para remover la fracción orgánica de los sedimentos, las muestras fueron tratadas con H_2O_2 al 15 % y lavadas con agua desionizada (milli-Q). Los sedimentos tratados fueron secados a 40 °C, homogenizados y molidos en un mortero de ágata.

Las relaciones isotópicas de carbono ($\delta^{13}\text{C}$) y oxígeno ($\delta^{18}\text{O}$) en los carbonatos se determinaron usando un espectrómetro de masas Thermo Finnigan MAT 253 acoplado con un Gas Bench II, siguiendo la metodología de McCrea (1950) en el laboratorio de Isótopos Estables del IGL en la UNAM. Las relaciones isotópicas ($\delta^{18}\text{O}$ y $\delta^{13}\text{C}$) se reportan relativas al estándar VPDB (Vienna Pee Dee Belemnite) con una desviación estándar de $\pm 0.2\%$.

IV.2.7 Análisis Estadísticos

Se utilizaron análisis estadísticos para determinar las correlaciones entre las diferentes variables geoquímicas de los sedimentos lacustres de Santiaguillo en el programa STATISTICA de Statsoft USA. Con este fin, las variables fueron normalizadas mediante la función $Z = [(x-\mu)/\sigma]$ donde, x es el valor, μ es el promedio de los datos y σ es la desviación estándar. Despues de esta normalización, el compendio de datos presenta una distribución normal y cada

variable tiene una media 0 y desviación estándar 1 (Davis, 1987; Swanson *et al.*, 2001). Los coeficientes de correlación (*r*) cercanos a 1 establecen fuerte correlación positiva entre las variables, los cercanos a -1 sugieren fuerte correlación negativa y los cercanos a 0 indican correlación nula.

Para los sedimentos de trinchera se determinaron los coeficientes de correlación (*r*) entre SM, CO₃, Ti, Fe, K, Ca, Sr, Zr, SiO₂/Al₂O₃ y Sr/Ti con un nivel de significancia *p*<0.05.

Para los sedimentos de núcleos se calcularon los índices de correlación (*r*) entre variables (IC, CaCO₃, CO₃, Ca, Si, Al, Ti, Fe, K, Sr, Ti/Ca, K/Ca, Sr/Ca y CIA) y se generaron matrices con valor *p*<0.05. Además, se generaron diagramas de agrupación (*Cluster*) conforme a las similitudes entre variables determinando la asociación total (*Complete Linkage*) y midiendo la distancia en 1-Pearson-*r*.

Tabla 1. Métodos analíticos empleados y número de muestras analizadas para generar los datos de los diferentes capítulos (artículos científicos).

	Capítulo V	Capítulo VI	Capítulo VII
	<i>Paleohydrology of the Santiagillo Basin (Mexico) since late last glacial and climate variation in southern part of western subtropical North America</i>	<i>Orbital-scale droughts in the central-northern Mexico during the late Quaternary and comparison with other subtropical and tropical records</i>	<i>Hydrological responses of the Chihuahua Desert of Mexico to possible Heinrich Stadials</i>
Metodología utilizada	Información obtenida	Número de muestras analizadas y variables utilizadas	
DRX Shimadzu 6000	Mineralogía	-	22
Bartington MS2E	Susceptibilidad de campo magnético bajo	150	-
¹⁴ C AMS	Dataciones	6	13
FRX Siemens SRS 3000	Elementos mayores y traza	69	38
FRX Niton FXL 950	Elementos mayores y traza	-	183
FRX Niton XLt3	Elementos mayores y traza	150	102
HiperTOC	TC	61	102
	IC	61	102
Perkin Elmer Series II CHNS/O	TN	31	-
Finnigan MAT 253	Isótopos Cy O	-	33

Referencias

- Alley, R.B., MacAyeal, D.R., 1994.** Ice rafted debris associated with binge/purge oscillations of the Laurentide ice sheet. *Paleoceanography* **9**, 503-511.
- Andrews, J.T., Tedesco, K., Jennings, A.E., 1993.** Heinrich events: chronology and processes, east-central Laurentide Ice Sheet and NW Labrador Sea. In: Peltier, W.R., (Ed.), *Ice in the Climate System*. NATO ASI Series, Springer-Verlag, New York **12**, 167-186.
- Andrews, J.T., Jennings A.E., Kerwin, M., Kirby, M., Manley, W., Miller, G.H., 1995.** A Heinrich-like event (DC-0): Source(s)for detrital carbonate in the North Atlantic during the Younger Dryas Chronozone. *Paleoceanography* **10**, 943-952.
- Asmerom, Y., Polyak, V., Burns, S., Rasmussen, J., 2007.** Solar forcing of Holocene climate: new insights from a speleothem record, southwestern United States. *Geology* **35**, 1-4.
- Barron J.A., David, B., Walter, E., 2005.** Paleoceanographic history of Guaymas Basin, Gulf of California during the past 15000 years based on diatoms, silicoflagellates, and biogenic sediments. *Marine Micropaleontology* **56**, 81-102.
- Barron, J.A., Metcalfe, S.E., Addison, J.A., 2012.** Response of the North American monsoon to regional changes in ocean surface temperature. *Paleoceanography* **27**, PA3206, doi:10.1029/2011PA002235, 2012
- Benson, L., Lund, S., Negrini, R., Linsley, B., Zic, M., 2003.** Response of North America Great Basin lakes to Dansgaard-Oeschger oscillations. *Quaternary Science Reviews* **22**, 2239-2251.
- Berger, A., Loutre, M.F., 1991.** Insolation values for the climate of the last 10 million years. *Quaternary Science Reviews* **10**, 297-317.
- Björck, S., Walker, M.J.C., Cwynar, L.C., Johnsen, S., Knudsen, K.-L., Lowe, J.J., Wohlfarth, B., and intimate members, 1998.** An event stratigraphy for the Last Termination in the North Atlantic region based on the Greenland ice-core record: A proposal by the INTIMATE group. *Journal of Quaternary Science* **13**, 283-292.
- Blanchet, C.L., Thouveny, N., Vidal, L., Leduc, G., Tachikawa, K., Bard, E., Beaufort, L., 2007.** Terrigenous input response to glacial/interglacial climatic variations over southern Baja California: a rock magnetic approach. *Quaternary Science Reviews* **26**, 3118-3133.

- Bond, G., Heinrich, H., Broecker, W., Labeyrie L., McManus, J., Andrews, J., Huon., S., Jantschik, R., Clasen, S., Simet, C., Tedesco, K., Klas, M., Bonani, G., Ivy, S., 1992.** Evidence for massive discharges of icebergs into the North Atlantic ocean during the last glacial period. *Nature* **360**, 245 – 249.
- Bond, G.C., Lotti, R., 1995.** Iceberg discharges into the North Atlantic on millennial time scales during the last glaciation. *Science* **267**, 1005.
- Bradley, R.S., 1999.** Paleoclimatology; Reconstructing Climates of the Quaternary. Academic Press, San Diego.
- Bradley, R.S., Eddy, J.A., 1991.** Records of past global changes. In: Global Changes of the Past (ed. R.S. Bradley) University Corporation for Atmospheric Research, Boulder, p.5-9.
- Broecker , W.S., Donk, J., 1970.** Insolation changes, ice volumes, and the O18 record in deep sea cores. *Reviews of Geophysics* **8**, 169-198.
- Broecker, W.S., 1994.** Massive iceberg discharge triggers for global climate change. *Nature* **372**, 421-424.
- Broecker, W.S., Bond, G., Klas, M., Clarck, E., McManus, J., 1992.** Origin of the northern Atlantic's Heinrich events. *Climate Dynamics* **6**, 265-273.
- Bronk Ramsey, C., 2008.** Deposition models for chronological records. *Quaternary Science Reviews* **27**, 42-60.
- Bronk Ramsey, C., 2009.** Bayesian analysis of radiocarbon dates. *Radiocarbon* **51**, 337-360.
- Castro, C.L., McKee, T.B., Pielke Sr., R.A., 2001.** The relationship of the North American Monsoon to tropical and North Pacific sea surface temperatures as revealed by observational analysis. *Journal of Climate* **14**, 4449-4473.
- Cohen, A.S., 2003.** Palaeolimnology: the history and evolution of lake systems. Oxford University Press. New York.
- Cohen, K.M., Finney, S.C., Gibbard, P.L., Fan, J.-X., 2013.** The ICS International Chronostratigraphic Chart. *Episodes* **36**, 3, 199-204.
- COHMAP members, 1988.** Climatic change of the past 18,000 years. Observations and model simulations. *Science* **241**, 1043-1052.
- COMPENDIUM OF INTERNATIONAL METHODS OF ANALYSIS (CIMA), 2002.** Quantification of total nitrogen according to the Dumas method (Musts and Wine). Method OIV-MA-AS323-02A.

- Cronin, T., 1999.** Principles of Paleoclimatology. Columbia University Press, 560.
- Cronin, T.M., 2010.** Paleoclimates: understanding climate change past and present. Columbia University press. New York.
- Dansgaard, W., Johnsen, S.J., Clausen, H.B., Dahl-Jensen, D., Gundestrup, N.S., Hammer, C.U., Hvldberg, C.S., Steffesen, J.P., Sveinbjörnsdottir, A.E., Jouzel, J., Bond, G., 1993.** Evidence for general instability of past climate from a 250-kyr ice-core record. *Nature* **364**, 218-220.
- Dansgaard, W., Johnsen, S.j., Clausen, H.B., Dahl-Jensen, D., Gundestrup, N., Hammer, C.U., Oeschger, H., 1984.** North Atlantic climatic oscillations revealed by deep Greenland ice cores. En Hansen, J. E y Takahashi, eds., Climate processes and Climate sensitivity, pp. 288-298. Washington, DC. American Geophisycal Union.
- Davis, O.K., Anderson, R. S., 1987.** Pollen in packrat (Neotoma) middens: pollen transport and the relationship of pollen to vegetation. *Palynology* **11**, 185-198.
- Denton, GH., Anderson, RF., Toggweiler, J.R., Edwards, RL., Schaefer, JM; Putnam, AE., 2010.** The Last Glacial Termination. *Science* **328**, 1652-1656.
- Emiliani, C.J., 1955.** Pleistocene temperatures. *Journal of Geology* **63**, 538-578.
- García, E., 1973.** Modificaciones al sistema de clasificación climática de Köppen: México. Universidad Nacional Autónoma de México, D.F.
- González-Elizondo, M., Jurado, J.E., Navar, M., González-Elizondo, S., Villanueva, J., Aguirre, O., Jiménez, J., 2005.** Tree-rings and climate relationships for Douglas-fir chronologies from the Sierra Madre Occidental, Mexico: a 1681-2001 rain reconstruction. *Forest Ecology Management* **213**, 39-53.
- Grimm, E.C., Watts, W.A., Jacobson Jr, G.L., Hansen, B.C.S., Almquist, H.R., Dieffenbacher-Krall, A.C., 2006.** Evidence for warm wet Heinrich events in Florida. *Quaternary Science Reviews* **25**, 2197-2211.
- Heinrich, H., 1988.** Origin and consequences of cyclic ice rafting in the northeast Atlantic Ocean during the past 130,000 years. *Quaternary Research* **29**, 142-152.
- Hemming, S.R., 2004.** Heinrich events: massive late Pleistocene detritus layers of the North Atlantic and their global climate imprint. *Review of Geophysics* **42**, RG1005.
- Jennerjahn, T.C., Ittekkot, V., Arz, H.W., Behling, H., Pätzold, J., Wefer, G., 2004.** Asynchronous terrestrial and marine signals of climate change during Heinrich events. *Science* **306**, 2236-2239.

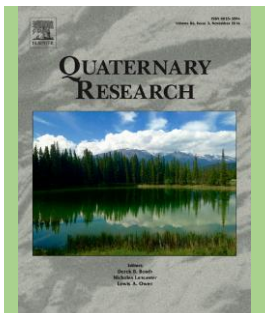
- Kirby, M.E., Feakins, S.J., Bonuso, N., Fantozzi, J.M., Hiner, C.A., 2013.** Latest Pleistocene to Holocene hydroclimates from Lake Elsinore, California. *Quaternary Science Reviews* **76**, 1-15.
- Lisieki, L.E., Raymo, M.E., 2005.** A Plio-Pleistocene stack of 57 globally distributed benthic d₁₈O records. *Paleoceanography* **20**; PA1003.
- Lozano Santa Cruz, R., Verma, S.P., Girón, P., Velasco, F., Morán Zenteno, D., Viera F., Chávez, G., 1995.** Calibración preliminar de Fluorescencia de Rayos-X para análisis cuantitativo de elementos mayores en rocas ígneas. *Actas INAGEQ* **1**, 203-208.
- Lyle, M., Heusser, L., Ravelo, C., Yamamoto, M., Barron, J., Diffenbaugh, N.S., Herbert, T., Andreasen, D., 2012.** Out of the tropics: the Pacific, Great Basin Lakes, and Late Pleistocene water cycle in the western United States. *Science* **337**, 1629-1633.
- Magaña, V.O., Vázquez, J.L., Pérez, J.L., Pérez, J.B., 2003.** Impact of El Niño in precipitation in Mexico. *Geofísica Internacional* **42**, 313-330.
- Maslin, M.A., y Shackleton, N.J., 1995.** Surface water temperatures, salinity, and density changes in the northeast Atlantic during the last 45,000 years: Heinrich events, deep water formation, and climatic rebounds. *Paleoceanography* **10**, 527-544.
- Mayewski, P.A., Rohling, E.E., Stager, J.C., Karlén, W., Maasch, K.A., Meeker, L.D., Meyerson, E.A., Gasse, F., van Kreveld, S., Holmgren, K., Lee-Thorp, J., Rosqvist, G., Rack, F., Staubwasser, M., Schneider, R.R., Steig, E.J., 2004.** Holocene climate variability. *Quaternary Research* **62**, 243-255.
- McCrea, J.M., 1950.** On the isotopic chemistry of carbonates and palaeo-temperature scale. *Journal of Chemical Physics* **18**, 849-857.
- Metcalfe, S.E., Barron, J.A., Davies, S.J., 2015.** The Holocene history of the North American Monsoon: 'known knowns' and 'known unknowns' in understanding its spatial and temporal complexity. *Quaternary Science Reviews* **120**, 1-27.
- Mitchell, D.L., Ivanova, D., Rabin, R., Brown, T.J., Redmond, K., 2002.** Gulf of California sea surface temperatures and the North American Monsoon: mechanistic implications from observations. *Journal of Climate* **15**, 2261-2281.
- Mix, A. C., Bard, E., Schneider, R., 2001.** Environmental processes of the ice age: land, oceans, glaciers (EPILOG). *Quaternary Science Reviews* **20**, 627-657.

- NEEM community members, 2013.** Eemian interglacial reconstructed from a Greenland folded ice core. *Nature* **493**, 489-494.
- Nesbitt, H.W., Young, G.M., 1984.** Prediction of some weathering trends of plutonic and volcanic rocks based on thermodynamic and kinetic considerations. *Geochimica et Cosmochimica Acta* **48**, 1523-1534.
- Nesbitt, H.W., Young, G.M., 1989.** Formation and diagenesis of weathering profiles. *Journal of Geology* **97**, 129-147.
- Northern Greenland Ice Core project members (NGRIP project), 2004.** High resolution record of Northern Hemisphere climate extending into the last interglacial period. *Nature* **431**, 147-151.
- Nieto-Samaniego, A.F., Barajas-Gea, C.I., Gómez-González, J.M., Rojas, A., Alaniz-Álvarez, S.A., Xu, S., 2012.** Geología, evolución estructural (Eoceno al actual) y eventos sísmicos del Graben de Santiagillo, Durango, México. *Revista Mexicana de Ciencias Geológicas* **29**, 115-130.
- National Institute of Standards and Technology NIST, 2016.** Certificate of Analysis, Standard Reference Material 2702, Inorganics in Marine Sediments.
- Peltier, W.R., Fairbanks, R.G., 2006.** Global glacial ice volume and Last Glacial Maximum duration from an extended Barbados sea level record. *Quaternary Science Reviews* **25**, 3322-3337.
- Rahmstorf, S., 2003.** Timing of abrupt climate change: A precise clock. *Geophysical Research Letters* **30**, 1510. doi: 10.1029/2003GL017115.
- Rasmussen, S.O., Andersen, K.K., Svensson, A.M., Steffensen, J.P., Vinther, B.M., Clausen, H.B., Siggaard-Andersen, M.L., Johnsen, S.J., Larsen, L.B., Dahl-Jensen, D., Bigler, M., Röhlisberger, R., Fischer, H., Goto-Azuma, K., Hansson, M. E., Ruth U., 2006.** A new Greenland ice core chronology for the last glacial termination. *Journal of Geophysical Research: Atmospheres* **111** D06102, doi:10.1029/2005JD006079.
- Reimer, P.J., Bard, E., Bayliss, A., Beck, J.W., Blackwell, P.G., Ramsey, C.B., Grootes, P.M., Guilderson, T.P., Haflidason, H., Hajdas, I., Hatté, C., Heaton, T.J., Hoffmann, D.L., Hogg, A.G., Hughen, K.A., Kaiser, K.F., Kromer, B., Manning, S.W., Niu, M., Reimer, R.W., Richards, D.A., Scott, E.M., Southon, J.R., Staff, R.A., Turney, C.S. M., van der Plicht, J., 2013.** IntCal13 and MARINE13 radiocarbon age calibration curves 0-50000 years cal BP. *Radiocarbon* **55**, 1869–1887.

- Roy, P.D., Caballero, M., Lozano, R., Ortega, B., Lozano, S., Pi, T., Israde, I., Morton, O., 2010. Geochemical record of Late Quaternary paleoclimate from lacustrine sediments of paleo-lake San Felipe, western Sonora Desert, Mexico. *Journal of South American Earth Sciences* **29**, 586-596.
- Roy, P.D., Jonathan, M.P., Pérez-Cruz, L.L., Sánchez-Córdova, M.M., Quiroz-Jiménez, J.D., Romero, F.M., 2012. A millennial-scale Late Pleistocene-Holocene palaeoclimatic record from the western Chihuahua Desert, Mexico. *Boreas* **41**, 707-717.
- Roy, P.D., Rivero-Navarrete, A., Lopez-Balbiaux, N., Pérez-Cruz, L.L., Metcalfe, S.E., Muthu Sankar, G., Sánchez-Zavala, J.L., 2013. A record of Holocene summer-season palaeohydrological changes from the southern margin of Chihuahua Desert (Mexico) and possible forcings. *The Holocene* **23**, 1105-1114.
- Roy, PD., Charles-Polo, M.P., López Balbiaux, N., Pi-Puig, T., Sankar, G.M., Lozano Santacruz, R., Lozano-García, M.S., Romero, F.M., 2014b. Last glacial hydrological variations at the southern margin of sub-tropical North America and regional comparison. *Journal of Quaternary Science* **29**, 495-505.
- Roy, P.D., Chávez-Lara, C.M., Beramendi-Orosco, L.E., Sánchez-Zavala, J.L., Muthu-Sankar, G., Lozano-Santacruz, R., Quiroz-Jimenez, J.D., López-Balbiaux, N., 2015. Paleohydrology of the Santiagillo Basin (Mexico) since late last glacial and climate variation in southern part of western subtropical North America. *Quaternary Research* **84**, 335-347.
- Sanchez-Goñi, M.F., Harrison, S.P., 2010. Millennial-scale climate variability and vegetation changes during the Last Glacial: Concepts and terminology. *Quaternary Science Reviews* **29**, 2823-2827.
- Schnurrenberger, D., Russell J., Kelts K., 2003. Classification of lacustrine sediments based on sedimentary components. *Journal of Paleolimnology* **29**, 141-154.
- Servicio Geológico Mexicano, 1998. Carta Geológico-Minera Durango, escala 1:250,000. G13-11.
- Shackleton, N.J., 1967. Oxygen isotope analyses and Pleistocene temperatures reassessed. *Nature* **215**, 15-17.
- Shackleton, N.J., 1969. Oxygen Isotopes, Ice Volume and Sea Level. *Quaternary Science Reviews* **6**, 183-190.
- Skinner, L.C., Shackleton, N.J., 2005. Rapid transient changes in northeast Atlantic deep water ventilation across Termination I. *Paleoceanography* **19**:PA2005.

- Steffensen, J.P., Andersen, K.A., Bigler, M., 2008.** High resolution Greenland ice core data show abrupt climate change happen in a few years. *Science* **321**, 680-684.
- Sutton, R.T., Hodson, D.L.R., 2005.** Atlantic Ocean forcing of North American and European summer climate. *Science* **309**, 115-118.
- Swanson, S.K., Bahr, J.M., Schwar, M.T., Potter, K.W., 2001.** Two-way cluster analysis of geochemical data to constrain spring waters. *Chemical Geology* **179**, 73-91.
- Thomson, R., Oldfield, F., 1986.** Environmental Magnetism. Allen & Unwin, London.
- Urrutia Fucugauchi, J., Ortega Ramirez, J., Cruz Gatica, R., 1997.** Rock magnetic study of late Pleistocene-Holocene sediments from the Babicora lacustrine basin, Chihuahua northern Mexico. *Geofísica Internacional* **10**, 77-86.
- Verma S.P., Lozano-Santa Cruz, R., Girón-García, P., Velasco, F., 1996.** Calibración preliminar de Fluorescencia de Rayos-X para análisis cuantitativo de elementos traza en rocas ígneas. *Actas INAGEQ* **2**, 237-242.
- Versteegh, G.J., 2005.** Solar forcing of climate. 2: evidence from the past. *Space Science Reviews* **120**, 243-286.
- Vidal, L., Labeyrie, L., Cortijo, E., Arnold, M., Duplessy, J. C., Michel, E., Becqué, S., van Weering, T. C. E., 1997.** Evidence for changes in the North Atlantic deep water linked to meltwater surges during the Heinrich events. *Earth and Planetary Science Letters* **146**, 13-27.
- Villanueva-Díaz, J., Paredes, J.C., Mata, S. R., López, J.C. A., Stahle, D.W., Corral, J.A.R., Sifuentes, A.R.M., 2014.** Variabilidad hidroclimática reconstruida con anillos de árboles para la cuenca alta del Río Mezquital, Durango. *Revista Mexicana de Ciencias Agrícolas* **10**, 1897-1912.
- Wang, Y.J., Cheng, H., Edwards, R.L., An, Z.S., Wu, J.Y., Shen, C.C., Dorale, J.A., 2001.** A high-resolution absolute-dated late Pleistocene Monsoon record from Hulu Cave, China. *Science* **294**, 2345-2348.
- Zic, M., Negrini, R., Wigand, P., 2002.** Evidence of synchronous climate change across the Northern Hemisphere between the North Atlantic and northwestern Great Basin, United States. *Geology* **30**, 635-638.

CAPÍTULO V



Paleohydrology of the Santiaguillo Basin (Mexico) since the late last glacial and climate variation in southern part of western subtropical North America



Paleohydrology of the Santiaguillo Basin (Mexico) since late last glacial and climate variation in southern part of western subtropical North America



Priyadarsi D. Roy ^{a,*}, Claudia M. Chávez-Lara ^b, Laura E. Beramendi-Orosco ^a, José L. Sánchez-Zavalta ^a, Gowrappan Muthu-Sankar ^c, Rufino Lozano-Santacruz ^a, Jesús D. Quiroz-Jimenez ^b, Nayeli López-Balbiaux ^d

^a Instituto de Geología, Universidad Nacional Autónoma de México, 04510 México DF, Mexico

^b Posgrado en Ciencias de la Tierra, Universidad Nacional Autónoma de México, 04510 México DF, Mexico

^c French Institute of Pondicherry, 11, St. Louis Street, Pondicherry 605001, India

^d USAI, Facultad de Química, Universidad Nacional Autónoma de México, 04510 México DF, Mexico

ARTICLE INFO

Article history:

Received 1 December 2014

Available online 6 November 2015

Keywords:

Paleoclimate

Geochemistry

Late last glacial–Holocene

Subtropical North America

Tropical Cyclone

North American Monsoon

Mexico

ABSTRACT

Stratigraphy, geochemistry and radiocarbon dating of a succession of sediment in the Santiaguillo Basin (central-northern Mexico) help reconstruct the millennial-scale dynamics of hydrological variability that occurred in the southern part of western subtropical North America since the late last glacial. Runoff was generally above average during the late last glacial from ~27 to 18 ka. Following this interval, runoff decreased and deposition of authigenic carbonate and aeolian transported sediment increased until ~4 ka. Heinrich 1 and 2, and Younger Dryas were intervals of reduced runoff and increased aeolian activity. The wetter climate of central-northern Mexico and arid conditions in north-northwestern Mexico during the late last glacial were probably related to formation of tropical cyclones in the eastern North Pacific during the autumn with restricted rainfall swaths and an absent/weaker North American Monsoon. Enhanced North American Monsoon and tropical cyclones with expanded rainfall swaths brought more summer and autumn precipitation to a broader region extending from the central-northern Mexico to the continental interiors of southwestern US during the early Holocene.

© 2015 University of Washington. Published by Elsevier Inc. All rights reserved.

Introduction

Modern day climate of the subtropical North America is controlled by summer and autumn rainfalls associated with the North American Monsoon (NAM) and tropical cyclones (Douglas et al., 1993; Stensrud et al., 1995; Higgins et al., 1997; Mitchell et al., 2002; Amador et al., 2006; Farfán and Fogel, 2007; Ritchie et al., 2011) as well as winter precipitation related to the westerly jet stream (Friedman et al., 1992; Cayan et al., 2008; Caldwell, 2010; Neelin et al., 2013). The Pacific coast of the southwestern US is dominated by winter precipitation (Friedman et al., 1992; Cayan et al., 2008; Caldwell, 2010; Neelin et al., 2013), whereas northern and northwestern Mexico are dominated by summer and autumn precipitation (Douglas et al., 1993; Stensrud et al., 1995; Mitchell et al., 2002; Xu et al., 2004; Farfán and Fogel, 2007). The continental interiors of southwestern US receive summer and autumn precipitation as well as winter rainfall (Sheppard et al., 2002). Figure 1 shows the present precipitation regimes from different sites (www.weatherbase.com) and divides the region into northern, central and southern parts based on locations of the comparison sites.

Numerous researchers suggest that more winter storms provided greater precipitation to the region during the global last glacial maximum (LGM) in western subtropical North America (COHMAP members, 1988; Thompson and Anderson, 2000; Enzel et al., 2003). COHMAP members (1988) and Kutzbach and Wright (1985) suggested that the Laurentide ice sheet split the jet streams into two different branches and the stronger southern branch carried more moisture into the region. However, the global climate simulations of Kim et al. (2008) and Toracinta et al. (2004) either did not support the split in the jet stream or indicated that the southern branch of the jet stream was weaker. The high-resolution model of Kim et al. (2008) locates the region of dominant winter precipitation in the western–southwestern US and region of dominant summer precipitation in northwestern Mexico. This model's simulation also shows that summer precipitation was occurring in the continental interiors of southwestern US. The juxtaposition of cold ice sheet and adjacent warm ice-free land caused a pronounced low-level thermal gradient and facilitated the development of synoptic cyclones at the southern margin of Laurentide ice sheet (Bromwich et al., 2005). Recently, Oster et al. (2015) compared a compilation of proxy precipitation reconstructions from the region with climate simulations and suggested that the hydroclimate of LGM is best explained by a stronger jet stream that is squeezed and steered across the continent.

* Corresponding author.

E-mail addresses: priyadarsi1977@gmail.com, roy@geologia.unam.mx (P.D. Roy).

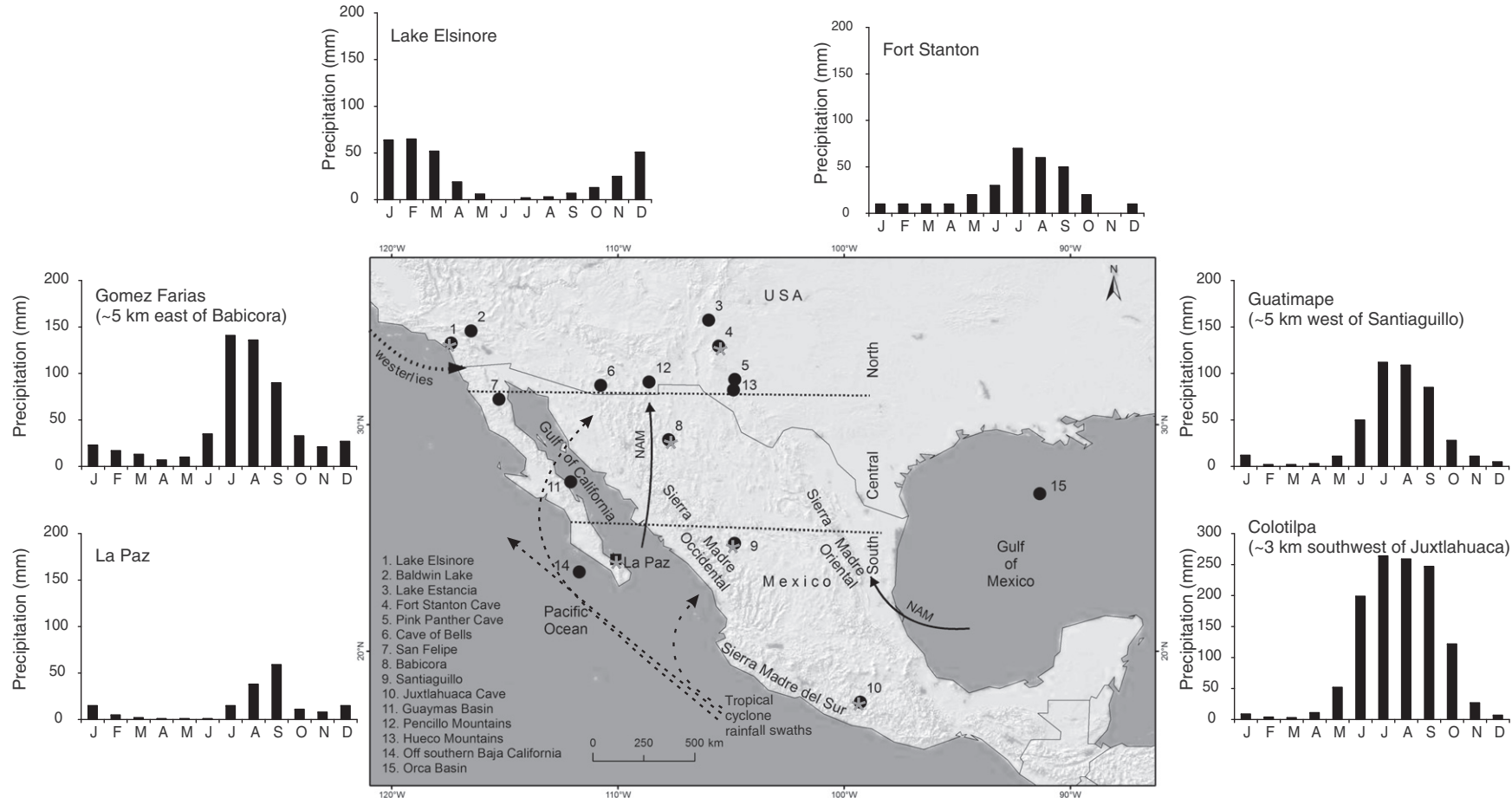


Figure 1. Location of paleoclimate archives (filled circle) from the western subtropical North America. The Santiagillo Basin is located at ~ 25°N in the eastern flank of Sierra Madre Occidental Mountains in central-northern Mexico. Modern precipitation data from different sites (star) of the region are shown (source: www.weatherbase.com).

Over the last two decades, the number of proxy-records from the region has increased thus improving the knowledge of LGM climate across the southwestern US and northwestern Mexico (Anderson et al., 2002; Holmgren et al., 2003, 2007; Kirby et al., 2005, 2006, 2013; Asmerom et al., 2010; Roy et al., 2010, 2012, 2013; Wagner et al., 2010; Lachniet et al., 2014) (Fig. 1). More winter precipitation in the southwestern US is reflected by the presence of permanent lakes in coastal southern California, negative excursions in $\delta^{18}\text{O}$ values of speleothems from Nevada, Arizona and New Mexico and absence of summer flowering annuals and C_4 grasses in the US and Mexico borderland (Kirby et al., 2005, 2006; Holmgren et al., 2007; Asmerom et al., 2010; Wagner et al., 2010). At the same time, the lacustrine basins from Baja California and Chihuahua received less runoff as a result of reduced summer precipitation in northern and northwestern Mexico (Roy et al., 2010, 2012).

Over the deglaciation, the amount of summer precipitation increased in northern and northwestern Mexico (Roy et al., 2010, 2012). Lyle et al. (2012) suggested that the northward expansion of summer precipitation brought humid air mass into the Great Basin in the interior of the western US. However, Kirby et al. (2013) and Lachniet et al. (2014) did not recognize any evidence of summer rainfall reaching the coastal southern California and central Great Basin and suggested that variations in the hydrological conditions of Lake Elsinore and Leviathan Cave were controlled by different amounts of winter precipitation. During the Pleistocene–Holocene transition, an interval of alluvial fan aggradation in the southwestern US is explained by the enhanced frequency of winter storms as well as increased penetration of tropical cyclones (Antinao and McDonald, 2013). In a regional synthesis of Holocene records, Metcalfe et al. (2015) re-analyzed the influences of both summer and autumn insolation and latitudinal migration of Inter-Tropical Convergence Zone (ITCZ) on climate signals of the NAM region. Barron et al. (2012) reported presence of enhanced moisture in a broader NAM region during the early Holocene (>8 ka; all ages in this paper are presented as calendar years before AD 1950) and related it to the moisture flow sourced from the subtropical Pacific compared to the regular Gulf of California (GoC).

Paleoclimatic details for central-northern Mexico come from our previous work in the Santiaguillo Basin (Roy et al., 2014). An enhancement in the amount of runoff into the Santiaguillo Basin during the Pleistocene–Holocene transition and early Holocene was associated with more monsoonal moisture sourced from GoC. In this study, we present new geochemical (organic carbon, carbonate, C/N, and elemental concentrations) and magnetic susceptibility data extending our knowledge about runoff, evaporation and lake salinity, provenance of organic productivity and clastic sediments in the basin, and aeolian activity up to 27 ka. The paleohydrological information is compared with our recently published register of paleoecology of ostracods from the same sediment profile (Chávez-Lara et al., 2015). The runoff record for the Santiaguillo Basin is compared with proxy records from the Juxtlahuaca Cave (southwestern Mexico; Lachniet et al., 2013) and Lake Elsinore (coastal southwestern US; Kirby et al., 2013). Both the Juxtlahuaca Cave (monsoonal only) and Lake Elsinore (winter only) are end member sites and the comparison enables us to estimate the influences of monsoonal and winter precipitations on the hydrological variations in the Santiaguillo Basin. We evaluated the influences of different forcings on the Santiaguillo Basin record through comparison to insolation values (Berger and Loutre, 1991), reconstructed North Hemisphere temperature (NGRIP project members, 2004), mean position of ITCZ (Deplazes et al., 2013), sea surface temperature (SST) records from GoC (McClymont et al., 2012) and Gulf of Mexico (GoM; Flower et al., 2004), and contemporary meteorological data about the NAM and tropical cyclones.

Material and methods

Study site

The ephemeral and endorheic Santiaguillo Basin is located in a half-graben in central-northern Mexico ($24^{\circ} 44' \text{N}$, $104^{\circ} 48' \text{W}$, 1960 m asl)

along the eastern flank of Sierra Madre Occidental Mountains (Fig. 1). The half-graben was formed at $\sim 39\text{--}32$ Ma (Nieto-Samaniego et al., 2012) and the present lacustrine basin is spread over an area of $\sim 2000 \text{ km}^2$. The basin is oriented NW–SE, and has a maximum length and width of $\sim 45 \text{ km}$ and $\sim 10 \text{ km}$, respectively (Fig. 2). The northern sub-basin is presently used as an irrigation reservoir and an artificial dam separates this from the southern natural part of the basin. During the summer months the deepest part of the southern sub-basin fills with water to a depth of $< 1 \text{ m}$.

The bedrock of the basin is composed of Cretaceous to Quaternary metamorphic, igneous, and sedimentary rocks (Nieto-Samaniego et al., 2012). Paleogene rhyolite and ignimbrite are the dominant lithology and are exposed in the $\sim 2500\text{--}3000 \text{ m}$ high mountains to the immediate east and west of the basin. A large outcrop of Pliocene–Pleistocene basalt is present $\sim 20 \text{ km}$ southeast of the basin, constituting the second most important lithology. Minor exposures of Paleogene andesite are present in the surroundings. The Quaternary deposits consist of lacustrine sediments and alluvium.

Modern climate

A meteorological station at the western margin of the Santiaguillo Basin (at Guatimape, Fig. 2) recorded an average annual precipitation of $\sim 430 \text{ mm}$ between AD 1951–2010 (Source: Servicio Meteorológico Nacional, Mexico). Summer and autumn precipitations (June–October) associated with the NAM and tropical cyclones contributed almost 90% ($\sim 385 \text{ mm}$) of the annual rainfall; the winter precipitation (November–March) contributes $< 10\%$ of the annual total. Average annual temperature is $\sim 18^{\circ}\text{C}$; it can reach $\sim 34^{\circ}\text{C}$ during the months of May–June and is sub-zero during December–February.

Sampling and analysis

Sediments were collected up to the depth of 300 cm in a pit dug in the modern shore of the southern sub-basin (Fig. 2). Chronology of the sediment column is based on 6 AMS ^{14}C ages on organic matter present in the bulk sediments collected at depths of 49, 73, 111, 167, 205, and 279 cm (Fig. 3, Table 1). Samples at 2 cm intervals ($n = 150$) were oven dried at 40°C , homogenized and ground with an agate pestle. Concentrations of total carbon and inorganic carbon (IC) were determined at $\sim 4\text{--}6 \text{ cm}$ intervals ($n = 61$) in a Thermo Scientific HiperTOC solid analyzer. Organic carbon (OC) content was calculated by subtracting IC from total carbon and we expressed IC as carbonate (CO_3). Total nitrogen (TN) was measured at $\sim 10 \text{ cm}$ intervals ($n = 31$) in a Perkin Elmer Series II CHNS/O elemental analyzer.

The concentrations of Ti, Fe, K, Ca, Sr, and Zr were measured in all samples using a Thermo Scientific Niton XL3t X-ray fluorescence (XRF) analyzer. The data were corrected after measuring the same elements in 61 samples using the traditional Siemens SRS 3000 XRF (e.g. Roy et al., 2012). Additionally, concentrations of Si, Al, Na, K, Ca and P were measured at $\sim 4\text{--}6 \text{ cm}$ intervals ($n = 61$) using traditional XRF. Low field magnetic susceptibility of all sediment samples was obtained using a Bartington MS2E high resolution surface scanning sensor at 2 kHz. A total of 8 different rock samples were collected from the two dominant lithologies (rhyolite and basalt) present in the watershed (see Fig. 2 for locations) and analyzed for major element concentrations using traditional XRF.

Results

Sediment

Sediment consists of silty-sand, silt, silty-clay and clay (Fig. 3). Intercalations of gray clay and yellow calcareous silt are evident at a depth of 300–278 cm. This is followed by massive yellow silt

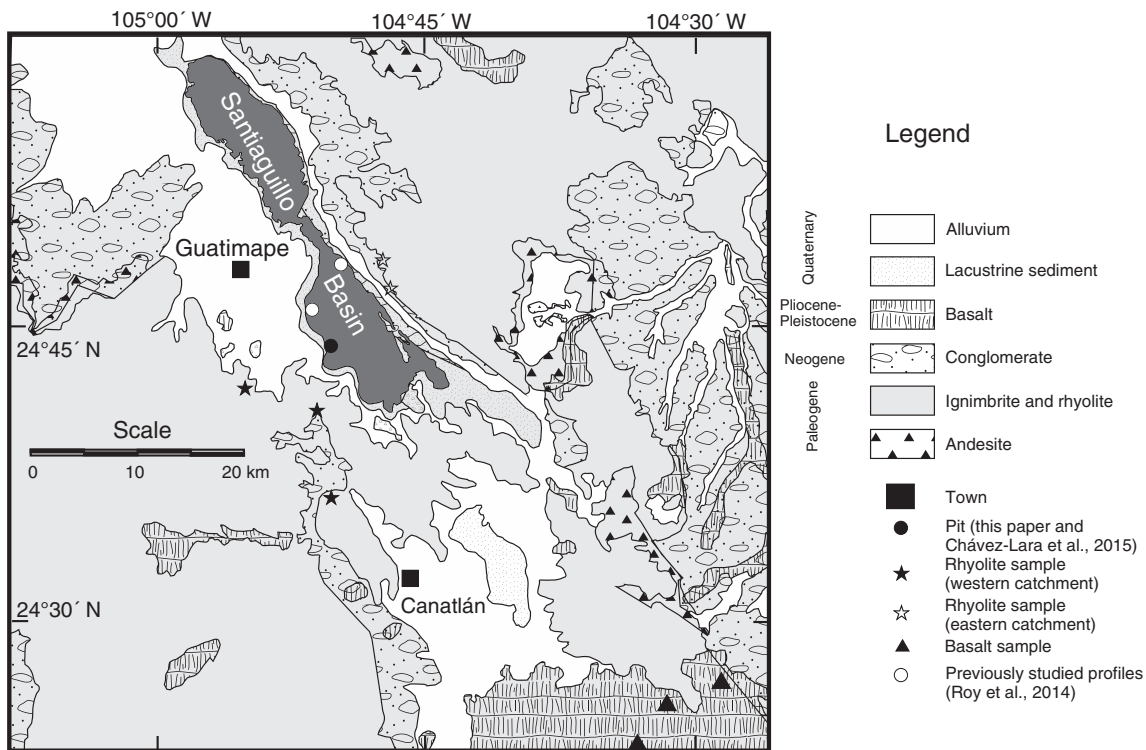


Figure 2. The geology of Santiaguillo Basin and sampling locations. A meteorological station at Guatimape provided the precipitation and temperature data between AD 1951–2010.

and silty-sand with occasional carbonate nodules to a depth of 75 cm. Intercalations of dark gray silty-clay and calcareous yellow silt occur above this zone to a depth of 50 cm, with vertical

desiccation fissures (~ 65 cm long) at the depth of 75 cm. Massive dark gray silty-sand with abundant root remnants occur in the upper 50 cm.

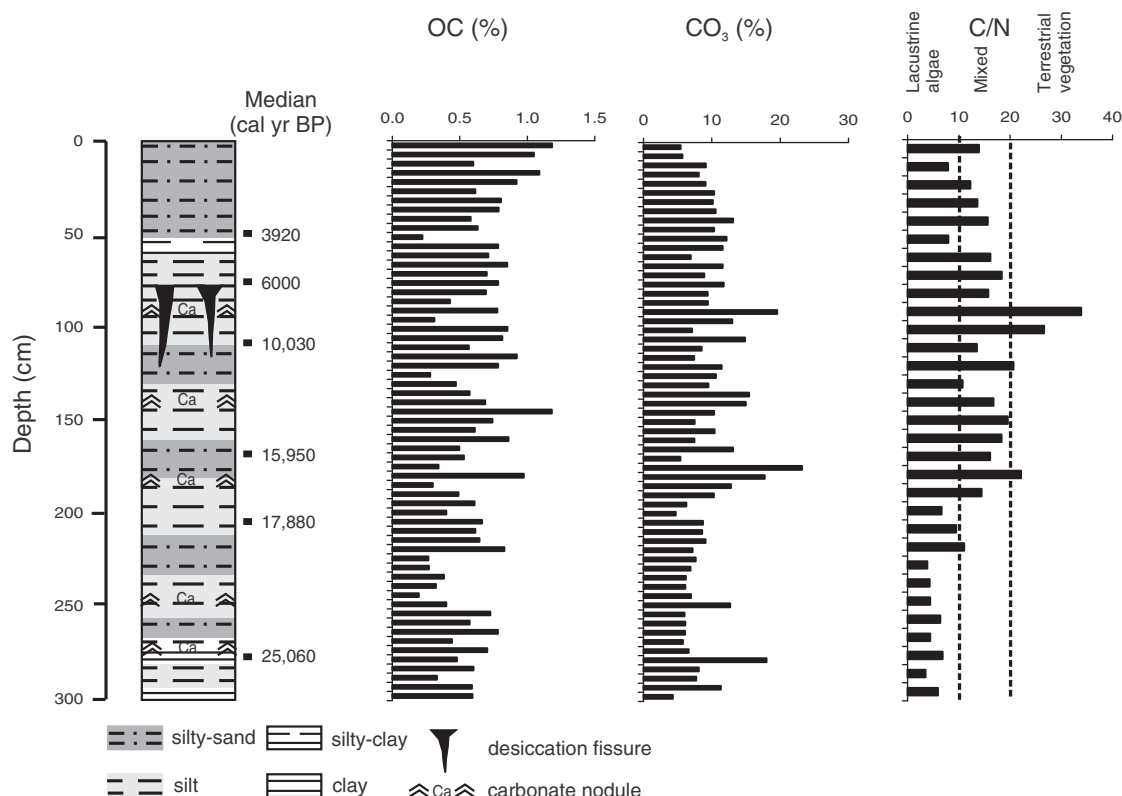


Figure 3. Stratigraphy of the sediment profile and median values of calibrated AMS ^{14}C ages at different depths. Distributions of organic carbon (OC), carbonate (CO_3) and organic carbon to total nitrogen relation (C/N) are presented along the depth.

Table 1

Radiocarbon ages of bulk sediment samples and calibration results for the Bayesian age–depth model constructed for a sediment succession from the Santiaguillo Basin.

Lab. code	Depth (cm)	$\delta^{13}\text{C}$ (‰)	Conventional age ($\pm 1\sigma$, yr BP)	Modeled calibrated age ^a (2σ , cal yr BP)	Median (cal yr BP)	Agreement Index ^b (%)
Beta-299072	49	−18.0	3610 ± 30	3830–4060	3920	99.7
Beta-299073	73	−19.3	5250 ± 30	5920–6180	6000	96.2
Beta-321663	111	−20.2	8900 ± 40	9890–10190	10,030	100.2
Beta-299074	167	−20.8	13,360 ± 60	15,750–16,160	15,950	70.8
Beta-299075	205	−20.7	14,610 ± 60	17,690–18,040	17,880	87.4
Beta-299076	279	−20.9	20,790 ± 100	24,590–25,380	25,060	98.1

^a Calibration using OxCal 4.2 (Bronk Ramsey, 2009) and IntCal_13 radiocarbon calibration curve (Reimer et al., 2013).

^b Agreement Index for the model = 79.6%.

OC and CO₃

OC content ranges from 0.2 to 1.2% and the amount of CO₃ ranges between 4 and 23% (Fig. 3). Higher values of CO₃ at depths of 281 cm (18%, n = 1), 181–175 cm (18–23%, n = 2), 141–135 cm (15–16%, n = 2) and 91 cm (20%, n = 1) are characterized by occasional carbonate nodules. The distributions of OC and CO₃ do not show any significant correlation ($r = 0.1$, $p < 0.05$).

TN and C/N ratio

TN varies between 0.02 and 0.10% and sediments have C/N (OC/TN) of 3–34 (Fig. 3). Lower and less variable C/N (≤ 10) values characterize the sediment at depths between 200 and 300 cm. In general, C/N is variable (≥ 10) in sediments from a depth of 200 cm to the surface. Lower values are associated with sediments deposited at depths of 51 cm and 11 cm (C/N = 8) and the highest value is observed in sediments at a depth of 91 cm (C/N = 34).

Chronology

An age–depth model (Fig. 4) was generated using the online OxCal version 4.2 (Bronk Ramsey, 2009). The Bayesian age model is constructed using 6 different stratigraphically consistent ¹⁴C ages, IntCal13 calibration curve (Reimer et al., 2013) and P sequence with k = 1 (Bronk Ramsey, 2008). Both the age model and calibrated ages were evaluated by the Agreement Index (A). This index is a measure of the correspondence between the data and model. More than 60% threshold for both indicates agreement between the age–depth model and observations, and suggests that there are no outliers within the radiocarbon ages. The calibrated ages and corresponding median values are presented in Table 1.

The age model incorporates uncertainties (1σ) of 44–195 years between the tie points and up to 480 years while extrapolating to bottom of the core at a depth of 300 cm. The model assigns a median age of ~27 ka to the base of sediment succession and estimates sedimentation of 9.4–19.8 cm/ka. The rate of sedimentation was highest (19.8 cm/ka) during ~17.8–15.9 ka and lowest (9.4 cm/ka) during ~15.9–6 ka. Sediments between depths of 49 and 300 cm were deposited between ~27 and 4 ka and sediments at depths from 49 cm to the surface represent the depositional history of last ~4 cal ka. Desiccation fissures at a depth of 75 cm suggest that the pit site was dry at ~6.5 ka. The comparable rates of sedimentation in the interval involving the desiccation (9.4 cm/ka) and two other intervals without any desiccation fissure, during ~25–17.8 ka (10.3 cm/ka) and ~10–6 ka (9.4 cm/ka) possibly suggest the absence of any hiatus or significant erosion at ~6.5 ka. However, the presence of hiatus and erosion of sediments in arid settings are common and the sediment profile representing the past 27 ka possibly contain many such events that were not detectable in the age model. The median calibrated age (with 1σ uncertainty) was assigned to sediments at 2 cm depth intervals using the interpolation option of OxCal.

Multi-element geochemistry

Basalt present to the southeast of the basin has Ti and Al concentrations of 1.8–2.3% and 3.9–4.3%, respectively. Rhyolite present in the east and west of the basin has Si concentrations of 34–37%. There are geochemical dissimilarities among the rhyolites. Rhyolite in the western catchment, for example, has more Ti (0.2–0.3%) and Al (3.4–3.7%) and less Si (34–35%) compared to the rhyolite in the eastern catchment. Rhyolite from the eastern catchment has 0.1% of Ti, 2.6–2.9% of Al and 37% of Si. The lacustrine sediments have Si concentrations of 21–31%, Al concentrations of 2.5–4.1% and Ti concentrations of 0.10–0.25%.

Degree of chemical alteration of the rocks and sediments is estimated by calculating the chemical index of alteration (CIA; Nesbitt and Young, 1984, 1989). CIA values of sediments and rocks are 48–86 and 43–55, respectively. Sediments in general have CIA ≥ 60 because most of them have undergone some degree of chemical weathering (Fig. 5A). Lower values (CIA < 60) at depths of 218, 251 and 91 cm

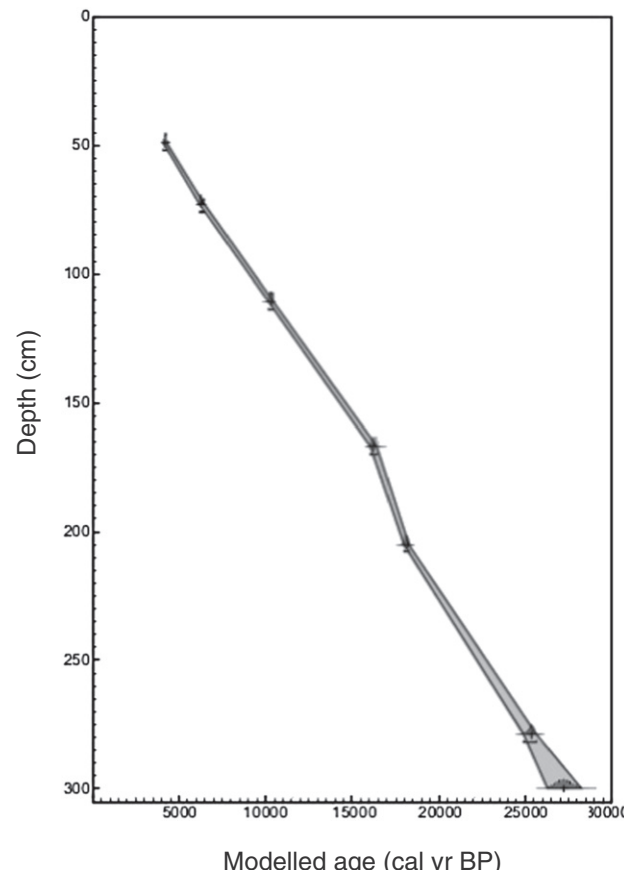


Figure 4. Age–depth model generated for the sediment profile using OxCal version 4.2.

represent events of deposition of unaltered to low altered sediments from the watershed into the basin. Irrespective of different degrees of chemical alteration, the linear trend of sediments in the A-CN-K ternary diagram indicates a uniform provenance over the past 27 ka. Presence of rhyolite samples collected from the western catchment along and close to the linear trend suggests that the lacustrine sediments were mainly sourced from erosion of the western rhyolite. Similarities in geochemical characteristics between the lacustrine sediments and western watershed rhyolite are also evident in the $\text{TiO}_2/\text{Al}_2\text{O}_3$ vs. $\text{SiO}_2/\text{Al}_2\text{O}_3$ binary plot (Fig. 5B). Both the lacustrine sediments and rhyolite from western watershed have comparable $\text{SiO}_2/\text{Al}_2\text{O}_3$ and $\text{TiO}_2/\text{Al}_2\text{O}_3$ values.

Concentrations of Ti, Fe, K, Ca, Sr, and Zr and relations of $\text{SiO}_2/\text{Al}_2\text{O}_3$ and Zr/Ti along the depth are presented in Figure 6. In general, both K (2.3–3.2%) and Zr (110–209 ppm) are similar to Ti ($r = 0.8$, $p < 0.05$) and represent the abundance of clastic sediment. Distribution of Ca (1.8–15.2%) is comparable ($r = 0.9$, $p < 0.05$) to CO_3 (Fig. 6) and it represents the abundance of carbonate minerals. Both Fe and Sr have distinct temporal distributions ($r = 0.4$, $p < 0.05$). Distributions of Fe and Ti are similar in some parts of the sediment profile and opposite in other parts ($r = 0.1$, $p < 0.05$). Occurrence of Fe, both in clastic grains and carbonate, could be due to the mobilization of Fe from the silicates and oxides in an anoxic environment and precipitation along with carbonate during the intervals of higher salinity (Cohen, 2003). Similarly, Sr is associated with both clastic grains (300–200 cm) and carbonate (200–0 cm). The strong positive correlation between Ti and Zr ($r = 0.8$, $p < 0.05$) suggests that both are present in the Ti-bearing and Zr-bearing clastic sediment sourced from erosion of the western rhyolite. The rhyolitic source of Ti and Zr is also suggested by similar temporal variations of Ti, Zr and $\text{SiO}_2/\text{Al}_2\text{O}_3$ ($r = 0.5$, $p < 0.05$). However, Zr/Ti values are variable along the depth ($670–1090 \times 10^{-4}$) and suggest that the basin received more Zr-bearing clastic grains compared to Ti-bearing clastic grains during certain intervals (e.g. sediments at 200–85 cm depth).

Magnetic susceptibility

Magnetic susceptibility values range between 6 and 17×10^{-5} SI (Fig. 6). Characterized with high amplitude variations, the sediments

from a depth of 300–223 cm have higher values ($10–17 \times 10^{-5}$ SI). Intermediate values ($11–12 \times 10^{-5}$ SI) are associated with the sediments at a depth of 155–147 cm. The upper 85 cm of the sediment column have lower values ($6–10 \times 10^{-5}$ SI). In general, the distribution of magnetic susceptibility is similar to Ti ($r = 0.6$, $p < 0.05$) and inverse of Ca ($r = -0.5$, $p < 0.05$). More Ti-bearing clastic sediments were deposited during the intervals of higher magnetic susceptibility, whereas more carbonates were precipitated during the intervals with lower magnetic susceptibility.

Discussion

Proxy

Concentrations of Ti and Ca, ratios of Zr/Ti and C/N, and calculated CIA values are used as proxies to document the paleohydrological variations (Fig. 7). CIA estimates chemical alteration of sediments and is used here as an indicator of the degree of sediment–water interaction in the watershed. In the absence of any carbonate-bearing rock in the watershed, the carbonate enriched sediments are related to intervals of more saline water and thus more evaporative/drier conditions in the basin. Both Ca and CO_3 have similar distributions and we consider that the sediments with more Ca represent intervals of more saline water and evaporative conditions. Ti reflects the contribution of detrital materials into the basin. The uniform provenance over the last 27 ka suggests that sediments with more Ti represent intervals of greater clastic deposition. Negative coefficient of correlation between Ti and Ca ($r = -0.9$, $p < 0.05$) suggests that more Ti-bearing clastic sediment were deposited during intervals of less saline water and thus less evaporative/wetter conditions. In general, sediments with more Ti are characterized by CIA of ≥ 60 . Moderate to highly altered sediments were transported from the watershed into the basin via runoff as recorded by higher Ti values. Consequently, we use Ti as a proxy to estimate runoff into the basin. Sediments with more Ti were deposited during the intervals of more runoff during wetter climates and vice versa.

The moderate positive relationship between Zr/Ti and Ca ($r = 0.4$, $p < 0.05$) suggests that more Zr-bearing clastic sediments were deposited during the intervals of more saline water and more evaporative/drier

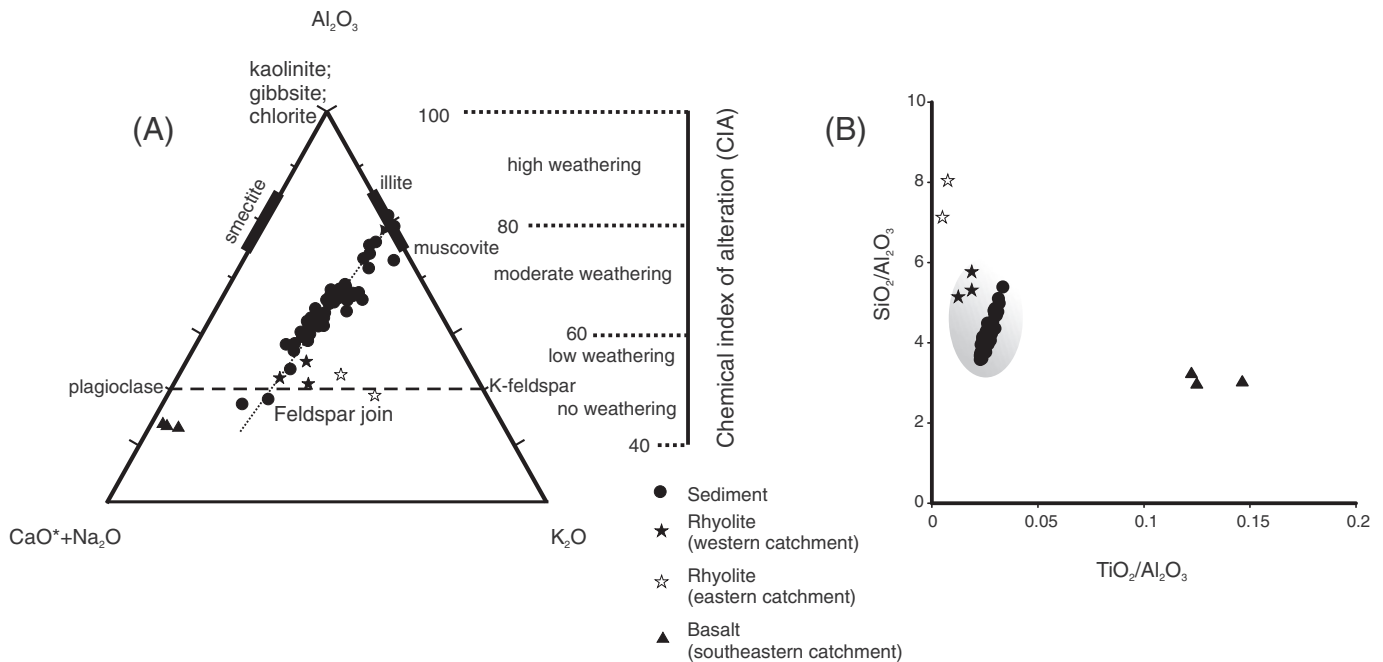


Figure 5. (A) Ternary diagram showing molar proportions of Al_2O_3 , $(\text{CaO}^* + \text{Na}_2\text{O})$ and K_2O and the scale of chemical index of alteration (CIA) of sediments and rocks. (B) Binary plot of $\text{TiO}_2/\text{Al}_2\text{O}_3$ vs. $\text{SiO}_2/\text{Al}_2\text{O}_3$ in sediments and rocks.

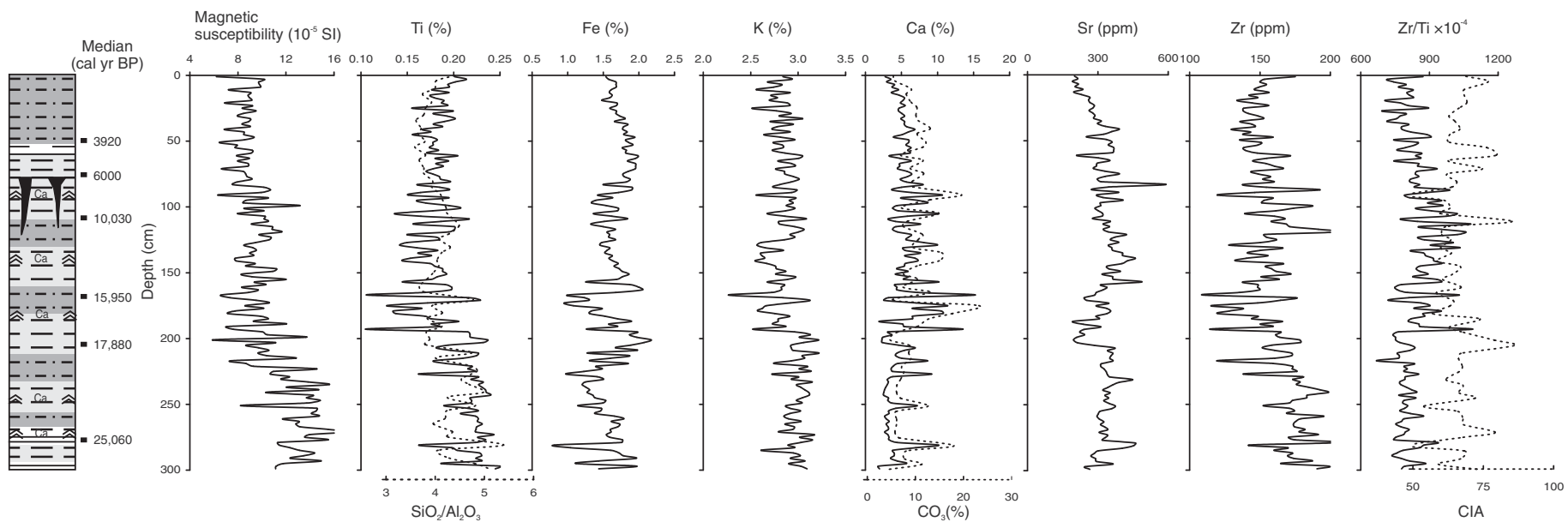


Figure 6. Distributions of magnetic susceptibility, concentrations of Ti, Fe, K, Ca, Sr, and Zr, CIA and ratios of $\text{SiO}_2/\text{Al}_2\text{O}_3$ and Zr/Ti along the depth. The distributions of Ti and Zr are similar to the variations of $\text{SiO}_2/\text{Al}_2\text{O}_3$. Both Ca and CO_3 have similar tendencies with depth.

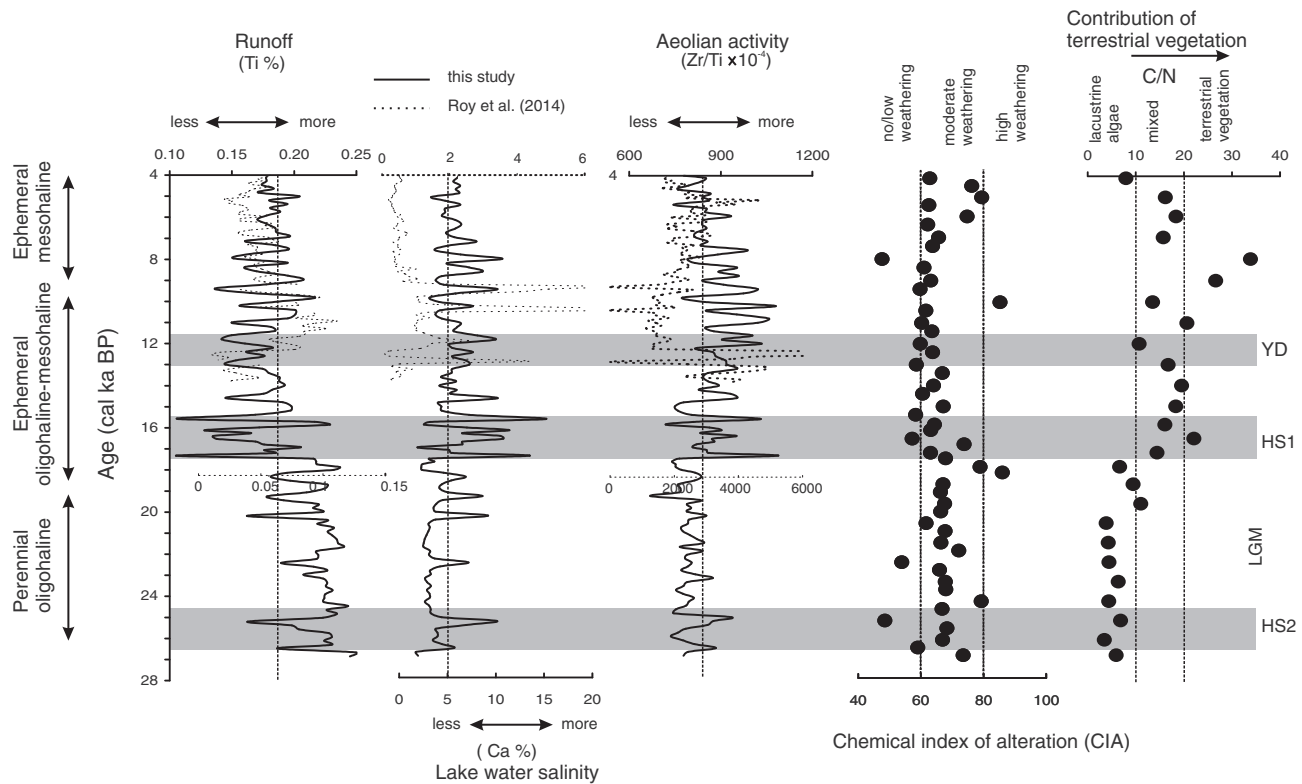


Figure 7. Proxy records indicating variations in runoff (Ti), lake water salinity (Ca) and aeolian activity (Zr/Ti) during ~27–4 ka. Sediment–water interaction in the watershed is estimated from CIA values and the source of sediment organic matter is inferred from C/N relation. The dotted lines show average values of Ti, Ca, and Zr/Ti. Heinrich 2 (HS2) and 1 (HS1), and Younger Dryas (YD) stadials are represented by dark gray bands.

conditions. Sediments with higher values of Zr/Ti are characterized by CIA of ≤ 60 . Zr-bearing clastic sediments along with minimally altered sediments were transported from the dry watershed by aeolian processes. Therefore, the ratio of Zr/Ti is used to infer aeolian activity. Contributions of terrestrial vegetation and lacustrine algae to the organic matter deposited in the basin are determined from C/N relation. Lacustrine algae are characterized by C/N < 10 , whereas terrestrial plants are characterized by C/N > 20 . Mixed contribution from lacustrine algae and terrestrial vegetation is reflected by C/N values between 10 and 20 (Talbot and Johannessen, 1992; Meyers and Ishiwatari, 1995).

The proxy data and interpretations are shown in Figure 7, but we do not provide paleohydrological reconstructions of the past 4 ka due to lack of chronological control in the upper part of the sediment column. The proxy records are compared with paleoecological data obtained from ostracod species assemblages from the same profile (Chávez-Lara et al., 2015). Concentrations of Ti, Ca and Zr/Ti ratio from another shallow core reported in Roy et al. (2014) are also shown along with our data (Fig. 7). Except for the Zr/Ti ratio, the variations of Ti and Ca are comparable between ~14 and 4 ka. Sediments with higher Ti in the shallow core (~12.3–9.3 ka; Roy et al., 2014) and pit (~11.5–9 ka; this paper) were deposited during contemporary intervals. Similarly, higher values of Ca in the shallow core sediments are present at ~13, 12, 10.5 and 9.5 ka (Roy et al., 2014) and above average Ca concentrations are observed in the pit sediments at ~13, 12, 10 and 9.5 ka. The slight offsets could be due to chronology of the interpolated parts of age models. Variation in Zr/Ti ratio is different in the previously published shallow core and the present study. Both records indicate higher values between ~14 and 12.3 ka. However, the above average Zr/Ti between ~12.3–7.5 ka is only registered in the pit sediments and not in the shallow core. The difference could be due to aeolian transported Zr-bearing clastic grains not reaching uniformly to all sites within the basin. The pit site possibly recorded more intervals of aeolian activity due to its location in the basin margin, whereas the shallow core

location received aeolian transported minerals only during some of the arid intervals.

Paleohydrological variation at Santiaguillo

Santiaguillo Basin received generally above average runoff between ~27 and 18 ka (Fig. 7). Aeolian activity around the basin was generally below average. Deposition of mostly moderate to highly altered sediments reflects more sediment–water interaction in the watershed during the late last glacial. C/N values of ≤ 10 indicate that the organic matter was dominantly sourced from lacustrine algae. Lower C/N along with above average Ti suggests that algal productivity increased during this interval of more runoff into the basin. Ostracod assemblage indicates presence of a diluted and perennial oligohaline water column at the modern dry pit site during the late last glacial and LGM (Chávez-Lara et al., 2015). However, the sediments deposited at ~26.5 ka and ~25 ka indicate brief events of average and below average runoff, enhanced aeolian transportation of Zr-bearing minerals, above average evaporative conditions and deposition of minimally altered sediments. Both the events of reduced runoff and above average aeolian activity occurred within the Heinrich Stadial 2 (26.5–24.3 ka; Sanchez Gofñ and Harrison, 2010). Other similar short lived intervals of more evaporative/drier conditions at ~22.5, 20, 19, and 18.5 ka characterize the late last glacial (Fig. 7).

Except for 3 brief events between ~11.5 and 9 ka, runoff into the basin was average and below average between ~18 and 4 ka. C/N values of > 10 indicate that the organic matter in the sediment was dominantly sourced from terrestrial vegetation during the deglaciation and Holocene. Terrestrial vegetation encroached into the modern littoral zone of the basin in this interval of reduced runoff. The ostracods suggest increased lake water salinity and presence of an ephemeral oligohaline to mesohaline water column at the pit site (Chávez-Lara et al., 2015). Changing hydrological conditions during this interval are reflected by

high amplitude variations in proxy records. Sediment–water interaction and its effect on weathering in the watershed were low–moderate between ~17 and 10.5 ka, and increased to moderate–high during ~10.5 to 9 ka and ~7 to 4 ka.

Two notable intervals of below average runoff occurred during ~17.5–16 ka and ~13–11.5 ka, and are coincident with Heinrich Stadial 1 (18–15.6 ka; [Sanchez Goñi and Harrison, 2010](#)) and the Younger Dryas Stadial (12.8–11.6 ka; [Pettet, 2009](#)). Both the intervals are represented by above average carbonate precipitation and aeolian activity. In summary, our data indicate a transition from wet late last glacial and LGM to a drier deglaciation and Holocene occurred at ~18 ka. Superimposed on this first order change in hydrologic conditions are the short-lived excursions in aridity and wetness.

Runoff into Santiaguillo Basin and seasonality of precipitation

To evaluate influences of different precipitation sources on the hydrological variations that occurred since the late last glacial, the new runoff record from the Santiaguillo Basin is compared with high-resolution records of monsoonal rainfall reconstructed from oxygen isotope composition of a speleothem from the Juxtlahuaca Cave ([Lachniet et al., 2013](#)) and winter precipitation reconstructed from sand contents in sediments from the Lake Elsinore ([Kirby et al., 2013](#)) ([Fig. 8](#)). Both these sites represent end members of the hydroclimatic regime. The speleothem reconstructs variations in amounts of monsoonal rainfall over the last 22 ka in the southwestern Mexico and the sand contents reconstruct variation in amounts of winter precipitation between 19 and 9 ka in the coastal southwestern US.

Runoff into Santiaguillo Basin and the $\delta^{18}\text{O}$ values from the speleothem have similar oscillations on millennial time scales. However, Ti concentrations of Santiaguillo Basin sediments and sand contents

of Lake Elsinore are inversely related. Enhanced monsoonal precipitation in the southwestern Mexico between 22–18 ka occurred within the interval of generally above average runoff into Santiaguillo between ~27 and 18 ka. Similarly, the regime of weaker monsoonal precipitation during 17.5 to 11 ka was contemporary to the interval of generally below average runoff into Santiaguillo at ~18–11.5 ka. Over a large part of this interval, ~19–12.9 ka, the coastal southwestern US recorded enhanced winter precipitation. We suggest that runoff into the Santiaguillo Basin was mainly controlled by the monsoonal precipitation and winter rainfall was not a significant contributor. The southern part of western subtropical North America received more monsoonal precipitation during the late last glacial and LGM (~27–18 ka). The amount of monsoonal rainfall decreased over the deglaciation into the Pleistocene–Holocene transition (~18–11.5 ka).

Regional hydrological variation

Paleoclimate records from 9 different sites from the northern and northwestern Mexico ([Blanchet et al., 2007](#); [Roy et al., 2010, 2012](#)), US–Mexico borderland ([Holmgren et al., 2007](#)) and coastal ([Kirby et al., 2006, 2013](#)) and continental interiors of southwestern US ([Anderson et al., 2002](#); [Asmerom et al., 2007, 2010](#); [Wagner et al., 2010](#)) are compared to evaluate the millennial-scale changes in hydroclimate during intervals of ~27–18 and 18–10 ka in [Figure 9](#).

Between ~27 and 18 ka, more monsoonal precipitation in the central-northern Mexico provided above average runoff into Santiaguillo Basin. The enhanced aeolian activity in Baja California Peninsula and reduced runoff into the lacustrine basins of Babicora and San Felipe suggest that northern and northwestern Mexico remained drier. Lack of macrofossils of summer flowering annuals and C_4 grasses in packrat middens from the Peloncillo and Hueco Mountains (i.e., US-

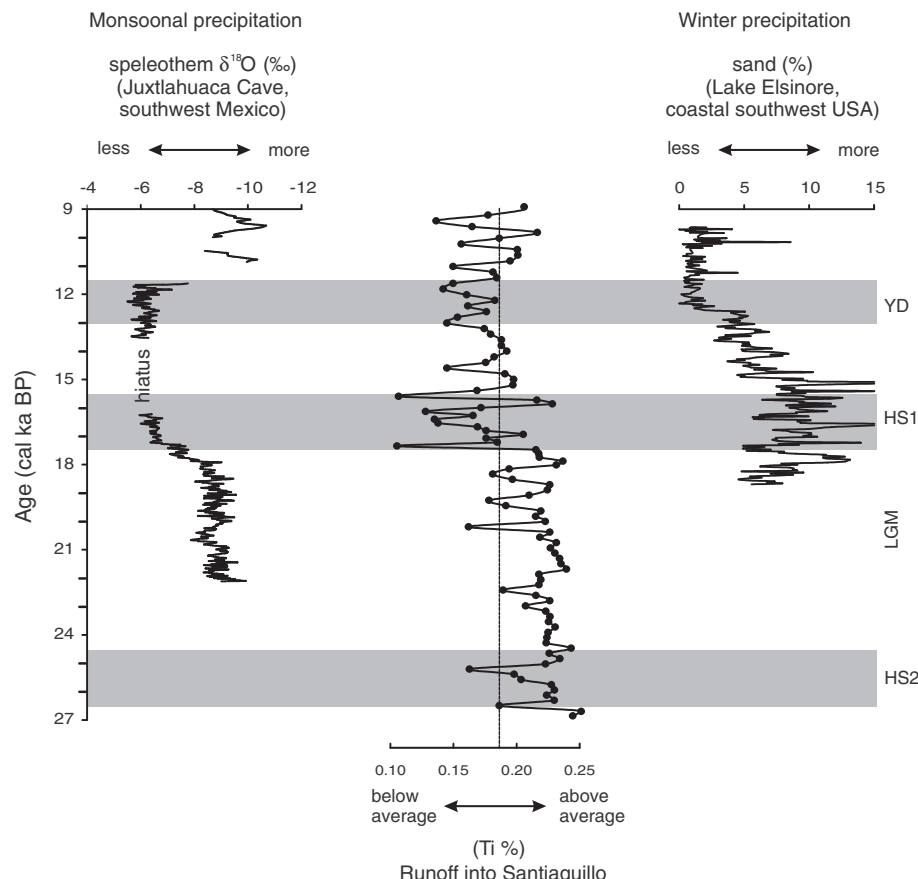


Figure 8. Comparison of runoff into Santiaguillo Basin with the proxy records of monsoonal precipitation estimated in a speleothem from Juxtlahuaca Cave ([Lachniet et al., 2013](#)) and winter precipitation estimated from sand contents in sediments of Lake Elsinore ([Kirby et al., 2013](#)). The dotted line indicates average Ti value of Santiaguillo Basin sediments.

Western subtropical North America

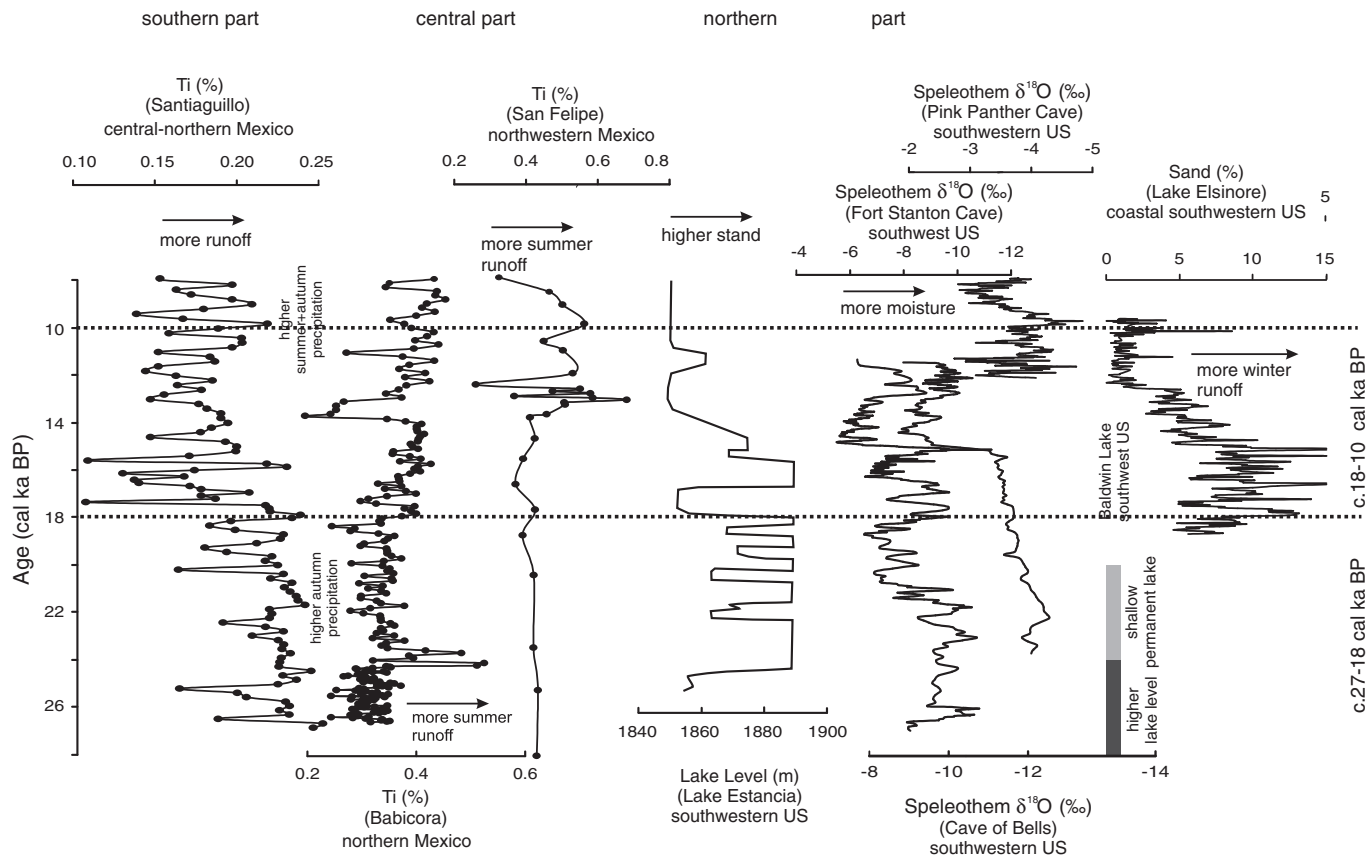


Figure 9. Regional hydrological variation estimated by comparison of proxy-records of runoff into the lacustrine basins of central-northern, northern and northwestern Mexico (Roy et al., 2010, 2012, this study), speleothem records of moisture variation in southwestern US (Asmerom et al., 2007, 2010; Wagner et al., 2010) and lake-level variations in coastal (Kirby et al., 2005, 2006, 2013) and continental interiors of southwestern US (Anderson et al., 2002) between ~27 and 10 ka. The grouping of registers in terms of southern, central and northern parts is based on location of the comparison sites.

Mexico borderland) suggests that little monsoonal precipitation fell at higher latitudes. However, the enhanced winter precipitation led to the development of permanent lakes in the coastal southwestern US (i.e. Baldwin Lake; Kirby et al., 2006). In a regime of monsoonal precipitation restricted to the central-northern Mexico, we relate the varying moisture contents in the continental interiors of southwestern US to different amounts of winter precipitation. More winter precipitation led to higher lake stands at Lake Estancia (Anderson et al., 2002) and more humidity in the Cave of Bells and Fort Stanton Cave (Asmerom et al., 2010; Wagner et al., 2010).

Between ~18 and 10 ka, the generally drier conditions of Santiagillo Basin indicate reduction in monsoonal precipitation in the central-northern Mexico. However, more summer precipitation in the northern Mexico provided increased runoff into Babicora after ~18 ka. Similarly, more summer precipitation was occurring in the Peloncillo and Hueco Mountains. This wetter climate over a broad region decreased the aeolian transported terrigenous material from the southern Baja California peninsula into the Pacific Ocean. Higher lake stand in Lake Estancia (~17–14 ka; Anderson et al., 2002) and more moisture in Fort Stanton Cave (18–15 ka; Asmerom et al., 2010) were contemporary to an interval of more winter precipitation in the coastal southwestern US as well as higher summer precipitation in northern Mexico. During the interval of lowest winter precipitation in coastal southwestern US at ~12.9–10 ka (Kirby et al., 2013), more moisture in Cave of Bells (13–11.5 ka; Wagner et al., 2010) and Pink Panther Cave (12.3–10 ka; Asmerom et al., 2007), higher stand of Lake Estancia (~12–11 ka; Anderson et al., 2002) and more runoff into San Felipe (~13–10 ka; Roy et al.,

2010) and Santiagillo (~11.5–9 ka) can only be explained by higher amounts of monsoonal/summer precipitation. We conclude that the monsoonal/summer precipitation gradually expanded to higher latitudes over the deglaciation and reached one of its greatest spatial extents during the Pleistocene–Holocene transition and early Holocene.

Forcing

Based on the Holocene records, Metcalfe et al. (2015) reported that both summer as well as autumn insolation influenced monsoonal precipitation of the NAM region. The modern summer precipitation is associated with NAM and the moisture flow is sourced from GoC and GoM (Adams and Comrie, 1997; Mitchell et al., 2002). Both the instrumental and proxy records indicate positive correlations between NAM and SST of both GoC and GoM (Mitchell et al., 2002; Barron et al., 2012; Metcalfe et al., 2015). Similarly, the northerly-located ITCZ in boreal summer strengthens the NAM (Amador et al., 2006). Figure 10 compares different forcings with proxy precipitation record for the Santiagillo Basin to help identify the possible moisture sources.

Except for Heinrich 1 and Younger Dryas stadials, the temporal variations in runoff show a first order negative correlation with mean position of ITCZ. Similarly, the influences of summer (June) insolation and North Hemisphere temperature on runoff were minimal. More runoff between ~27–18 ka was contemporary to a southerly positioned ITCZ, lower summer insolation and cooler temperature in the North Hemisphere. The amount of runoff decreased over the deglaciation as the

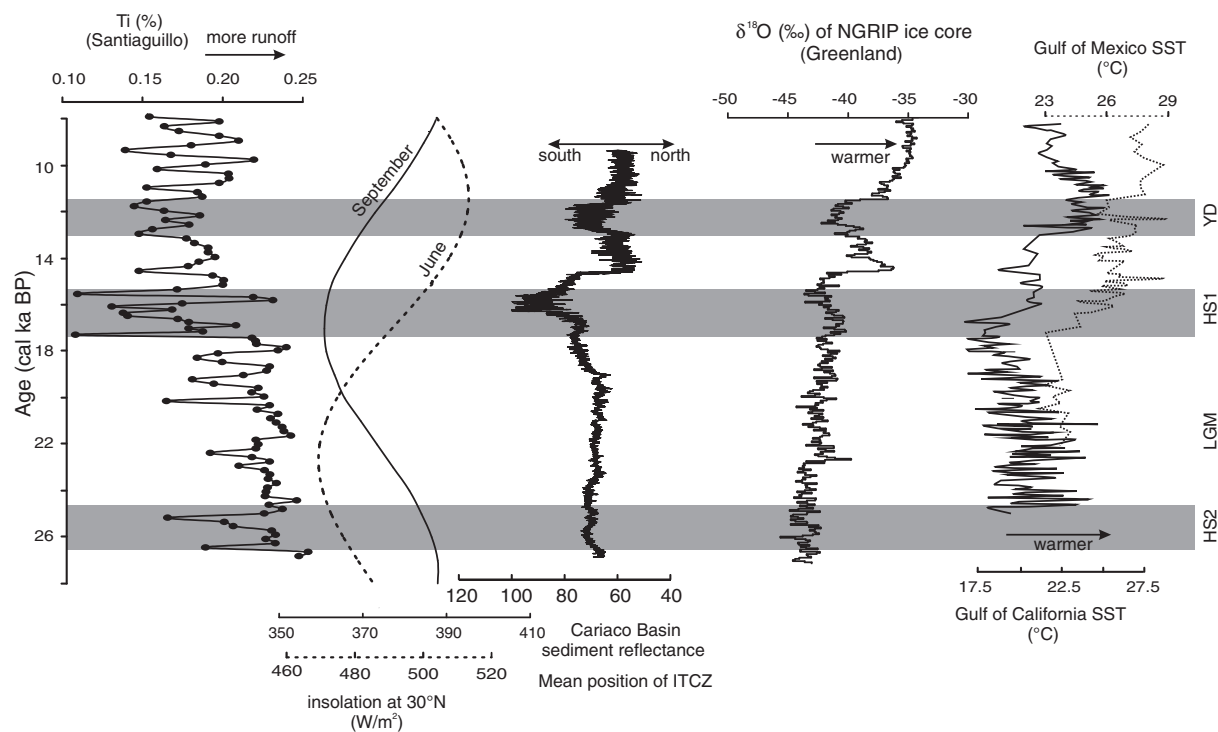


Figure 10. Evaluation of possible forcings on the variable monsoonal precipitation in the southern part of western subtropical North America by comparing the proxy record of runoff into the Santiagillo Basin with June and September insolations at 30°N latitude (Berger and Loutre, 1991), reconstructed North Hemisphere temperature (NGRIP project members, 2004), mean position of ITCZ (Deplazes et al., 2013) and SST records from Gulf of California (McClymont et al., 2012) and Gulf of Mexico (Flower et al., 2004).

ITCZ shifted northward, summer insolation increased and North Hemisphere became warmer. A proxy SST record from the Guaymas Basin indicates that GoC did not have the precondition for NAM onset (i.e. ~26°C; Mitchell et al., 2002) during the late last glacial and deglaciation. The contrasts between runoff and another proxy SST record from the Orca Basin suggest that minimal amount of moisture reaching the Santiagillo Basin was sourced from GoM. We propose that NAM was either absent or weaker during the late last glacial and deglaciation.

Tropical cyclones forming in the eastern North Pacific during the autumn provide an additional source of moisture for the region (Ritchie and Elsberry, 2007; Corbosiero et al., 2009; Ritchie et al., 2011). As the North Hemisphere summer progresses into the autumn, the interaction between mid-latitude upper-level troughs and northward moving tropical cyclones drop a large quantity of precipitation over Mexico and across the southwestern US (Jones et al., 2003). The runoff record for

the Santiagillo Basin shows a first order positive correlation with the autumn insolation (September). During the late last glacial and early Holocene, the Santiagillo Basin received above average runoff and autumn insolation was higher. Runoff decreased (below average) in an interval of lower autumn insolation during the deglaciation. A compilation of the meteorological data during AD 1992–2005 by Ritchie et al. (2011) indicates that the highest numbers of tropical cyclones remnants were formed in September and the tropical cyclones had different rainfall swaths. Tropical cyclones grouped as a south recurring track (e.g. Hurricane Kenna, AD 2002) and rain in Mexico only (e.g. Hurricane Ileana, AD 1994) had rainfall swaths restricted to the central-northern Mexico. However, the tropical cyclones with a north recurring track (e.g. Hurricane Hilary, AD 1993) had expanded rainfall swaths and brought moisture into the northern-northwestern Mexico as well as continental interiors of southwestern US.

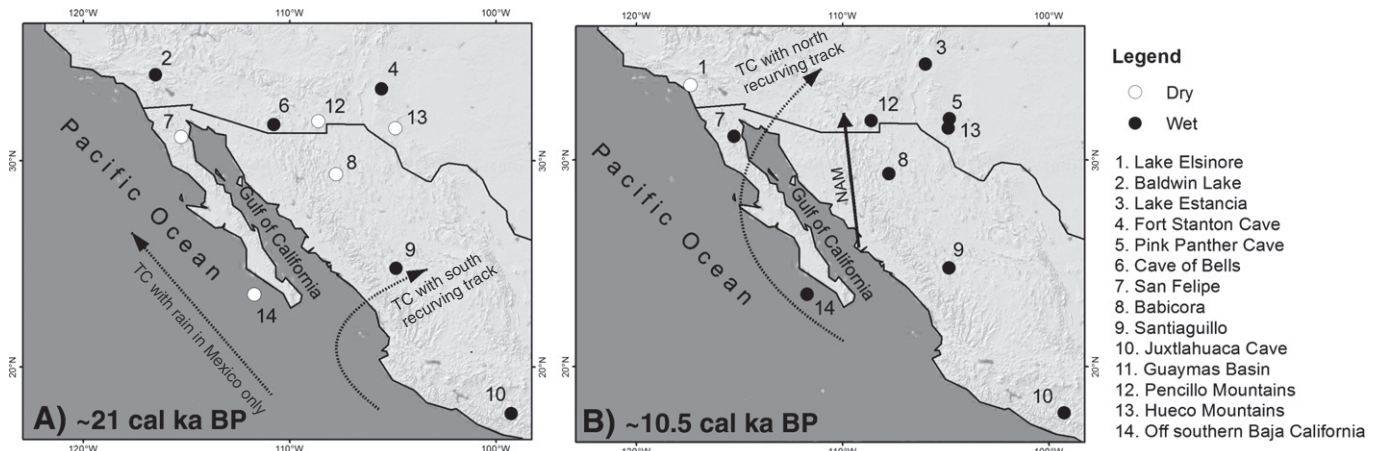


Figure 11. Map showing the regional hydroclimate at ~21 cal ka BP (A: LGM) and ~10.5 cal ka BP (B: early Holocene). Arrows indicate different modern tropical cyclone (TC) rainfall swath patterns transporting moisture from the eastern North Pacific (Ritchie et al., 2011) and North American Monsoon (NAM) transporting moisture from Gulf of California (Mitchell et al., 2002).

We chose to discuss the hydroclimate at ~21 ka (LGM) and ~10.5 ka (early Holocene) as both intervals had different moisture sources (Fig. 11). In the absence or occurrence of a weaker NAM, we relate the LGM wetter climate of the central-northern Mexico to frequent formation of tropical cyclones in the eastern North Pacific with restricted rainfall swaths. During the early Holocene, SST of GoC attended the precondition required for the NAM onset (Mitchell et al., 2002) and tropical cyclones increasingly penetration into the southwestern US (~11.5–9 ka; Antinao and McDonald, 2013). We assume that the occurrence of more rainfall in a broader region extending from the central-northern Mexico in the south up to the continental interiors of southwestern US in the north were caused by stronger NAM during the summer and tropical cyclones with expanded rainfall swaths during the autumn.

Conclusions

Geochemical characteristics of sediments in the Santiagillo Basin provided information about runoff, evaporation and lake salinity, provenance of organic productivity and clastic sediments in the basin, and aeolian activity in the central-northern Mexico over the past 27 ka. Comparison of the proxy runoff record with pure end member sites suggests that the hydrological variations were controlled by the millennial-scale dynamics of summer and autumn precipitations related to the NAM and tropical cyclones. More specifically:

- A transition from wet late last glacial and LGM to a drier deglaciation and Holocene occurred at ~18 ka. Superimposed on this first order change in hydrologic conditions are the short-lived excursions in aridity and wetness. Runoff decreased during Heinrich 1 and 2, and Younger Dryas stadials. The deposition of authigenic carbonate and aeolian transported sediment increased during these arid intervals.
- Difference between the Santiagillo runoff record and summer insolation (June), North Hemisphere temperature, mean position of ITCZ and SST records from the Gulf of California and Gulf of Mexico suggests that the NAM had minimal influence on the hydroclimate of late last glacial and deglaciation.
- Frequent formation of tropical cyclones in the eastern North Pacific with restricted rainfall swaths brought more autumn precipitation to the central-northern Mexico during the late last glacial. However, the absence or occurrence of a weaker NAM caused drier conditions in the northern-northwestern Mexico.
- During the early Holocene, an enhanced NAM and tropical cyclones with expanded rainfall swath patterns brought more summer and autumn moisture from the Gulf of California and eastern North Pacific to a broader region extending from the central-northern Mexico in the south up to the continental interiors of southwestern US in the north.

Acknowledgments

This research was supported by Papiit-UNAM IN100413 and Conacyt CB-237579. Technical assistance was provided by Patricia Girón García (IGL), Victor Lemus Neri (USAI), Fernando Nuñez and Marcela Charles Polo. Suggestions and comments of both the anonymous reviewers and Prof. Lewis Owen (editor) are thankfully acknowledged. Staffs of Heroico Cuerpo de Bomberos and Protección Civil of Durango provided assistance and security to the expedition members during field visits and sampling.

References

- Adams, D.K., Comrie, A.C., 1997. The North American monsoon. *Bulletin of the American Meteorological Society* 78, 2197–2213.
- Amador, J.A., Alfaro, E.J., Lizano, O.G., Magaña, V.O., 2006. Atmospheric forcing of the eastern tropical Pacific: a review. *Progress in Oceanography* 69, 101–142.
- Anderson, R.S., Power, M.J., Smith, S.J., Springer, K., Scott, E., 2002. Paleoecology of a middle Wisconsin deposit from Southern California. *Quaternary Research* 58, 310–317.
- Antinao, J.L., McDonald, E., 2013. An enhanced role for the Tropical Pacific on the humid Pleistocene–Holocene transition in southwestern North America. *Quaternary Science Reviews* 78, 319–341.
- Asmerom, Y., Polyak, V., Burns, S., Rasmussen, J., 2007. Solar forcing of Holocene climate: new insights from a speleothem record, southwestern United States. *Geology* 35, 1–4.
- Asmerom, Y., Polyak, V.J., Burns, S.J., 2010. Variable winter moisture in the southwestern United States linked to rapid glacial climate shifts. *Nature Geoscience* 3, 114–117.
- Barron, J.A., Metcalfe, S.E., Addison, J.A., 2012. Response of the North American Monsoon to regional changes in ocean surface temperature. *Paleoceanography* 27, 1–17, PA3206.
- Berger, A., Loutre, M.F., 1991. Insolation values for the climate of the last 10 million years. *Quaternary Science Reviews* 10, 297–317.
- Blanchet, C.L., Thouveny, N., Vidal, L., Leduc, G., Tachikawa, K., Bard, E., Beaufort, L., 2007. Terrigenous input response to glacial/interglacial climatic variations over southern Baja California: a rock magnetic approach. *Quaternary Science Reviews* 26, 3118–3133.
- Bromwich, D.H., Toracinta, E.R., Oglesby, R.J., Fastook, J.L., Hughes, T.J., 2005. LGM summer climate on the southern margin of the Laurentide ice sheet: wet or dry? *Journal of Climate* 18, 3317–3338.
- Bronk Ramsey, C., 2008. Deposition models for chronological records. *Quaternary Science Reviews* 27, 42–60.
- Bronk Ramsey, C., 2009. Bayesian analysis of radiocarbon dates. *Radiocarbon* 51, 337–360.
- Caldwell, P., 2010. California wintertime precipitation bias in regional and global climate models. *Journal of Applied Meteorology and Climatology* 49, 2147–2158.
- Cayan, D.R., Mauer, E.P., Dettinger, M.D., Tyree, M., Hayhoe, K., 2008. Climate change scenarios for the California region. *Climatic Change* 87, S21–S42.
- Chávez-Lara, C.M., PROY, P.D., Perez, L., Muthu Sankar, G., Lemus-Neri, V.H., 2015. Ostracode and C/N based paleoecological record from Santiagillo Basin of subtropical Mexico over last 27 cal kyr BP. *Revista Mexicana de Ciencias Geológicas* 32, 1–10.
- Cohen, A.S., 2003. *Paleolimnology: the History and Evolution of Lake Systems*. Oxford University Press, New York.
- COHMAP members, 1988. Climatic change of the past 18,000 years: observations and model simulations. *Science* 241, 1043–1052.
- Corbosiero, K.L., Dickinson, M.J., Bosart, L.F., 2009. The contribution of eastern North Pacific tropical cyclones to the rainfall climatology of the southwest United States. *Monthly Weather Review* 137, 2415–2435.
- Deplazes, G., Lückge, A., Peterson, L.C., Timmermann, A., Hamann, Y., Hughen, K.A., Röhl, U., Laj, C., Cane, M.A., Sigman, D.M., Haug, G.H., 2013. Links between tropical rainfall and North Atlantic climate during the last glacial period. *Nature Geoscience* 6, 213–217.
- Douglas, M.W., Maddox, R.A., Howard, K., Reyes, S., 1993. The Mexican Monsoon. *Journal of Climate* 6, 1665–1677.
- Enzel, Y., Wells, S.G., Lancaster, N., 2003. Late Pleistocene lakes along the Mojave river, southwest California. In: Enzel, Y., Wells, S.G., Lancaster, N. (Eds.), *Paleoenvironments and Paleohydrology of the Mojave and Southern Great Basin Deserts*. Geological Society of America Special Paper 368, pp. 61–77.
- Farfán, L.M., Fogel, I., 2007. Influence of tropical cyclones on humidity patterns over southern Baja California, Mexico. *Monthly Weather Review* 135, 1208–1224.
- Flower, B.P., Hastings, D.W., Hill, H.W., Quinn, T.M., 2004. Phasing of deglacial warming and Laurentide icesheet melt water in the Gulf of Mexico. *Geology* 32, 597–600.
- Friedman, I., Smith, G.I., Gleason, J.D., Warden, A., Harris, J.M., 1992. Stable isotope composition of waters in Southeastern California 1. Modern precipitation. *Journal of Geophysical Research* 97, 5795–5812.
- Higgins, R.W., Yao, Y., Wang, X.L., 1997. Influence of the North American Monsoon system on the U.S. summer precipitation regime. *Journal of Climate* 10, 2600–2622.
- Holmgren, C.A., Peñalba, M.C., Rylander, K.A., Betancourt, J.L., 2003. A 16,000 ^{14}C yr B.P. packrat midden series from the USA–Mexico borderlands. *Quaternary Research* 60, 319–329.
- Holmgren, C.A., Norris, J., Betancourt, J.L., 2007. Inferences about winter temperature and summer rains from the late Quaternary record of C_4 perennial grasses and C_3 desert shrubs in the northern Chihuahua Desert. *Journal of Quaternary Science* 22, 141–161.
- Jones, S., Harr, P.A., Abraham, J., Bosart, L.F., Bowyer, P.J., Evans, J.L., Hanley, D.E., Hanstrum, B.N., Hart, R.E., Lalaurette, F., Sinclair, M.R., Smith, R.K., Thorncroft, C., 2003. The extratropical transition of tropical cyclones: forecast challenges, current understanding, and future directions. *Weather and Forecasting* 18, 1052–1092.
- Kim, S.-J., Crowley, T.J., Erickson, D.J., Govindasamy, B., Duffy, P.B., Lee, B.Y., 2008. High-resolution climate simulation of the last glacial maximum. *Climate Dynamics* 31, 1–16.
- Kirby, M.E., Lund, S.P., Poulsen, C.J., 2005. Hydrologic variability and the onset of modern El Niño–Southern Oscillation: a 19250 year record from Lake Elsinore, southern California. *Journal of Quaternary Science* 20, 239–254.
- Kirby, M.E., Lund, S.P., Bird, B.W., 2006. Mid-Wisconsin sediment record from Baldwin Lake reveals hemispheric climate dynamics (Southern CA, USA). *Palaeogeography, Palaeoclimatology, Palaeoecology* 241, 267–283.
- Kirby, M.E., Feakins, S.J., Boniso, N., Fantozzi, J.M., Hinrichs, C.A., 2013. Latest Pleistocene to Holocene hydroclimates from Lake Elsinore, California. *Quaternary Science Reviews* 76, 1–15.
- Kutzbach, J.E., Wright, H.E., 1985. Simulation of the climate of 18,000 yr B.P.: results for North America/North Atlantic/European Sector. *Quaternary Science Reviews* 4, 147–187.
- Lachnit, M.S., Asmerom, Y., Bernal, J.P., Polyak, V.J., Vazquez-Selem, L., 2013. Orbital pacing and ocean circulation-induced collapses of the Mesoamerican monsoon over the past 22,000 y. *Proceedings of the National Academy of Sciences* 110, 9255–9260.

- Lachniet, M.S., Denniston, R.F., Asmerom, Y., Olyak, V.J., 2014. Orbital control of Western North America atmospheric circulation and climate over two glacial cycles. *Nature Communications* 5, 3805. <http://dx.doi.org/10.1038/ncomms4805>.
- Lyle, M., Heusser, L., Ravelo, C., Yamamoto, M., Barron, J., Daffenbaugh, N.S., Herbert, T., Andreassen, D., 2012. Out of the Tropics: the Pacific, Great Basin Lakes, and Late Pleistocene water cycle in the western United States. *Science* 337, 1629–1633.
- McClintock, E.L., Ganeshram, R.S., Pichevin, L.E., Talbot, H.M., van Dongen, B.E., Thunell, R.C., Haywood, A.M., Singarayer, J.S., Valdes, P.J., 2012. Sea-surface temperature records of Termination 1 in the Gulf of California: challenges for seasonal and interannual analogues of tropical Pacific climate change. *Paleoceanography* 27, 1–15, PA2202.
- Metcalf, S.E., Barron, J.A., Davies, S.J., 2015. The Holocene history of the North American Monsoon: ‘known knowns’ and ‘known unknowns’ in understanding its spatial and temporal complexity. *Quaternary Science Reviews* 120, 1–27.
- Meyers, P.A., Ishiwatari, R., 1995. Organic matter accumulation records in lake sediments. In: Lerman, A., Imboden, D., Gat, J. (Eds.), *Physics and Chemistry of Lakes*. Springer-Verlag, New York, pp. 279–328.
- Mitchell, D.L., Ivanova, D., Rabin, R., Brown, T.J., Redmond, K., 2002. Gulf of California sea surface temperatures and the North American Monsoon: mechanistic implications from observations. *Journal of Climate* 15, 2261–2281.
- Neelin, J.D., Langenbrunner, B., Meyerson, J.E., Hall, A., Berg, N., 2013. California winter precipitation change under global warming in the coupled model intercomparison project phase 5 ensemble. *Journal of Climate* 26, 6238–6257.
- Nesbitt, H.W., Young, G.M., 1984. Prediction of some weathering trends of plutonic and volcanic rocks based on thermodynamic and kinetic considerations. *Geochimica et Cosmochimica Acta* 48, 1523–1534.
- Nesbitt, H.W., Young, G.M., 1989. Formation and diagenesis of weathering profiles. *Journal of Geology* 97, 129–147.
- NGRIP project members, 2004. High-resolution record of Northern Hemisphere climate extending into the last interglacial period. *Nature* 431, 147–151.
- Nieto-Samaniego, A.F., Barajas-Gea, C.I., Gómez-González, J.M., Rojas, A., Alaniz-Álvarez, S.A., Xu, S., 2012. *Geología, evolución estructural (Eoceno al actual) y eventos sísmicos del Graben de Santiago, Durango, México*. Revista Mexicana de Ciencias Geológicas 29, 115–130 (In Spanish).
- Oster, J.L., Ibarra, D.E., Winnick, M.J., Maher, K., 2015. Steering of westerly storms over western North America at the Last Glacial Maximum. *Nature Geoscience* 8, 201–205.
- Pettet, D.M., 2009. Younger Dryas. In: Gorntz, V. (Ed.), *Encyclopedia of Paleoclimatology and Ancient Environments*. Springer, Dordrecht, pp. 993–995.
- Reimer, P.J., Bard, E., Bayliss, A., Beck, J.W., Blackwell, P.G., Ramsey, C.B., Grootes, P.M., Guilderson, T.P., Hajdas, I., Hatté, C., Heaton, T.J., Hoffmann, D.L., Hogg, A.G., Hughen, K.A., Kaiser, K.F., Kromer, B., Manning, S.W., Niu, M., Reimer, R.W., Richards, D.A., Scott, E.M., Southon, J.R., Staff, R.A., Turney, C.S.M., van der Plicht, J., 2013. IntCal13 and MARINE13 radiocarbon age calibration curves 0–50000 years cal BP. *Radiocarbon* 55, 1869–1887.
- Ritchie, E.A., Elsberry, R.L., 2007. Simulations of the extratropical transition of tropical cyclones: phasing between the upper-level trough and tropical cyclone. *Monthly Weather Review* 135, 862–876.
- Ritchie, E.A., Wood, K.M., Gutzler, D.S., White, S.R., 2011. The influence of eastern Pacific tropical cyclone remnants on the Southwestern United States. *Monthly Weather Review* 139, 192–210.
- Roy, P.D., Caballero, M., Lozano, R., Ortega, B., Lozano, S., Pi, T., Israde, I., Morton, O., 2010. Geochemical record of Late quaternary paleoclimate from lacustrine sediments of paleo-lake San Felipe, western Sonora Desert, Mexico. *Journal of South American Earth Sciences* 29, 586–596.
- Roy, P.D., Jonathan, M.P., Pérez-Cruz, L.L., Sánchez-Córdova, M.M., Quiroz-Jiménez, J.D., Romero, F.M., 2012. A millennial-scale Late Pleistocene–Holocene palaeoclimatic record from the western Chihuahua Desert, Mexico. *Boreas* 41, 707–717.
- Roy, P.D., Quiroz-Jiménez, J.D., Pérez-Cruz, L.L., Lozano-García, S., Metcalfe, S.E., Lozano-Santacruz, R., López-Balbiaux, N., Sánchez-Zavala, J.L., Romero, F.M., 2013. Late Quaternary palaeohydrological conditions in the drylands of northern Mexico: a summer precipitation proxy record of the last 80 ka. *Quaternary Science Reviews* 78, 342–354.
- Roy, P.D., Quiroz-Jiménez, J.D., Chávez-Lara, C.M., Sánchez-Zavala, J.L., Pérez-Cruz, L.L., Muthu Sankar, G., 2014. Humid Pleistocene–Holocene transition and early Holocene at sub-tropical Northern Mexico and possible Gulf of California forcing. *Boreas* 43, 577–587.
- Sanchez Goñi, M.F., Harrison, S.P., 2010. Millennial-scale climate variability and vegetation changes during the Last Glacial: Concepts and terminology. *Quaternary Science Reviews* 29, 2823–2827.
- Sheppard, P.R., Comrie, A.C., Packin, G.D., Angersbach, K., Hughes, M.K., 2002. The climate of the US Southwest. *Climate Research* 21, 219–238.
- Stensrud, D.J., Gall, R.L., Mullen, S.L., Howard, K.W., 1995. Model climatology of the Mexican Monsoon. *Journal of Climate* 8, 1775–1794.
- Talbot, M.R., Johannessen, T., 1992. A high-resolution palaeoclimatic record for the last 27,500 years in tropical West Africa from carbon and nitrogen isotope composition of lacustrine organic matter. *Earth and Planetary Science Letters* 110, 23–37.
- Thompson, R.S., Anderson, K.H., 2000. Biomes of western North America at 18,000, 6,000 and 0 ^{14}C yr BP reconstructed from pollen and packrat midden data. *Journal of Biogeography* 27, 555–584.
- Toracinta, E.R., Oglesby, R.J., Bromwich, D.H., 2004. Atmospheric response to modified CLIMAP ocean boundary conditions during the Last Glacial Maximum. *Journal of Climate* 17, 504–522.
- Wagner, J.D.M., Cole, J.E., Beck, J.W., Patchett, P.J., Henderson, G.M., Barnett, H.R., 2010. Moisture variability in the southwestern United States linked to abrupt glacial climate change. *Nature Geoscience* 3, 110–113.
- Xu, J., Gao, X., Shuttleworth, J., Sorooshian, S., Small, E., 2004. Model climatology of the North American Monsoon onset period during 1980–2001. *Journal of Climate* 17, 3892–3906.

CAPÍTULO VI



Orbital-scale droughts in the central-northern Mexico during the late Quaternary and comparison with other subtropical and tropical records

Orbital-scale droughts in central-northern Mexico during the late Quaternary and comparison with other subtropical and tropical records

JESÚS DAVID QUIROZ-JIMÉNEZ¹*, PRIYADARSI D. ROY², LAURA E. BERAMENDI-OROSCO²,
SOCORRO LOZANO-GARCÍA² and LORENZO VÁZQUEZ-SELEM³

¹Posgrado en Ciencias de la Tierra, Universidad Nacional Autónoma de México, Ciudad de México, Mexico

²Instituto de Geología, Universidad Nacional Autónoma de México, Ciudad Universitaria, Ciudad de México, Mexico

³Instituto de Geografía, Universidad Nacional Autónoma de México, Ciudad Universitaria, Ciudad de México, Mexico

Palaeoclimate research in subtropical arid Mexico is mainly focused to infer dynamics and geographic distributions of different precipitation regimes, but droughts have received less attention. We present a new sedimentary core record indicating orbital-scale dynamics of droughts that occurred in central-northern Mexico during the late Quaternary. This record is reconstructed from abundances of authigenic carbonate and windblown clastic sediments in a 1026-cm-long sediment core from the Santiaguillo ephemeral lake. The Marine Isotope Stage (MIS) 2 lacked drought, and at least two different droughts were centred at c. 13.5 ka and at c. 7 ka during the MIS 1. The drought of c. 13.5 ka in the Santiaguillo ephemeral lake was contemporary to an interval of droughts in the Basin of Mexico (central Mexico) and stronger aeolian activity in the Baja California peninsula (northwestern Mexico). This synchronous arid condition, observed in the subtropical as well as tropical Mexico, occurred during an interval of higher spring insolation, relatively warmer but fluctuating global temperature, and stronger El Niño-Southern Oscillation. Unsuccessful radiocarbon dating for the lower part of the sediment core led to an assignment of uncertain chronology to droughts that occurred possibly between MIS 5 and MIS 3. Copyright © 2017 John Wiley & Sons, Ltd.

Received 13 January 2016; accepted 4 October 2016

KEY WORDS drought; geochemistry; palaeoclimate; orbital scale; late Quaternary; Santiaguillo; subtropical Mexico

1. INTRODUCTION

The Cooperative Holocene Mapping Project (COHMAP, 1988) presented the first major hypothesis and explained the principal mechanism behind climate variations that occurred during the late Quaternary in subtropical North America. Higher lake levels and expansive woodlands in the southwestern US during the Last Glacial Maximum (LGM) were related to more winter storms associated with a stronger southern branch of the westerly jet streams due to the presence of a larger ice sheet in North America. Over the deglaciation and Holocene, the winter moisture into the region decreased as the ice sheet gradually reduced in size and the strength of the jet stream decreased. This hypothesis did not include palaeoclimate data from northern Mexico, as only a couple of published proxy records were available at that time (i.e. Cuatro Cienegas; Meyer, 1973; and Bolson de Mapimi; Van Devender and Burgess, 1985). Both of

these records were discontinuous and lacked a robust chronological control. However, palaeoclimate research of the subtropical Mexico witnessed increasing interest following the COHMAP hypothesis. A literature compilation of the last three decades indicate at least 40 published papers with proxy records from more than 27 different sites across the region. Most of these records are focused on the Holocene deposits (Anderson and Van Devender, 1995; Davis, 2003; Caballero *et al.*, 2005; Castiglia and Fawcett, 2006; Ortega-Rosas *et al.*, 2008; Roy *et al.*, 2013a), and longer records providing information about the last glacial hydrological variations are relatively few in number (Murillo De Nava *et al.*, 1999; Ortega-Guerrero *et al.*, 1999; Lozano-García *et al.*, 2002; Metcalfe *et al.*, 2002; Roy *et al.*, 2010, 2013b, 2014; Holmgren *et al.*, 2011).

More continuous records, improved chronology of the sedimentary sequences, and regional comparisons between reconstructed hydroclimates of north-northwestern Mexico and south-western US have provided an opportunity to test the earlier hypothesis and propose a new hypothesis in order to explain the mechanisms of climate change in the region (Lyle *et al.*, 2012; Kirby *et al.*, 2013; Roy *et al.*, 2013b,

*Correspondence to: J. D. Quiroz-Jiménez, Posgrado en Ciencias de la Tierra, Universidad Nacional Autónoma de México, 04510, Ciudad de México, México. E-mail: quiroz_271085@hotmail.com

2014; Metcalfe *et al.*, 2015; Oster *et al.*, 2015). Recent reviews of Barron *et al.* (2012), Antinao and McDonald (2013), Metcalfe *et al.* (2015), and Roy *et al.* (2015) have attempted to understand the dynamics of moisture sourced from the Pacific Ocean and evaluated different forcings controlling the geographic distributions of the winter storms and summer precipitation related to the North American Monsoon (NAM) and tropical cyclone. In a sedimentary record reaching up to the Marine Isotope Stage (MIS) 4, Roy *et al.* (2013b) proposed that the winter storms had minimal influence in the regions located south of 29°N latitude during the last glacial period and the hydroclimate of northern Mexico was mainly influenced by the dynamics of the summer precipitation. During the LGM, precipitation was restricted to central-northern Mexico, and a broader region in north-northwestern Mexico remained dry (Roy *et al.*, 2015). Northward expansion of the summer moisture during the deglaciation brought more humidity up to the Great Basin (Lyle *et al.*, 2012). However, the observations of Kirby *et al.* (2013) and Lachniet *et al.* (2014), indicating an absence of summer rainfall in coastal southern California as well as central parts of the Great Basin, improved our understanding of geographic coverage of the summer precipitation during this interval. Antinao and McDonald (2013) related the humid conditions during the Pleistocene–Holocene transition in the southwestern US to enhanced winter storms as well as increased penetration of tropical cyclones. A contemporary interval in the central-northern Mexico received more precipitation as a result of stronger NAM with moisture sourced from the Gulf of California (Roy *et al.*, 2014). However, the source of dominant moisture flow was changed from the Gulf of California to the subtropical Pacific Ocean during the early Holocene (Barron *et al.*, 2012). Over the late Holocene, other forcings such as the Pacific Decadal Oscillation (PDO), El Niño Southern Oscillation (ENSO) and Atlantic Multidecadal Oscillation (AMO) caused significant changes to precipitation regimes (Metcalfe *et al.*, 2015).

Compared with multiple investigations to understand the variable precipitation regimes, fewer studies have attempted to decipher drought dynamics in the region (i.e. Murillo de Nava *et al.*, 1999; Blanchet *et al.*, 2007). In this paper, we present a new drought record and provide information about orbital-scale dynamics of droughts that occurred in central-northern Mexico during the late Quaternary from abundances of authigenic carbonate and windblown clastic sediments deposited in the Santiaguillo ephemeral lake. We evaluated influences of insolation, inter-tropical convergence zone (ITCZ), ENSO, and North Hemisphere temperature on the drought dynamics. Comparisons of the new data with a drought record from central Mexico (Basin of Mexico; Torres-Rodríguez *et al.*, 2015) and proxy records of aridity from northern (palaeolake Babicora; Roy *et al.*, 2013b) and northwestern Mexico (southern Baja California

peninsula; Blanchet *et al.*, 2007) estimated the geographic distributions of arid intervals across the subtropical as well as tropical Mexico.

2. REGIONAL SETTINGS

2.1. Study site

The Santiaguillo ephemeral lake (24° 44' N, 104° 48' W, 1960 m asl) is located at the southern part of a tectonic basin (Nieto-Samaniego *et al.*, 2012) in the subtropical central-northern Mexico (Fig. 1). It is situated ~75 km north of Durango City and in the eastern foothills of the western Sierra Madre. It is surrounded by ~2500–3000-m-high mountains and fed by several intermittent streams. The tectonic basin is ~45 km long and is divided into two different parts by a man-made dam. The smaller part at the northern sector has a reservoir for irrigation purposes (i.e. artificial), and the larger southern natural part is natural. The ephemeral southern part is less than a metre depth in the summer and autumn months and remains dry for the rest of the year.

2.2. Climate

This basin is located in the southern NAM region as defined by Metcalfe *et al.* (2015), and it has a temperate semi-arid climate (BS1kw) (García, 1973). Three different weather stations (i.e. Guatimapé: AD 1978–2006, El Pino: AD 1964–2006 and Canatlán: AD 1964–2006) located at distances between 1 and 13 km from the basin provide the instrumental meteorological data (Fig. 2) (source: Servicio Meteorológico Nacional, México). Average annual precipitation varied between 430 and 554 mm, and almost 90% of the total precipitation reached through NAM and tropical cyclones during summer and autumn months (June–October) (Fig. 1). Spring is the driest season of the year with <4% of total annual rainfall occurring from March to May. The average annual temperature fluctuated between 16 and 18°C; it reached ~38°C in the month of June and fell below zero from December to January.

Both the instrumental data and the tree-ring records representing the last 600 years relate the interannual precipitation variability with sea surface temperature (SST) of the tropical Pacific and Atlantic Oceans modulated ENSO, PDO and AMO (Cleveland *et al.*, 2003; Magaña *et al.*, 2003; González-Elizondo *et al.*, 2005; Sutton and Hodson, 2005; Versteegh, 2005; Cerano-Paredes *et al.*, 2010; Villanueva-Díaz *et al.*, 2014). Positive (warmer) phases of ENSO and PDO and cooler phases of AMO in general reduce the amount of total annual precipitation (drought) in the region. The amounts of summer precipitation also decreased during intervals of warmer conditions in the

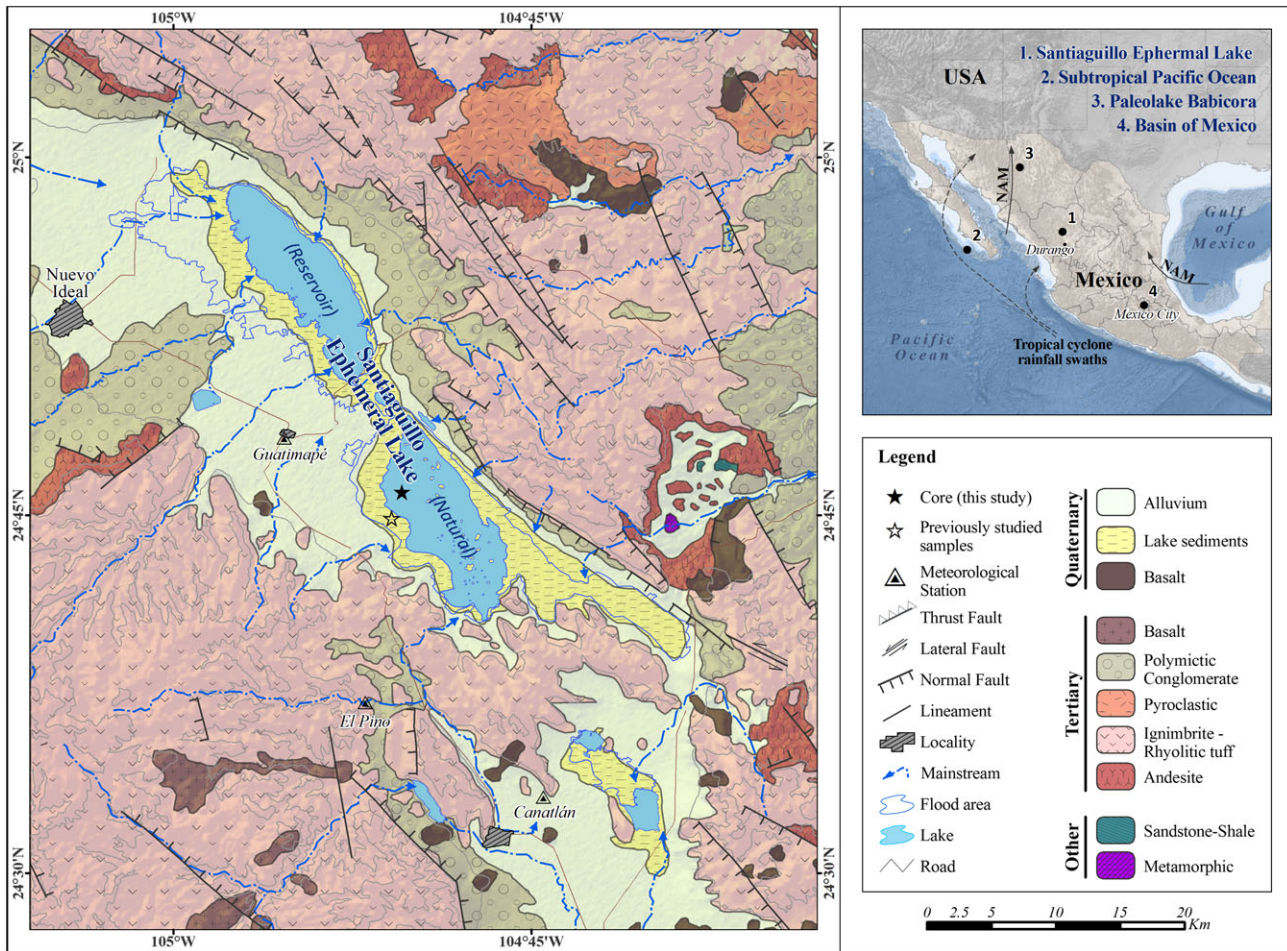


Figure 1. Map showing location and geology of the Santiaguillo ephemeral lake in the subtropical central-northern Mexico. Chemical composition and mineralogical abundance of a 1026-cm-long sediment core from the basin provides information about orbital-scale drought dynamics during the late Quaternary. Locations of other records of aridity from different sites across the northern, northwestern and central Mexico are shown in filled circles.

eastern tropical Pacific Ocean and location of ITCZ closer to the equator (Castro *et al.*, 2001; Magaña *et al.*, 2003).

2.3. Geology

The catchment rocks exposed in the mountains located in the vicinity of the basin are predominantly ignimbrites and rhyolites (Nieto-Samaniego *et al.*, 2012) (Fig. 1). Andesites are exposed both in the eastern and western catchment, whereas basalts are exposed in the southern part of the basin. Smaller outcrops of metamorphic rocks and Jurassic sandstone-siltstone are present to the east of the basin (Servicio Geológico Mexicano, 1998). Other sedimentary deposits include conglomerates and alluvium.

3. SAMPLING AND ANALYSIS

A 1026-cm-long sediment core was collected from the Santiaguillo ephemeral lake (Fig. 1). It was split in the

laboratory and photographed. Sediment texture was defined after macroscopic inspection and microscopic observation of smear slides using the protocol of Schnurrenberger *et al.* (2003) in order to understand the sediment grain size distributions and, hence, depositional energy in the basin. The core was sampled at 2-cm intervals, and all the samples were oven dried at 40°C, homogenized and grounded with an agate pestle. Clastic and non-clastic minerals were identified in 22 samples collected at different depths along the core using a Shimadzu-6000 X-ray diffractometer (XRD) in order to identify the intervals of higher erosion in the watershed and higher lake water salinity. Organic carbon and inorganic carbon contents were measured in 102 samples (at every ~10-cm interval) in a Thermo Scientific HiperTOC solid analyser. Both of them provide proxy information to identify the intervals of different productivity and quantify the abundance of authigenic carbonates. Concentrations of Ti, Fe, K, Ca and Sr were measured in the same samples using a non-destructive Thermo Scientific Niton XL3t X-ray fluorescence (XRF)

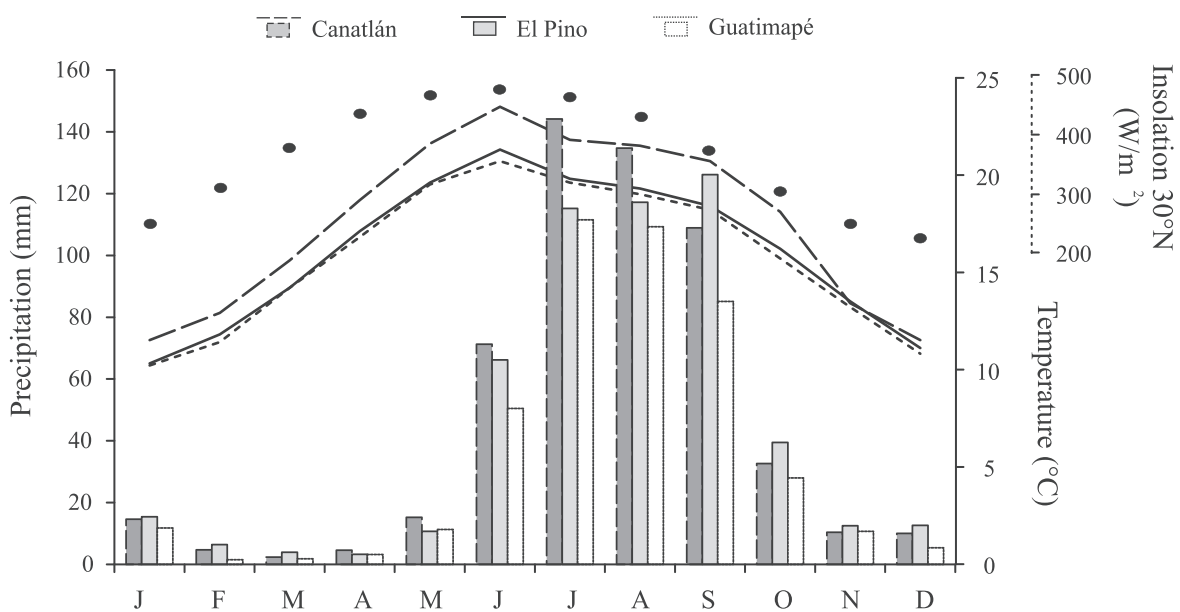


Figure 2. Modern meteorological data (precipitation: bars and temperature: lines) is provided by three different stations (i.e. Guatimapé: AD 1978–2006, El Pino: AD 1964–2006 and Canatlán: AD 1964–2006) located at distances of 1–13 km from the basin. Temperature follows the monthly insolation values of last 1 ka (Berger and Loutre, 1991).

analyser for the chemical characterization of primary clastic minerals and authigenic evaporites deposited in the basin. All these elements were also measured in a traditional and destructive Siemens SRS 3000 XRF in 38 samples collected all along the core. Data obtained in both XRF analysers show the coefficient of correlations of 0.8 for K and Sr and 0.9 for Ti, Fe and Ca. Compared with traditional XRF, Niton XL3t XRF overestimated the concentrations of Ti and Ca and underestimated the concentrations of Fe, K and Sr. Obtained data were corrected using the linear regression equations (e.g. Roy *et al.*, 2012). Additionally, concentration of Al was measured in 38 samples along the core using the traditional XRF in order to estimate the degree of chemical alteration (CIA) of the clastic sediments by using the concentrations of oxides in siliciclastic fractions of sediments and the formula of Nesbitt and Young (1984, 1989): $CIA = [Al_2O_3/(Al_2O_3 + CaO + Na_2O + K_2O)] \times 100$. For chronological control of the sediment core, bulk organic carbon present in 13 different samples at depths of 25, 49, 78, 89, 110, 136, 174, 266, 291, 319, 355, 385, and 410 cm was analysed for ^{14}C AMS. Statistical analysis (correlation matrix and cluster) was performed using the STATISTICA software to identify the associations of different chemical parameters.

4. RESULTS

4.1. Core sediment and mineralogy

The core sediments comprise silty sand, sandy silt, silt, silty clay, and sand textures (Fig. 3). The basal part of the sequence

(1026–646 cm) has massive calcareous sandy silt. Silty sand is present at depths of 961–945 cm and 890–862 cm, and silty clay is present at depths of 704–686 cm. Intercalations of calcareous and non-calcareous silty sand and sandy silt are present in the intermediate part (646–266 cm). Two dominantly fine to medium sand layers are observed at depths of 469–420 cm and 297–266 cm. Both these sand layers also contain gravel-size rock fragments. The upper most part of the core (266–0 cm) contains intercalations of massive sandy silt and silt. A silty-clay layer is present at depths of 34–20 cm. More root remnants are observed at depths of 34–0 cm. Sediments have different abundances of clastic minerals as well as non-clastic calcite (Table 1). The clastic minerals are composed of quartz, K-feldspars, cristobalite, zircon, montmorillonite and illite. Quartz and calcite are the most abundant minerals, and all others are present in trace amounts.

4.2. Organic carbon (OC) and inorganic carbon (IC)

Sediments have 0.1–2.6% of OC and 0.3–5.5% of IC (Fig. 3). There is no clear relationship between sediment texture and OC. OC > 1% is observed in sediments at depths of 976 cm (1.3%), 936 cm (1.3%), 846 cm (1.6%), 679 cm (1.3%), 374 cm (1.9%), 344 cm (1.6%), 126 cm (2%) and 20 cm (2.6%). The rest of the sediment column has ≤ 1% of OC.

As calcite is the only carbonate mineral present, we expressed IC as $CaCO_3$. Abundance of $CaCO_3$ varies between 2.1% and 45.5% (Fig. 3). Sediments with higher values are present at depths of 1016 cm (20.1%), 886 cm (18.3%), 846 cm (30.4%), 726 cm (45.5%), 544 cm (36.2%), 394 cm

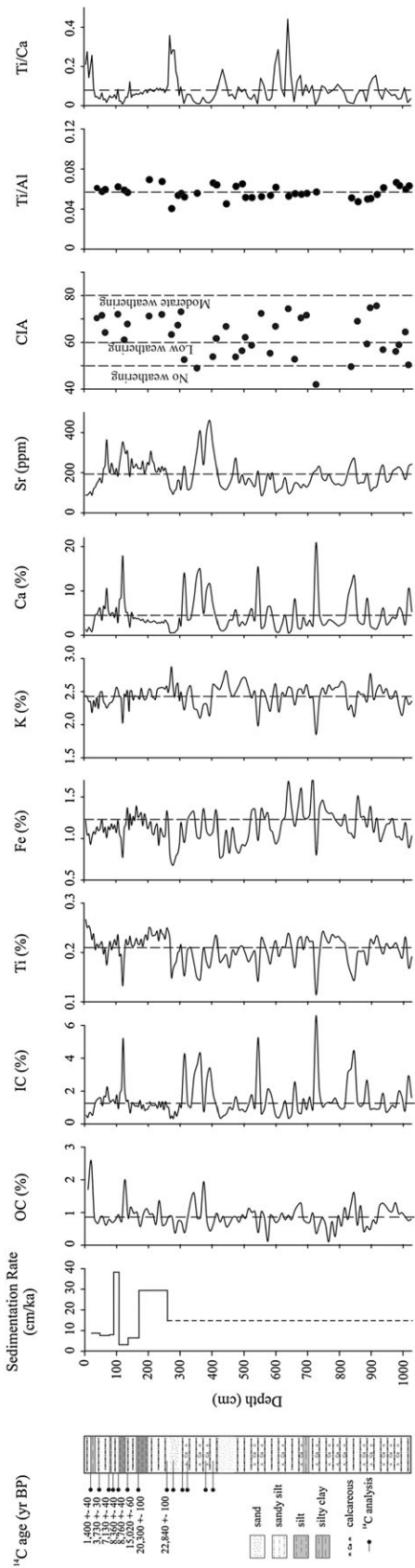


Figure 3. Stratigraphy of the core along with AMS ^{14}C dates and sedimentation rates at different depths. Abundances of organic carbon (OC) and inorganic carbon (IC), concentrations of Ti, Fe, K, Ca and Sr, and ratios of Ti/Al and Ti/Ca are presented along the core. The dotted lines show average values of each element and element ratios. Degree of chemical weathering of clastic minerals is estimated by CIA.

Table 1. Clastic and authigenic minerals present in sediments of the Santiaguillo ephemeral lake

	Abundance
Clastic mineral	Quartz
	Feldspar
	(orthoclase, anorthoclase)
	Cristobalite
	Zircon
	Montmorillonite
	Illite
Authigenic mineral	Calcite

(23.4%), 364 cm (29.4%), 314 cm (29.5%), 121 cm (43.4%) and 71 cm (19%). In general, CaCO_3 of $\leq 10\%$ is observed in sediments representing the rest of the core.

4.3. Multi-element concentration and statistical analysis

Sediments have 0.1–0.3% of Ti, 0.7–1.7% of Fe, 1.8–2.9% of K, 0.5–21% of Ca and 88–460 ppm of Sr (Fig. 3). The ratio of Ti/Al is homogeneous (0.04–0.07), and chemical index of alteration (CIA) varies between 42 and 77 all along the core (Fig. 3). CIA values (e.g. Nesbitt and Young, 1984, 1989) suggest that clastic sediments have undergone varying degrees of chemical weathering during the transportation from the watershed to the basin. Sediments with $\text{CIA} < 60$ had minimal chemical weathering (no/less sediment–water interaction) and preserved the primary silicate minerals (i.e. feldspar). Sediments with $\text{CIA} > 60$ had undergone up to moderate chemical weathering (more sediment–water interaction) and hosted both primary silicates (i.e. feldspar) and secondary clay minerals (i.e. montmorillonite and illite).

In general, the distribution of Ti is comparable with the distributions of Fe and K, and the distribution of Ca is comparable with that of Sr. Table 2 presents the correlation coefficient matrix of all the geochemical parameters. The first group of elements is sourced from different primary minerals present in the clastic sediments. Fe and K are mobile, whereas Ti is an insoluble element and is insensitive to environmental redox variation (e.g. Mason and Moore, 1982; Yarincik *et al.*, 2000). The relatively lower coefficients of correlations ($r=0.5$, $p < 0.05$) of Fe and K with Ti suggest that a part of Fe and K was released from the Fe and K-bearing primary minerals in conditions of increasing sediment–water interaction in the watershed (e.g. Mason and Moore, 1982; Cohen, 2003). Partial mobility of both these elements is also suggested by the higher correlation of Ti with CIA ($r=0.8$, $p < 0.05$) and lower correlations of Fe and K with CIA ($r=0.6$, $p < 0.05$). Subsequently, the soluble Fe and K might have reprecipitated as authigenic minerals or adsorbed onto the

Table 2. Correlation coefficient matrix (r) with $p < 0.05$ of the geochemical variables of sediments deposited in the Santiaguillo ephemeral lake

	IC	OC	Ca	Sr	Ti	K	Fe	Ti/Ca	Fe/Ca	K/Ca	Sr/Ca	CIA
IC	1.0											
OC	-0.2	1.0										
Ca	1.0	-0.1	1.0									
Sr	0.6	0.0	0.6	1.0								
Ti	-0.7	0.2	-0.7	-0.3	1.0							
K	-0.7	0.0	-0.7	-0.4	0.5	1.0						
Fe	-0.2	0.1	-0.2	-0.1	0.5	0.1	1.0					
Ti/Ca	-0.6	0.1	-0.6	-0.6	0.3	0.4	-0.1	1.0				
Fe/Ca	-0.6	0.1	-0.6	-0.6	0.3	0.4	0.2	0.9	1.0			
K/Ca	-0.6	0.0	-0.6	-0.6	0.2	0.4	-0.2	1.0	0.9	1.0		
Sr/Ca	-0.6	0.0	-0.6	-0.4	0.3	0.4	-0.2	0.9	0.8	0.9	1.0	
CIA	-0.7	-0.1	-0.8	-0.5	0.8	0.6	0.6	0.6	0.5	0.5	0.5	1.0

secondary clay minerals. However, mineralogical composition of the sediments and negative correlations of Fe ($r=-0.2$, $p < 0.05$) and K ($r=-0.8$, $p < 0.05$) with IC suggest the absence of Fe and K in carbonates and their possible adsorption onto the clay minerals such as montmorillonite and illite. An absence of any correlation between both ($r=0.1$, $p < 0.05$) indicates that different processes led to the release of Fe and K from the primary clastic minerals. Compared with the partly mobile Fe and K, Ti represents the abundance of primary minerals present in clastic sediments.

The second group of elements comprising Ca and Sr is positively correlated with IC ($r=1.0$ and 0.6 , $p < 0.05$, respectively) and represent the calcite abundance. A negative correlation between IC and CIA ($r=-0.7$, $p < 0.05$)

indicates that the clastic sediments deposited along with calcite were either unaltered or experienced lower degree of sediment–water interaction during transportation from the watershed to the basin. Relatively lower positive correlation of Sr with IC ($r=0.6$, $p < 0.05$) is due to the association of a part of Sr in non-carbonate minerals (e.g. feldspar). Negative correlations of Ca with Ti ($r=-0.7$, $p < 0.05$), Fe ($r=-0.2$, $p < 0.05$) and K ($r=-0.7$, $p < 0.05$) indicate that calcite has a diluting effect on the clastic mineral abundance. Element ratios (i.e. proxies) are insensitive to the noise factor associated with dilution effects (e.g. Weltje and Tjallingii, 2008). Hence, we used ratios of Ti/Ca, Fe/Ca, K/Ca and Sr/Ca in order to characterize the chemical compositions of clastic minerals. The cluster analysis groups Ti/Ca, Fe/Ca, K/Ca and Sr/Ca along with CIA (cluster 1) (Fig. 4). All these

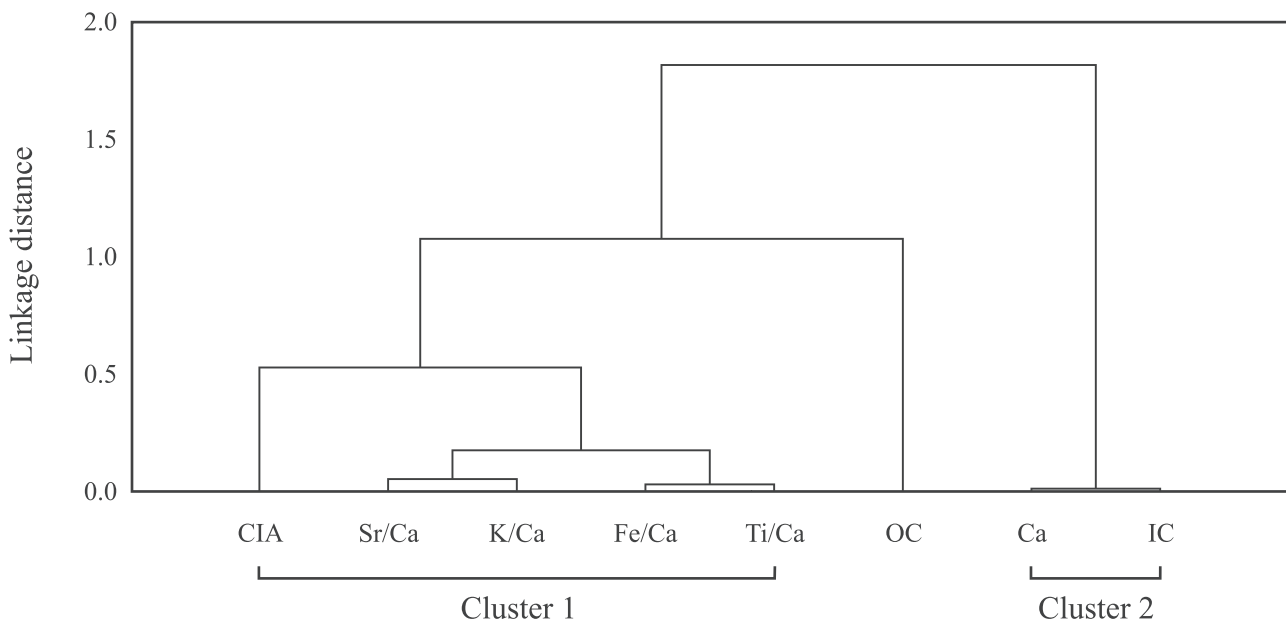


Figure 4. Dendrogram based on 1-Pearson-r complete linkage method for geochemical variables of sediments from the Santiaguillo ephemeral lake.

DROUGHTS IN MEXICO DURING LATE QUATERNARY

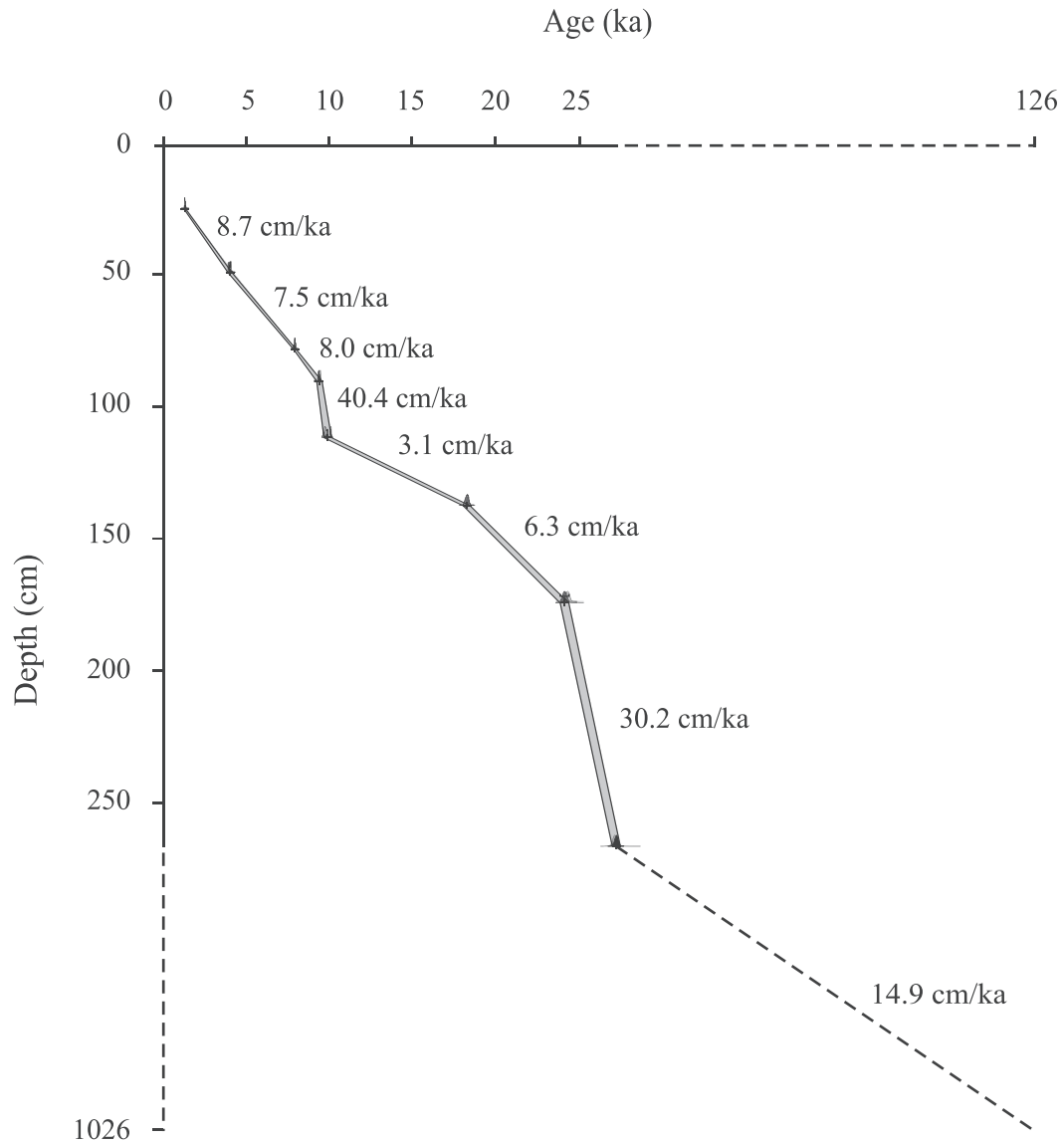


Figure 5. A Bayesian age–depth model constructed using eight different ^{14}C ages in sediments between depths of 266 and 25 cm. Chronology to sediments at depths of 1026–266 cm was assigned by extrapolating an average sedimentation of 14.9 cm/ka calculated for sediments at depths of 266–25 cm.

Table 3. Radiocarbon date, calibrated value and agreement index of samples from different depth intervals from the core collected from the Santiaguillo ephemeral lake

Lab code	Depth (cm)	^{14}C year BP	$\delta^{13}\text{C}$ (‰)	Modelled age		Agreement index (A)
				2 σ range (cal. year BP)	Median age (cal. year BP)	
OS/0506	25	1400 ± 40	-21.2	1380–1270	1310	99.2
Beta-346907	49	3730 ± 30	-22.8	4220–3980	4080	99.6
Beta-367219	78	7130 ± 40	-19.2	8020–7860	7960	99.9
Beta-355322	89	8360 ± 40	-21.4	9470–9150	9340	91.8
OS/0507	110	8760 ± 40	-25.0	10 150–9670	9860	77.0
Beta-346908	136	$15 020 \pm 60$	-20.6	18 440–18 020	18 240	99.2
Beta-367220	174	$20 300 \pm 100$	-21.0	24 510–23 970	24 240	80.8
Beta-346910	266	$22 840 \pm 100$	-21.2	27 500–27 050	27 290	96.1

element ratios are linked to chemical variables (Ca and IC) representing the calcite (cluster 2) with a higher linkage distance, and the cluster of element ratios is negatively related ($r=-0.6$, $p<0.05$) to the chemical variables associated with calcite. It suggests that sediments characterized by the lower values of these element ratios were deposited during the intervals of higher calcite deposition.

4.4. Chronology

The radiocarbon analysis was successfully done for eight samples. A Bayesian age–depth model was constructed using the successful ^{14}C ages in sediments deposited between depths of 266 and 25 cm, IntCal13 calibration curve (Reimer *et al.*, 2013) and P sequence with $k=0.3$ (Fig. 5) (Bronk Ramsey, 2008). Table 3 presents the calibrated ages and corresponding median values. This age model was generated using the online OxCal version 4.2 (Bronk Ramsey, 2009) and has an Agreement Index (A) of 80. It incorporates uncertainties (2σ) of 40–290 years between the tie points and assigns median ages between *c.* 27.3 ka (age in thousands of calendar years before 1950 AD are presented as ka) and 1.3 ka for sediments of 266–25-cm depths. The upper 25 cm of the sediment core was deposited over the last *c.* 1.3 ka. Sedimentation rate varies between 3.1 and 40.4 cm/ka with an average of 14.9 cm/ka (Figs. 3 and 5). Samples analysed for geochemistry were separated from each other by 130 to 3210 years (~10-cm interval) and hence documented millennial to orbital-scale variations in the depositional history.

Higher sedimentation rates of 30.2 cm/ka (266–174 cm) and 40.4 cm/ka (110–89 cm) occurred during *c.* 27.3–24.2 ka and *c.* 9.9–9.3 ka, respectively. The lowest sedimentation of 3.1 cm/ka (136–110 cm) is observed during *c.* 18.2–9.9 ka. We assigned a chronology to sediments present at depths of >266 cm by extrapolating an average sedimentation of 14.9 cm/ka (calculated between 266- and 25-cm depths) to the base of the core. This method was followed as the depositional history of the last *c.* 27.3 ka was characterized by both heterogeneous sediment texture and different sedimentation rates. The core base (i.e. 1026 cm) has a possible median age of *c.* 126 ka. In the absence of radiocarbon dates in the lower part of the sediment sequence collected from the subtropical Pacific Ocean, Blanchet *et al.* (2007) assigned a chronology up to *c.* 120 ka by interpolating between the last radiocarbon age and the sediments representing the Blake magnetic excursion. However, our approach is similar to extrapolation of the chronology to lower parts of sediment columns as followed by Blazevic *et al.* (2009) and Burnett *et al.* (2011) in different studies.

5. DISCUSSION

5.1. Palaeohydrological proxy

The Santiaguillo sediments comprise primary silicates (quartz, K-feldspar and zircon), secondary alumino-silicates (montmorillonite and illite) and calcite in varying proportions. The watershed geology indicates the presence of non-carbonate volcanic, metamorphic and sedimentary rocks (Fig. 1). Hence, calcite is an authigenic mineral, and it was deposited in the basin by evaporation of the water column during the arid intervals. We estimated the abundance of calcite from CaCO_3 values, and sediments with more calcite represent evaporative intervals.

Using a provenance diagram, Roy *et al.* (2015) have reported a uniform provenance for clastic sediments deposited over the last 27 ka in the Santiaguillo ephemeral lake. Homogeneous values of Ti/Al along the new core indicate that clastic sediments present in the 1026-cm-long core were also sourced from the erosion of similar association of rocks. Chemical characteristics of primary clastic sediments deposited in the basin are inferred from varying Ti/Ca, Fe/Ca, K/Ca and Sr/Ca ratios (i.e. clastic sediments with lower elemental ratio or clastic sediments with higher elemental ratio). As all the element ratios show better correlations ($r=0.8\text{--}0.9$, $p<0.05$) with each other, we used only Ti/Ca as a proxy to characterize the clastic minerals. Negative correlation of CaCO_3 with Ti/Ca ($r=-0.6$, $p<0.05$) and CIA ($r=-0.7$, $p<0.05$) indicates that clastic sediments with less Ti/Ca were transported into the basin from a drier watershed and deposited along with the carbonate-enriched sediments. Minimal or absence of sediment–water interaction suggest that less Ti/Ca-bearing clastic sediments were windblown and hence represent the intervals of higher aeolian activity in the watershed. We demarcated the droughts by identifying sediments with both above-average amounts of calcite and below-average values of Ti/Ca (Fig. 6). More calcite precipitation represents the intervals of enhanced evaporative conditions, and deposition of windblown clastic sediments represents the intervals of drier watershed and enhanced aeolian activity.

5.2. Drought record

MIS 2 and 1: Below-average amounts of calcite deposition and minimal abundance of windblown clastics suggest an absence of drought during the MIS 2 (*c.* 28–15 ka; Fig. 6). At least two different events of drought occurred in the MIS 1 (last *c.* 15 ka), and they were centred at *c.* 13.5 ka and *c.* 7 ka. However, sediments deposited during the drought of *c.* 13.5 ka are characterized by more calcite and less Ti/Ca compared with sediments representing the drought of *c.* 7 ka. In previous studies, Chávez-Lara *et al.*

DROUGHTS IN MEXICO DURING LATE QUATERNARY

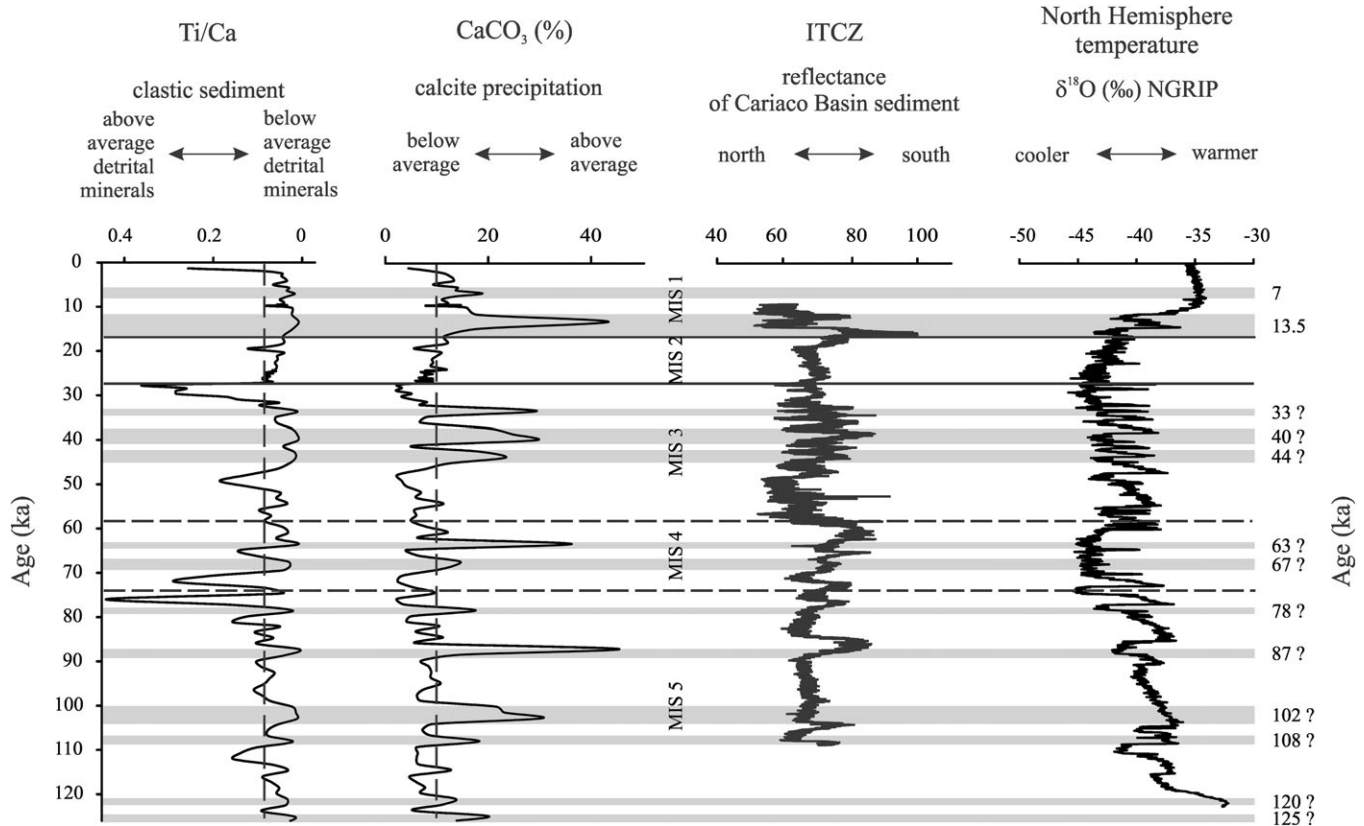


Figure 6. Droughts are indicated by sediments with above-average amounts of calcite and clastics with below-average abundance of Ti/Ca-bearing minerals. Dotted lines indicate the average values.

(2015) and Roy *et al.* (2015) reconstructed runoff and water column salinity of the Santiagillo lake between *c.* 27 and 4 ka. The new core is collected from a relatively central part of the lake, while both the previous studies are based on sediments from the modern shore. Irrespective of different sampling resolutions and age models of the previous studies and the present paper, tendencies of the drought record and water column salinity were almost synchronous in orbital time scale (Fig. 7). Absence of drought during the MIS 2 was contemporary to an interval (*c.* 27–18 ka) of more runoff and presence of diluted and perennial oligohaline water column at the modern shore. Similarly, MIS 1 (*c.* last 15 ka) had two different droughts, and Santiagillo received less runoff and hosted more saline (oligohaline–mesohaline) ephemeral water column at the shore.

The extrapolation of a uniform sedimentation rate for the rest of the core might be erroneous. Hence, we discussed about droughts occurred during the MIS 5, 4 and 3 by providing information about the depth and uncertain chronologies (Fig. 6).

MIS 5, 4 and 3: Droughts represented by sediments at depths of 1026–1016 cm (*c.* 125 ka?), 996–986 cm (*c.* 120 ka?), 896–886 cm (*c.* 108 ka?), 856–826 cm

(*c.* 102 ka?), 736–716 cm (*c.* 87 ka?) and 669–659 cm (*c.* 78 ka?) possibly occurred during the MIS 5. However, sediments at depths of 856–826 cm and 736–716 cm have more calcite and less Ti/Ca compared with the rest. The droughts registered by sediments at depths of 589–564 cm (*c.* 67 ka?) and 554–544 cm (*c.* 63 ka?) possibly represent the MIS 4. Sediments deposited at depths of 554–544 cm have more calcite compared with sediments of 589–564 cm. The earlier part of MIS 3 lacked drought, and the later part had at least three different droughts represented by sediments at depths of 404–384 cm (*c.* 44 ka?), 364–344 cm (*c.* 40 ka?) and 324–304 cm (*c.* 33 ka?). Droughts of the late MIS 3 have almost comparable amounts of calcite deposition.

5.3. Forcing

In a regional synthesis of palaeoclimate records, Metcalfe *et al.* (2015) observed that the hydroclimate of the NAM region was affected by changes in the summer and autumn solar irradiances, location of ITCZ and ENSO variability. An earlier proxy-based precipitation record representing the late

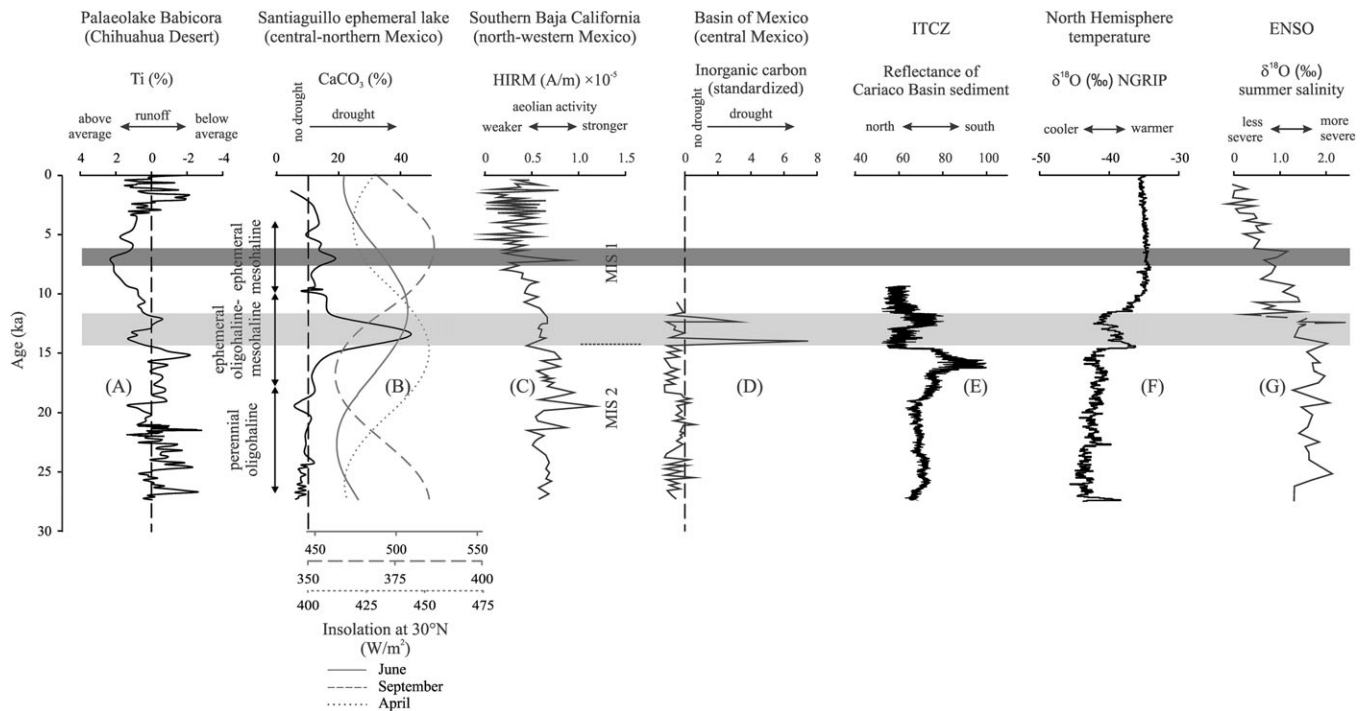


Figure 7. Proxy records indicating (A) runoff into palaeolake Babicora (Roy *et al.*, 2013a, 2013b), (B) drought from Santiaguillo ephemeral lake (this study), (C) aeolian activity in southern part of the Baja California peninsula (Blanchet *et al.*, 2007) and (D) droughts in the Basin of Mexico (Torres-Rodríguez *et al.*, 2015) provide hydroclimatic information of the subtropical and tropical Mexico. Droughts recorded in Santiaguillo is compared with (B) April (spring), June (summer) and September (autumn) insolations (Berger and Loutre, 1991), (E) mean position of ITCZ (Deplazes *et al.*, 2013), (F) North Hemisphere temperature (NGRIP project members, 2004) and (G) ENSO activity (Stott *et al.*, 2002). The event shown in dark-grey band has lower regional expansion compared with the interval marked in lighter-grey band. Arid conditions during the early MIS 1 (*c.* 13.5 ka) had the highest regional expansion.

last glacial–early Holocene from Santiaguillo showed first-order positive correlation with the autumn insolation (Roy *et al.*, 2015). We intended to identify possible climatic forcings on orbital-scale drought dynamics of central-northern Mexico and evaluated geographic coverage of the arid intervals that occurred only during the well-constrained MIS 2 and MIS 1 (Fig. 7). The drought record is compared with seasonal insolations (Berger and Loutre, 1991), mean position of the ITCZ (Deplazes *et al.*, 2013), North Hemisphere temperature (NGRIP project members, 2004) and super-ENSO activity (Stott *et al.*, 2002).

As droughts are intervals of moisture scarcity, we expected negative relationship between the drought record and the autumn (September) insolation. For example, the autumn insolation was higher, and Santiaguillo lacked drought during the late last glacial (early part of MIS 2). However, the tendencies of calcite abundance and autumn insolation do not show similar relationship during the middle Holocene drought. The drought of *c.* 7 ka (middle MIS 1) occurred in an interval of higher autumn insolation. However, the proxy drought record shows a first-order positive relationship with the spring (April) insolation. The drought of *c.* 13.5 ka occurred during an interval of highest spring insolation. Meteorological data from the basin

indicate that spring (March–May) is the driest season and it contributes less than 4% of the total rainfall (Fig. 2). Solar irradiance of the spring is also comparable with insolation of the summer months (Fig. 2). Field observation and modern instrumental data suggest that moderate to higher temperature and an almost absence of runoff during the spring lead to enhanced evaporation of the water column and more calcite precipitation. The similarity between the calcite abundance and the spring insolation suggests that droughts of central-northern Mexico during the MIS 2 and 1 were also controlled by the precession-modulated spring insolation.

Modern instrumental records and tree-ring reconstructions show that ENSO has a dipole impact in Mexico. The warmer phase of ENSO (El Niño) produces drier summer conditions in the central-northern Mexico (including Durango) but humid winter–spring conditions for the northwestern Mexico. On the other hand, the cold phase of ENSO (La Niña) causes drier conditions in northwestern Mexico during the winter–spring (Seager *et al.*, 2009; Mendez and Magaña, 2010; Stahle *et al.*, 2016). Based on the oxygen isotope composition of coralline aragonite from Papua New Guinea, Tudhope *et al.* (2001) suggested the existence of ENSO (with substantial changes in strength) over the last 130 ka. ENSO occurred even during the glacial period of

substantially reduced global temperature. Considering the modern analogue of higher salinity in the western Pacific Ocean during the years of El Niño conditions (Mo and Higgins, 1998), Stott *et al.* (2002) reconstructed millennial-scale oscillations of super-ENSO from $\delta^{18}\text{O}$ measured in the surface-dwelling planktonic foraminifera from a marine sequence collected from the eastern edge of the Indonesian archipelago. We observe that both the droughts of *c.* 13.5 ka and *c.* 7 ka identified in sediments of the Santiagillo ephemeral lake were contemporary to intervals of El Niño conditions. Another proxy record of ENSO (Laguna Pallcacocha; Moy *et al.*, 2002) suggested that ENSO activity remained higher during the early–middle Holocene (i.e. post 7 ka) compared with the early Holocene (*c.* 12–7 ka). Similarly, the marine sediments collected near the Galapagos Islands reported that ENSO activity remained weaker during the early–middle Holocene compared with the late Holocene (Koutavas *et al.*, 2006). The proxy record of Santiagillo did not reconstruct droughts that occurred over the last 1.3 ka, and hence, it is beyond the scope of this paper to evaluate droughts of the late Holocene with respect ENSO. We observe that the drought of *c.* 13.5 ka was contemporary to an interval of fluctuating global temperature and unstable ITCZ. Some of the droughts identified in the extrapolated part of the age model with uncertain chronology also maintain this relationship with the North Hemisphere temperature and mean position of ITCZ (Fig. 6).

5.4. Regional comparison

The proxy record of drought in the Santiagillo ephemeral lake is compared with records indicating runoff (palaeolake Babicora; Roy *et al.*, 2013b) and aeolian activity (southern Baja California peninsula; Blanchet *et al.*, 2007) in the subtropical north and northwestern Mexico and droughts (Basin of Mexico; Torres-Rodríguez *et al.*, 2015) in the tropical central Mexico in order to evaluate the geographic coverage of arid intervals (Fig. 7). Ti concentration reconstructs variable runoff into the palaeolake Babicora and precipitation in the Chihuahua Desert. Coercivity (HIRM) changes of sediments deposited in the subtropical Pacific Ocean reflect the strength of aeolian activity in southern part of the Baja California peninsula. Abundance of inorganic carbon in sediments of the Lake Chalco provides information about drought regimes in the central Mexico up to *c.* 10.8 ka.

Hydroclimates of central-northern Mexico, Chihuahua Desert (northern Mexico) and the southern part of the Baja California peninsula (northwestern Mexico) behaved differently. During the MIS 2, the palaeolake Babicora received reduced runoff (arid conditions), and the southern part of the Baja California peninsula experienced higher

aeolian activity. However, both the Santiagillo ephemeral lake and the Basin of Mexico lacked droughts. Restriction of the arid conditions to higher latitudes (i.e. north and northwestern Mexico) was contemporary to an interval characterized by stronger ENSO and lower global temperature. After evaluating the modern conditions (Mitchell *et al.*, 2002; Ritchie *et al.*, 2011) in palaeo-records, Roy *et al.* (2015) associated this interval without droughts in the central-northern Mexico and southwest Mexico to an interval of weaker NAM. But the frequent formation of tropical cyclones with restricted rainfall swath patterns brought more rainfall to the region. The drought centred at *c.* 13.5 ka in Santiagillo was contemporary to intervals of stronger aeolian activity in the Baja California peninsula and droughts in the Basin of Mexico. This arid interval was spread across subtropical as well as tropical Mexico and occurred during an interval of relatively warmer and variable North Hemisphere temperature and stronger ENSO. Similarly, the contemporary occurrence of another drought in both Santiagillo and Basin of Mexico at *c.* 7 ka also happened in an interval of warmer global temperature and stronger ENSO.

6. CONCLUSIONS

Varying abundances of authigenic carbonate and wind-blown clastic sediments in a 1026-cm-long sediment core from the Santiagillo ephemeral lake provide information about orbital-scale drought dynamics in central-northern Mexico during the late Quaternary. Droughts were represented by deposition of above-average amounts of calcite and clastic sediments with below-average Ti/Ca. Comparison of the new data with proxy records indicating aridity in different parts of Mexico provides an estimation of the geographic distributions of the arid intervals across subtropical as well as tropical Mexico. More specifically,

- i. Central-northern Mexico lacked a drought during the MIS 2, whereas the droughts of MIS 1 were centred at *c.* 13.5 ka and *c.* 7 ka.
- ii. The drought record of central-northern Mexico shows first-order positive relationships with precession-modulated spring insolation. The droughts of *c.* 13.5 ka occurred during an interval of higher spring insolation, relatively warmer but unstable global temperature and stronger ENSO.
- iii. A synchronous arid interval in different sites across the subtropical and tropical Mexico occurred during the early part of MIS 1 and centred at *c.* 13.5 ka. It is indicated by droughts in the Santiagillo ephemeral lake, stronger aeolian activity in southern Baja

California peninsula and droughts in the Basin of Mexico. We suggest that the combination of Milankovitch forcing along with warmer global temperature and ENSO possibly led to regional expansion of the arid conditions.

ACKNOWLEDGEMENTS

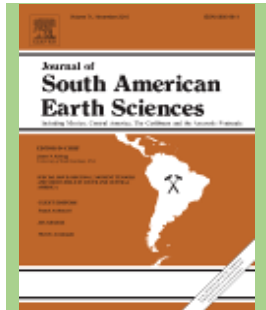
This paper is product of a project (CB-237579) with financial support received from CONACyT. The first author (JDQJ) was awarded a scholarship from CONACyT (235509) for his doctoral study. A part of this manuscript was redrafted during the sabbatical of PDR with a scholarship from DGAPA-UNAM. Jose Luis Sánchez Zavala, Carolina Castelán Hernández and Nayeli López Balbiaux provided field work and laboratory assistance. Rufino Lozano Santacruz and María Patricia Girón García analysed the samples for elemental concentrations and mineralogy. Oscar Sandate of Ecoterra Servicios Ambientales helped in the sediment core collection. Suggestions and comments from Cecile L. Blanchet, an anonymous reviewer and editor (Prof. Ian D. Somerville) are thankfully acknowledged.

REFERENCES

- Anderson, R.S., Van Devender, T.R.** 1995. Vegetation history and paleoclimates of the coastal lowlands of Sonora, Mexico – pollen records from packrats middens. *Journal of Arid Environments* **30**, 295–306.
- Antinao, J.L., McDonald, E.** 2013. An enhanced role for the tropical Pacific on the humid Pleistocene-Holocene transition in southwestern North America. *Quaternary Science Reviews* **78**, 319–341.
- Barron, J.A., Metcalfe, S.E., Addison, J.A.** 2012. Response of the North American monsoon to regional changes in ocean surface temperature. *Paleoceanography* **27**, PA3206, doi: 10.1029/2011PA002235, 2012.
- Berger, A., Loutre, M.F.** 1991. Insolation values for the climate of the last 10 million years. *Quaternary Science Reviews* **10**, 297–317.
- Blanchet, C.L., Thouveny, N., Vidal, L., Leduc, G., Tachikawa, K., Bard, E., Beaufort, L.** 2007. Terrigenous input response to glacial/interglacial climatic variations over southern Baja California: a rock magnetic approach. *Quaternary Science Reviews* **26**, 3118–3133.
- Blazevic, M.A., Kirby, M.E., Woods, A.D., Browne, B.L., Bowman, D.D.** 2009. A sedimentary facies model for glacial-age sediments in Baldwin Lake, Southern California. *Sedimentary Geology* **219**, 151–168.
- Bronk Ramsey, C.** 2008. Deposition models for chronological records. *Quaternary Science Reviews* **27**, 42–60.
- Bronk Ramsey, C.** 2009. Bayesian analysis of radiocarbon dates. *Radiocarbon* **51**, 337–360.
- Burnett, A.P., Soreghan, M.J., Scholz, C.A., Brown, E.T.** 2011. Tropical East African climate change and its relation to global climate: a record from Lake Tanganyika, Tropical East Africa, over the past 90+ kyr. *Palaeogeography, Palaeoclimatology, Palaeoecology* **303**, 155–167.
- Caballero, M., Peñalba, M.C., Martínez, M., Ortega-Guerrero, B., Vázquez, L.** 2005. A Holocene record from a former coastal lagoon in Bahía Kino, Gulf of California, Mexico. *The Holocene* **15**, 1236–1244.
- Castiglia, P.J., Fawcett, P.J.** 2006. Large Holocene lakes and climate change in the Chihuahuan Desert. *Geology* **34**, 113–116.
- Castro, C.L., McKee, T.B., Pielke, R.A., Sr.** 2001. The relationship of the North American monsoon to tropical and North Pacific sea surface temperatures as revealed by observational analysis. *Journal of Climate* **14**, 4449–4473.
- Cerano-Paredes, J., Villanueva Díaz, J., Fulé, P.Z.** 2010. Reconstrucción de incendios y su relación con el clima para la Reserva Cerro El Mohinora, Chihuahua. *Revista Mexicana de Ciencias Forestales* **1**, 63–74.
- Chávez-Lara, C.M., Roy, P.D., Pérez, L., Sankar, G.M., Neri, V.H.L.** 2015. Ostracode and C/N based paleoecological record from Santiago basin of subtropical Mexico over last 27 cal kyr BP. *Revista Mexicana de Ciencias Geológicas* **32**, 1–10.
- Cleveland, M.K., Stahle, D.W., Therrell, M.D., Villanueva-Díaz, J., Burns, B.T.** 2003. Tree-ring reconstructed winter precipitation and tropical teleconnections in Durango, Mexico. *Climatic Change* **59**, 369–388.
- Cohen, A.S.** 2003. *Palaeolimnology: The History and Evolution of Lake Systems*. Oxford University Press: New York.
- COHMAP members.** 1988. Climatic change of the past 18,000 years. Observations and model simulations. *Science* **241**, 1043–1052.
- Davis, L.G.** 2003. Geoarchaeology and geochronology of pluvial lake Chapala, Baja California, Mexico. *Geoarchaeology* **18**, 205–223.
- Deplazes, G., Lückge, A., Peterson, L.C., Timmermann, A., Hamann, Y., Hughen, K.A., Röhl, U., Laj, C., Cane, M.A., Sigman, D.M., Haug, G.H.** 2013. Links between tropical rainfall and North Atlantic climate during the last glacial period. *Nature Geoscience* **6**, 213–217.
- García, E.** 1973. *Modificaciones al sistema de clasificación climática de Köppen*. México. Universidad Nacional Autónoma de México, D.F.
- González-Elizondo, M., Jurado, J.E., Navar, M., González-Elizondo, S., Villanueva, J., Aguirre, O., Jiménez, J.** 2005. Tree-rings and climate relationships for Douglas-fir chronologies from the Sierra Madre Occidental, Mexico: a 1681–2001 rain reconstruction. *Forest Ecology Management* **213**, 39–53.
- Holmgren, C.A., Betancourt, J.L., Rylander, K.A.** 2011. Vegetation history along the eastern, desert escarpment of the Sierra San Pedro Mártir, Baja California, Mexico. *Quaternary Research* **75**, 647–657.
- Kirby, M.E., Feakins, S.J., Bonuso, N., Fantozzi, J.M., Hiner, C.A.** 2013. Latest Pleistocene to Holocene hydroclimates from Lake Elsinore, California. *Quaternary Science Reviews* **76**, 1–15.
- Koutavas, A., DeMenocal, P.B., Lynch-Stieglitz, J.** 2006. Holocene trends in tropical Pacific sea surface temperatures and the El Niño-Southern Oscillation. *PAGES News* **14**, 22–23.
- Lachnić, M.S., Denniston, R.F., Asmerom, Y., Polyak, V.J.** 2014. Orbital control of western North America atmospheric circulation and climate over two glacial cycles. *Nature Communications* **5**, 3805. DOI:10.1038/ncomms4805.
- Lozano-García, M.S., Ortega-Guerrero, B., Sosa-Nájera, S.** 2002. Mid to Late Wisconsin pollen record of San Felipe Basin, Baja California. *Quaternary Research* **58**, 84–92.
- Lyle, M., Heusser, L., Ravelo, C., Yamamoto, M., Barron, J., Difffenbaugh, N.S., Herbert, T., Andreassen, D.** 2012. Out of the tropics: the Pacific, Great Basin Lakes, and Late Pleistocene water cycle in the western United States. *Science* **337**, 1629–1633.
- Magaña, V.O., Vázquez, J.L., Pérez, J.L., Pérez, J.B.** 2003. Impact of El Niño in precipitation in Mexico. *Geofísica Internacional* **42**, 313–330.
- Mason, B., Moore, C.B.** 1982. *Principles of Geochemistry*. John Wiley and Sons: New York.
- Mendez, M., Magaña, V.** 2010. Regional aspects of prolonged meteorological droughts over Mexico and Central America. *American Meteorological Society* **23**, 1175–1188.
- Metcalfe, S., Say, A., Black, S., McCulloch, R., O'Hara, S.** 2002. Wet conditions during the last glaciation in the Chihuahuan Desert, Alta Babicora Basin, Mexico. *Quaternary Research* **57**, 91–101.
- Metcalfe, S.E., Barron, J.A., Davies, S.J.** 2015. The Holocene history of the North American monsoon: ‘known knowns’ and ‘known unknowns’ in understanding its spatial and temporal complexity. *Quaternary Science Reviews* **120**, 1–27.

- Meyer, E.R.** 1973. Late Quaternary paleoecology of the Cuatro Cienegas basin, Coahuila, Mexico. *Ecology* **54**, 982–985.
- Mitchell, D.L., Ivanova, D., Rabin, R., Brown, T.J., Redmond, K.** 2002. Gulf of California sea surface temperatures and the North American monsoon: mechanistic implications from observations. *Journal of Climate* **15**, 2261–2281.
- Mo, K.C., Higgins, R.W.** 1998. Tropical convection and precipitation regimes in the western United States. *Journal of Climate* **11**, 2404–2423.
- Moy, C.M., Seltzer, G.O., Rodbell, D.T., Anderson, D.M.** 2002. Variability of El Niño/Southern Oscillation activity at millennial timescales during the Holocene epoch. *Nature* **420**, 162–165.
- Murillo de Nava, J.M., Gorsline, D.S., Goodfriend, G.A., Vlasov, V.K., Cruz-Orozco, R.** 1999. Evidence of Holocene climatic changes from aeolian deposits in Baja California Sur, Mexico. *Quaternary International* **56**, 141–154.
- Nesbitt, H.W., Young, G.M.** 1984. Prediction of some weathering trends of plutonic and volcanic rocks based on thermodynamic and kinetic considerations. *Geochimica et Cosmochimica Acta* **48**, 1523–1534.
- Nesbitt, H.W., Young, G.M.** 1989. Formation and diagenesis of weathering profiles. *Journal of Geology* **97**, 129–147.
- Nieto-Samaniego, A.F., Barajas-Gea, C.I., Gómez-González, J.M., Rojas, A., Alaniz-Álvarez, S.A., Xu, S.** 2012. Geología, evolución estructural (Eoceno al actual) y eventos sísmicos del Graben de Santiago, Durango, México. *Revista Mexicana de Ciencias Geológicas* **29**, 115–130.
- Northern Greenland Ice Core project members, (NGRIP project).** 2004. High resolution record of Northern Hemisphere climate extending into the last interglacial period. *Nature* **431**, 147–151.
- Ortega-Guerrero, B., Caballero-Miranda, M., Lozano-García, S., De la O Villanueva, M.** 1999. Palaeoenvironmental record of the last 70,000 yr un San Felipe Basin, Sonora desert Mexico: preliminary results. *Geofísica Internacional* **38**, 153–163.
- Ortega-Rosas, C.I., Guiot, J., Peñalba, M.C., Ortiz-Acosta, M.E.** 2008. Biomization and quantitative climate reconstructions techniques in northwestern Mexico-With an application to four Holocene pollen sequences. *Global and Planetary Change* **61**, 242–266.
- Oster, J.L., Ibarra, D.E., Winnick, M.J., Maher, K.** 2015. Steering of westerly storms over western North America at the Last Glacial Maximum. *Nature Geoscience* **8**, 201–205.
- Reimer, P.J., Bard, E., Bayliss, A., Beck, J.W., Blackwell, P.G., Ramsey, C.B., Grootes, P.M., Guilderson, T.P., Haflidason, H., Hajdas, I., Hatté, C., Heaton, T.J., Hoffmann, D.L., Hogg, A.G., Hughen, K.A., Kaiser, K.F., Kromer, B., Manning, S.W., Niu, M., Reimer, R.W., Richards, D.A., Scott, E.M., Southon, J.R., Staff, R.A., Turney, C.S.M., van der Plicht, J.** 2013. IntCal13 and MARINE13 radiocarbon age calibration curves 0–50000 years cal BP. *Radiocarbon* **55**, 1869–1887.
- Ritchie, E.A., Wood, K.M., Gutzler, D.S., White, S.R.** 2011. The influence of eastern Pacific tropical cyclone remnants on the southwestern United States. *Monthly Weather Review* **139**, 192–210.
- Roy, P.D., Caballero, M., Lozano, R., Ortega, B., Lozano, S., Pi, T., Israde, I., Morton, O.** 2010. Geochemical record of late Quaternary paleoclimate from lacustrine sediments of paleo-lake San Felipe, western Sonora Desert, Mexico. *Journal of South American Earth Sciences* **29**, 586–596.
- Roy, P.D., Jonathan, M.P., Pérez-Cruz, L.L., Sánchez-Córdova, M.M., Quiroz-Jiménez, J.D., Romero, F.M.** 2012. A millennial-scale Late Pleistocene–Holocene palaeoclimatic record from the western Chihuahua Desert, Mexico. *Boreas* **41**, 707–717.
- Roy, P.D., Rivero-Navarette, A., Lopez-Balbiaux, N., Pérez-Cruz, L.L., Metcalfe, S.E., Muthu Sankar, G., Sánchez-Zavala, J.L.** 2013a. A record of Holocene summer-season palaeohydrological changes from the southern margin of Chihuahua Desert (Mexico) and possible forcings. *The Holocene* **23**, 1105–1114.
- Roy, P.D., Quiroz-Jiménez, J.D., Pérez-Cruz, L.L., Lozano-García, S., Metcalfe, S.E., Lozano-Santacruz, R., López-Balbiaux, N., Sánchez-Zavala, J.L., Romero, F.M.** 2013b. Late Quaternary paleohydrological conditions in the dryland of northern Mexico: a summer precipitation proxy record of the last 80 cal ka BP. *Quaternary Science Reviews* **78**, 342–354.
- Roy, P.D., Quiroz-Jiménez, J.D., Chávez-Lara, C.M., Sánchez-Zavala, J.L., Pérez-Cruz, L.L., Sankar, G.M.** 2014. Humid Pleistocene–Holocene transition and early Holocene in sub-tropical northern Mexico and possible Gulf of California forcing. *Boreas* **43**, 577–587.
- Roy, P.D., Chávez-Lara, C.M., Beramendi-Oroso, L.E., Sánchez-Zavala, J.L., Muthu-Sankar, G., Lozano-Santacruz, R., Quiroz-Jimenez, J.D., López-Balbiaux, N.** 2015. Paleohydrology of the Santiago basin (Mexico) since late last glacial and climate variation in southern part of western subtropical North America. *Quaternary Research* **84**, 335–347.
- Schnurrenberger, D., Russell, J., Kelts, K.** 2003. Classification of lacustrine sediments based on sedimentary components. *Journal of Paleolimnology* **29**, 141–154.
- Seager, R., Ting, M., Davis, M., Cane, M., Nike, N., Nakamura, J., Lie, C., Cook, E., Stahle, D.W.** 2009. Mexican drought: an observational modeling and tree ring study of variability and climate change. *Atmosfera* **22**, 1–31.
- Servicio Geológico Mexicano.** 1998. *Carta Geológico-Minera Durango, scale 1:250,000*. G13-11.
- Stahle, D.W., Cook, E.R., Burnette, D.J., Villanueva, J., Cerano, J., Burns, J.N., Griffin, D., Cook, B.I., Acuña, R., Torbenson, M.C.A., Sjezner, P., Howard, J.M.** 2016. The Mexican drought atlas: tree-ring reconstructions of the soil moisture balance during the late pre-Hispanic, colonial, and modern eras. *Quaternary Science Review* **149**, 34–60.
- Stott, L., Poulsen, C., Lund, S., Thunell, R.** 2002. Super ENSO and global climate oscillations at millennial time scales. *Science* **297**, 222–226.
- Sutton, R.T., Hodson, D.L.R.** 2005. Atlantic Ocean forcing of North American and European summer climate. *Science* **309**, 115–118.
- Torres-Rodríguez, E., Lozano-García, S., Roy, P., Ortega, B., Beramendi-Oroso, L., Correa-Metrio, A., Caballero, M.** 2015. Last glacial droughts and fire regimes in the central Mexican highlands. *Journal of Quaternary Science* **30**, 88–89.
- Tudhope, A.W., Chilcott, C.P., McCulloch, M.T., Cook, E.R., Chappell, J., Ellam, R.M., Lea, D.W., Lough, J.M., Shimmield, G.B.** 2001. Variability in the El Niño–Southern Oscillation through a glacial–interglacial cycle. *Science* **291**, 1511–1517.
- Van Devender, T.R., Burgess, T.L.** 1985. Late Pleistocene woodlands in the Bolson de Mapimi: a refugium for the Chihuahuan Desert biota? *Quaternary Research* **24**, 346–353.
- Versteegh, G.J.** 2005. Solar forcing of climate. 2: evidence from the past. *Space Science Reviews* **120**, 243–286.
- Villanueva-Díaz, J., Paredes, J.C., Mata, S.R., López, J.C.A., Stahle, D.W., Corral, J.A.R., Sifuentes, A.R.M.** 2014. Variabilidad hidroclimática reconstruida con anillos de áboles para la cuenca alta del Río Mezquital, Durango. *Revista Mexicana de Ciencias Agrícolas* **10**, 1897–1912.
- Weltje, G.J., Tjallingii, R.** 2008. Calibration of XRF core scanners for quantitative geochemical logging of sediment cores: theory and application. *Earth and Planetary Science Letters* **274**, 423–438.
- Yarincik, K.M., Murray, R.W., Peterson, L.C.** 2000. Climatically sensitive eolian and hemipelagic deposition in the Cariaco Basin, Venezuela, over the past 578,000 years: results from Al/Ti and K/Al. *Paleoceanography* **15**, 210–228.

CAPÍTULO VII



*Hydrological responses of the Chihuahua
Desert of Mexico to possible Heinrich
Stadials*



Hydrological responses of the Chihuahua Desert of Mexico to possible Heinrich Stadials

Jesús David Quiroz-Jimenez ^a, Priyadarsi D. Roy ^{b,*}, Rufino Lozano-Santacruz ^b, Patricia Giron-García ^b

^a Posgrado en Ciencias de la Tierra, Universidad Nacional Autónoma de México, Ciudad Universitaria, Del. Coyoacan, Ciudad de México, C.P. 04510, Mexico

^b Instituto de Geología, Universidad Nacional Autónoma de México, Ciudad Universitaria, Del. Coyoacan, Ciudad de México, C.P. 04510, Mexico



ARTICLE INFO

Article history:

Received 7 August 2016

Received in revised form

10 October 2016

Accepted 4 November 2016

Available online 5 November 2016

Keywords:

Geochemistry

Sediment

Paleoclimate

Last glacial

Heinrich stadial

Chihuahua desert

Mexico

ABSTRACT

Hydrological response of the Chihuahua Desert of Mexico to six different Heinrich Stadials (H6 to H1) is inferred with element ratio, carbonate abundance, and oxygen and carbon isotope compositions of lacustrine calcite in sediments collected from the Santiagillo Basin. Overall runoff and hence precipitation remained below average during H6, H4, H2 and H1, and above average during H5 and H3. Similarly, runoff of H4 showed the least variability and it was most variable during H5. In general, dissolved HCO_3^- was dominantly sourced from atmospheric CO_2 during the intervals of less runoff. However, lacustrine productivity as well as atmospheric CO_2 influenced carbon isotope composition of dissolved HCO_3^- during the regimes of fluctuating hydrological conditions. H2 was an interval of relatively warmer water column and enhanced lacustrine productivity. Comparison with other records indicates occurrence of similar millennial-scale hydrological variability in the southwest US. However, we did not always observe concurrency in proxy records from the Chihuahua Desert of Mexico and southwest US. Similarity in tendencies of runoff into the Santiagillo Basin and $\delta^{18}\text{O}$ of speleothem from the Hulu Cave during the six different Heinrich Stadials suggests a possible hemispheric link between hydroclimate of the Chihuahua Desert of Mexico and the East Asian Monsoon.

© 2016 Elsevier Ltd. All rights reserved.

1. Introduction

Global climate change occurred during the last glacial period in the Northern Hemisphere is archived in oxygen isotope compositions of the Greenland ice cores and sediments deposited in the North Atlantic Ocean (Dansgaard et al., 1982, 1993; Heinrich, 1988; Bond et al., 1992). Heinrich Stadials (H1 to H6) were cooler intervals with duration varying between 1.4 and 3.1 ka (thousand years before present) and all of them were characterized by discharge of icebergs from the Laurentide Ice Sheet (LIS) mainly through the Hudson Straight into the Atlantic Ocean (Andrews et al., 1993; Sanchez-Goñi and Harrison, 2010). Sedimentological data from the North Atlantic Ocean indicates that the Hudson Straight was not the primary ice source for all these cold intervals and H4 was associated with larger ice sheet collapse and dirtier icebergs compared to other Heinrich Stadials (Kirby and Andrews, 1999). It was assumed that disruptions in the Atlantic Meridional

OVERTURNING CIRCULATION (AMOC) and North Atlantic Deep Water (NADW) formation caused instabilities in the LIS and led to deposition of ice-raftered debris (IRD) in the North Atlantic (Calov et al., 2002; Hulbe et al., 2004). However, new paleoclimate data constrained the IRD events at few hundreds to almost a thousand year after the slowing down of AMOC and collapse of NADW (Roche et al., 2004; Hall et al., 2006; Jonkers et al., 2010). The climate models of Álvarez-Solas et al. (2011) suggested that an already weakened AMOC and reduced NADW caused subsurface warming in the North Atlantic and triggered the ice surges. Subsequent freshwater discharge into the North Atlantic eventually led to complete shutdown of NADW.

Terrestrial and marine systems in different latitudes responded differently to these high amplitude cooler conditions (Ruehleman et al., 1999; Hendy and Kennet, 2000; Wang et al., 2001; Zic et al., 2002; Jennerjahn et al., 2004; Prasad et al., 2004; Grimm et al., 2006; Leduc et al., 2007; Flower et al., 2004; Asmerom et al., 2010; Wagner et al., 2010; McClymont et al., 2012; Roy et al., 2012, 2015, 2016). Proxy records from the eastern Mediterranean and northwest Great Basin registered arid conditions (Zic et al., 2002; Prasad et al., 2004). Similarly, marine sediments off the

* Corresponding author.

E-mail addresses: roy@geologia.unam.mx, priyadarsi1977@gmail.com (P.D. Roy).

northeast Brazil suggested occurrence of more summer season fluvial discharge (Jennerjahn et al., 2004). In the subtropical North America, speleothems from the Fort Stanton Cave recorded more winter precipitation for the southwest US during all the Heinrich Stadials (Asmerom et al., 2010). Similarly, fossil pollens in sediments of the Lake Tulane suggested that the southeast US experienced warmer winter and wetter summer (Grimm et al., 2006; Donders et al., 2011). Both the Atlantic and Pacific Oceans retained heat during some of these stadials. Over the H1, the Gulf of Mexico experienced an increase of ~3 °C in sea surface temperature (SST) and the tropical Atlantic experienced ~1.5 °C increase in SST (Ruehleman et al., 1999; Flower et al., 2004). Warmer SST and presence of stratified water in the Gulf of California indicated conditions similar to the modern day summer or El-Niño regime (McClymont et al., 2012).

The subtropical Mexico hosts a large part of the southern Chihuahua Desert and proxy records from this region provide hydrological information for H2 and H1. Summer and autumn runoff into the Santiaguillo Basin reduced during H2 and H1 (Roy et al., 2015) and the El Potosi Basin received less runoff during the earlier part of H1 compared to the later part (Roy et al., 2016). The tropical central as well as southwest Mexico also remained drier during H1 (Lachniet et al., 2013; Lozano-García et al., 2015). In this paper, we present a proxy record to infer hydrological responses of the Chihuahua Desert of Mexico to six different Heinrich Stadials from elemental concentration and carbonate abundance in bulk sediments, and oxygen and carbon isotope compositions of carbonates deposited in the Santiaguillo Basin. Sediments deposited during different Heinrich Stadials were identified by radiocarbon dating up to ~27.3 ka, extrapolation of an average sediment rate and comparing the chronological variation of carbonate abundance with insoluble in rest of the sequence, and oxygen isotope composition of authigenic carbonate. Runoff is inferred from Al/Ca, Ti/Ca, Si/Ca and K/Ca ratios, water column salinity and temperature are estimated from carbonate abundance and oxygen isotope composition of carbonate, and carbon isotope composition provide information about sources of dissolved inorganic carbon in the water column.

2. Regional settings

2.1. Location and geology

The Chihuahua Desert of Mexico is spread over at least six different states of northern Mexico (i.e., Chihuahua, Durango, Zacatecas, Coahuila, Nuevo Leon and San Luis Potosi). The Santiaguillo Basin is present in an endorheic tectonic basin at western margin of the desert. It is located in the state of Durango and at eastern foothills of the Sierra Madre Occidental Mountains (Fig. 1a). The basin is NW-SE oriented and spreads over an area of ~2000 km². It is surrounded by volcanic mountains with elevation between 2500 and 3000 m asl and is fed by several intermittent streams. The basin hosts two water bodies: the northern perennial part is used as an irrigation reservoir and the southern part hosts a natural ephemeral lake. Both the water bodies are separated by construction of an artificial dam. The ephemeral lake hosts less than 1 m water column in its deepest part during the summer and autumn months and it mostly remains dry for a large part of the year. Geology of this basin comprised of the Paleogene to Quaternary igneous and sedimentary rocks, as well as small outcrops of Cretaceous metamorphic rocks (Munguía-Rojas et al., 1998; Nieto Samaniego et al., 2012). Ignimbrite and rhyolite are the dominant lithologies present in vicinity of the basin. Both andesite and conglomerate are present in the eastern and western catchment, whereas minor exposures of basalt are present to the east and south of the basin (Fig. 1b).

2.2. Modern climate

Three different meteorological stations present near the basin (Fig. 1c) recorded 430–554 mm of average annual precipitation during 1964–2006 CE (Source: Servicio Meteorológico Nacional, Mexico). Almost 90% (395–502 mm) of this rainfall occurred during the months of summer (June–August; average temperature of 19.8–22.3 °C) by the North American Monsoon and months of autumn (September–November; average temperature of 15.7–17.4 °C) by tropical cyclones. Both the summer and autumn precipitations were controlled by dynamics of the Inter Tropical Convergence Zone and sea surface temperature of the eastern tropical Pacific Ocean (Castro et al., 2001; Magaña et al., 2003). Winter (December–February; average temperature 10.8–12.0 °C) and spring (March–May; average temperature 16.8–18.6 °C) are the drier seasons and contributes <10% (16–22 mm) of annual precipitation. The average annual temperature varied between 16 °C and 18 °C and reached 38 °C during the month of June and remains sub-zero during the month of January.

3. Sampling and analysis

Two parallel sediment cores were collected from the ephemeral lake of the Santiaguillo Basin (Fig. 1). One of the cores (1026 cm long) was sampled at 1 cm interval and all the sub-samples were oven dried at 40 °C, homogenized and ground with an agate pestle. The present study is based on sediments deposited at depths between 560 and 78 cm and chronologically constrained with 6 different AMS ¹⁴C dates (Table 1). Radiocarbon analysis of 5 more samples at deeper part of the studied sequence (267–560 cm) resulted unsuccessful due to lower organic carbon content (Fig. 2). Sediments are characterized by texture observed in macroscopic inspection and microscopic observations (e.g., Schnurrenberger et al., 2003), abundance of organic carbon (OC) and relation between organic carbon and nitrogen (C/N). OC and N contents were measured in 48 samples in Thermo Scientific HiperTOC Solid Analyzer and Perkin Elmer Series II CHNS/O elemental analyzer. Carbonate and silicate minerals were identified using Shimadzu-6000 X-ray diffractometer (XRD).

The paleohydrological reconstruction was based on concentrations of Si, Al, Fe, K, Ti and Ca and CO₃ abundance in a total of 183 samples. Elemental concentrations were determined using a Thermo Scientific Niton FXL 950 X-ray Fluorescence (XRF) analyzer and the obtained data were corrected using the linear regression equations generated after comparing results of 38 samples obtained in Niton FXL and traditional Siemens XRF (e.g., Roy et al., 2012). Carbonate (CO₃) content was measured using a Thermo Scientific HiperTOC Solid Analyzer. Stable isotopes of carbon and oxygen were analyzed in carbonates of 33 different samples. Prior to the isotope analysis, organic material was removed by treating with 15% H₂O₂ and stable isotope ratios of carbon and oxygen were determined in carbonates using a Thermo Finnigan MAT 253 mass spectrometer coupled with Gas Bench II following the methodology of McCrea (1950). Isotope ratios are reported relative to the VPDB (Vienna Pee Dee Belemnite) standard with a standard deviation of ±0.2‰. Correlation coefficient and associations of different geochemical variables were obtained using the STATISTICA software.

4. Results

4.1. Sediment (texture, OC and C/N)

Sediments deposited between depths of 560 and 78 cm comprised sand, sandy-silt and silt (Fig. 2). Intercalations of

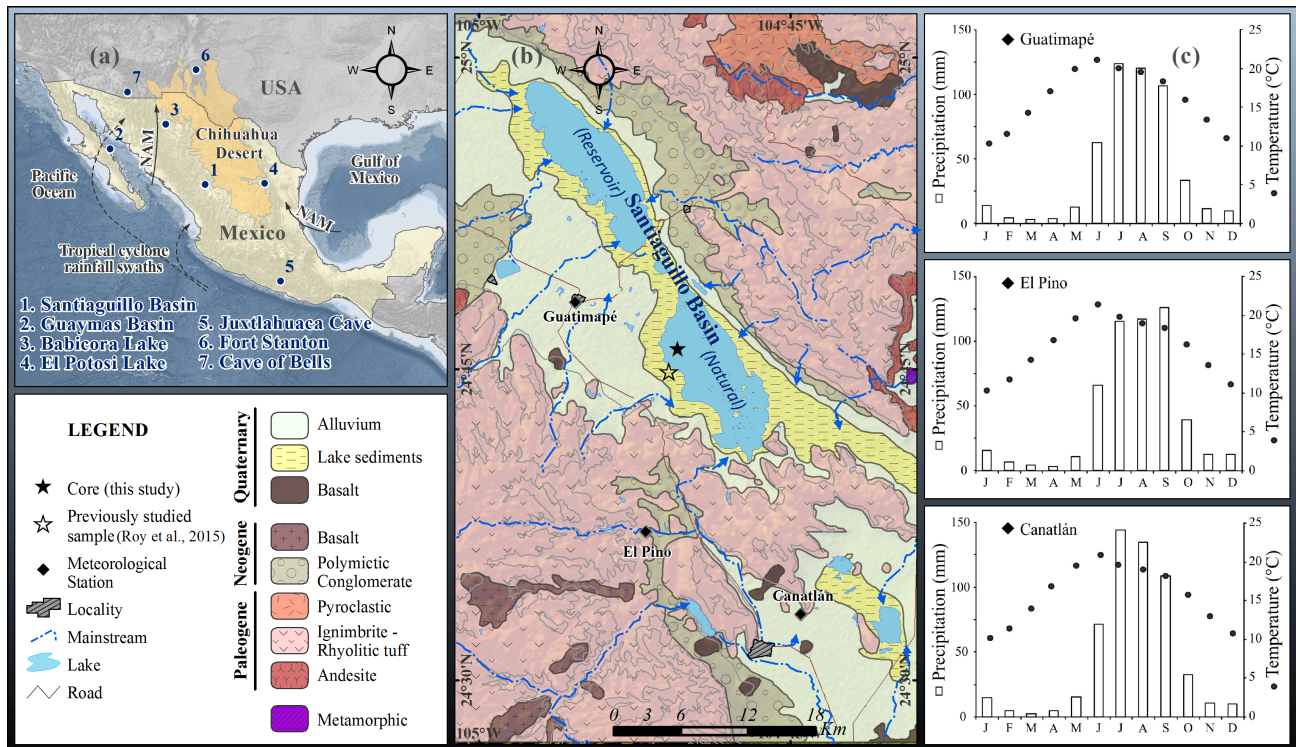


Fig. 1. (a) Map showing locations of the Santiaguillo Basin and other proxy records from northern Mexico and southwest US. (b) Cores were collected from ephemeral part of the basin and (c) three different nearby meteorological stations recorded an average annual precipitation varying between 430 and 554 mm during 1964–2006 CE.

Table 1

Depth, radiocarbon date, calibrated value and agreement index of samples in a sediment core from the Santiaguillo Basin.

Lab code	Depth (cm)	^{14}C yr BP	$\delta^{13}\text{C}$ (‰)	Modeled age		
				2σ range (cal. yr BP)	Median age (cal. yr BP)	Agreement index (A)
Beta-367219	78	7130 ± 40	-19.2	7860–8020	7960	100
Beta-355322	89	8360 ± 40	-21.4	9150–9470	9340	92
OS/0507	110	8760 ± 40	-25.0	9670–10,150	9860	77
Beta-346908	136	$15,020 \pm 60$	-20.6	18,020–18,440	18,240	99
Beta-367220	174	$20,300 \pm 100$	-21.0	23,970–24,510	24,240	81
Beta-346910	266	$22,840 \pm 100$	-21.2	27,050–27,500	27,290	96

calcareous and non-calcareous sandy-silt represent sediments present at depths of 560–469 cm. Fine to medium sand (with some gravel size fragments) is visible at depth of 469–420 cm. Sediments at 420–297 cm consist of calcareous sandy-silt and another fine to medium sand layer is present at 297–266 cm depth. Intercalations of sandy-silt and silt represent sediments present at 266–78 cm depth.

OC varies between 0.4 and 2.0% with an average of 0.9%. In general, some of the calcareous sandy-silt (414–334 cm) and intercalations of sandy-silt and silt (234–126 cm) have above average OC. Rest of the sediments have below average or average OC. Sediments are characterized by $\text{C}/\text{N} < 10$ and distribution of C/N is similar to OC ($r > 0.9$, $p < 0.05$). C/N relation fluctuates between 1.3 and 8.0 with an average of 3.3 (Fig. 2).

4.2. Carbonate mineralogy and abundance

Calcite is the only carbonate mineral and its abundance is reflected by CO_3 and Ca contents (Fig. 3). Both CO_3 and Ca have similar distributions ($r > 0.9$, $p < 0.05$). Abundance of CO_3 varies between 0.6 and 26% with an average of 6.7%. Concentration of Ca fluctuates between 0.2 and 21.7% with an average of 5.6%. Sediments between

depths of 560 and 297 cm are characterized by high amplitude variations of Ca (0.3–21.7%) and CO_3 (0.6–25.5%) and both of them in general are above average. Similarly, sediments of 130–78 cm are characterized by low amplitude variations (Ca: 1.8–10.6%; CO_3 : 4–11.8%) except for one sample and contain above average values of CO_3 and Ca. Sediment deposited at a depth of 121 cm has 21.7% of Ca and 26% of CO_3 . Sediments at 297–130 cm depth have homogeneous (Ca: 0.2–7.0%; CO_3 : 1.2–7.2%) and in general below average concentrations.

4.3. Stable isotopes in carbonate

Carbon and oxygen isotopes ($\delta^{18}\text{O}$ and $\delta^{13}\text{C}$) relative to VPDB are positively correlated ($r = 0.5$, $p < 0.05$). $\delta^{18}\text{O}$ fluctuates between -8.6 and -0.8‰ with an average of -4.4‰. Carbonates present in sediments at 326–114 cm depth are characterized by above average $\delta^{18}\text{O}$ and sediments in rest of the core in general have below average or average $\delta^{18}\text{O}$ (Fig. 3). $\delta^{13}\text{C}$ varies between -6.5 and 1.0‰ with an average of -2.3‰. It is above average in sediments deposited between 502–402 cm and 299–114 cm and in general below average or average in rest of the

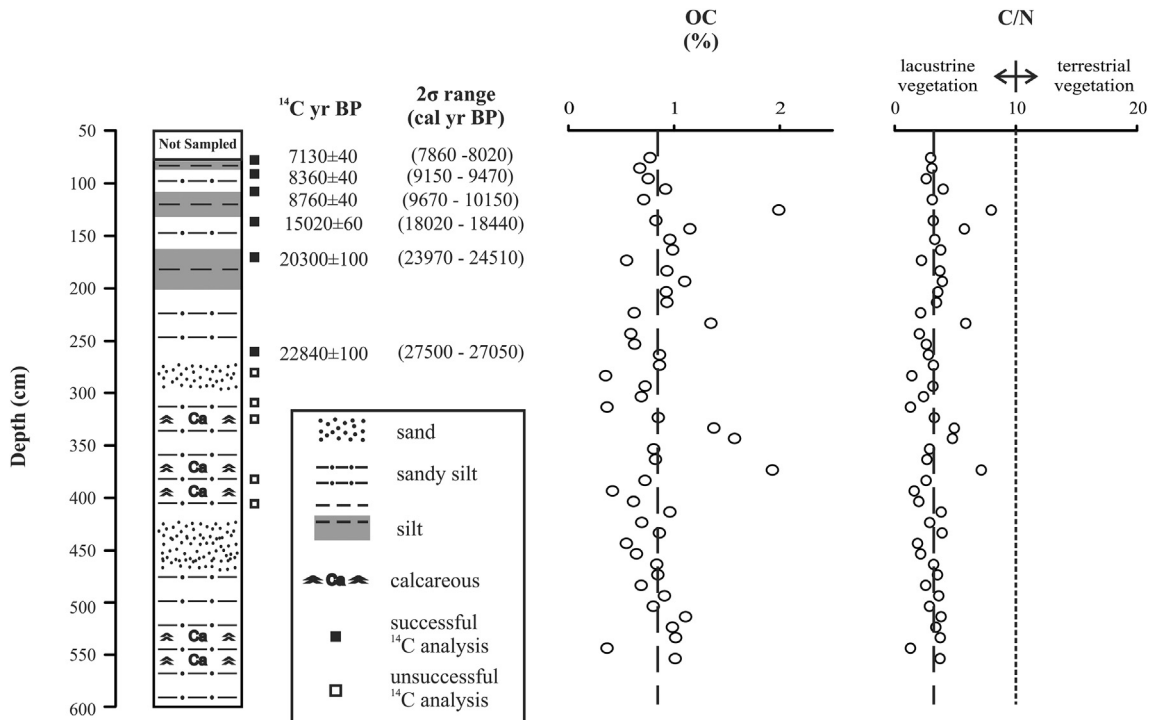


Fig. 2. Stratigraphy of the sediment profile, radiocarbon dates at different depths and their calibrated values. Distributions of total organic carbon (OC) and carbon to nitrogen ratio (C/N) are shown along the depth.

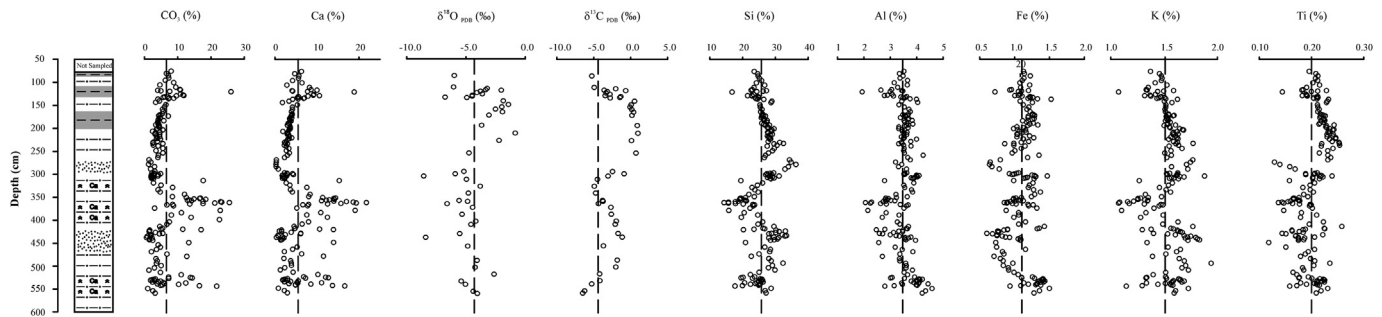


Fig. 3. Distributions of carbonate (CO₃) abundance, carbon and oxygen isotopes ($\delta^{18}\text{O}$ and $\delta^{13}\text{C}$) and concentrations of Ca, Si, Al, Fe, K and Ti along the depth.

sediments. Both the isotopes show absence of any significant negative correlation with Ca ($r = 0.1\text{--}0.3$, $p < 0.05$) and CO₃ ($r = 0.1\text{--}0.2$, $p < 0.05$).

4.4. Clastic minerals and multi-elements

Clastic minerals are comprised of dominant quartz and lower abundances of K-feldspar, cristobalite, zircon, montmorillonite and illite. Concentrations of Si (14.3–36.3%; average = 25.9%), Al (1.9–4.6%; average = 3.5%), Fe (0.6–1.5%; average = 1.1%), K (1.0–1.9%; average = 1.5%) and Ti (0.1–0.3%; average = 0.2%) reflect different abundances of clastic minerals present along the sediment profile (Fig. 3) and their distributions are comparable ($r = 0.5\text{--}0.7$, $p < 0.05$). However, concentration of most of the elements representing clastic minerals is lower in sediments with more carbonate. The diluting effect of calcite on clastic mineral abundance is suggested by negative correlations of Si, Al, K and Ti with Ca ($r = 0.6\text{--}0.9$, $p < 0.05$) and CO₃ ($r = 0.6\text{--}0.9$, $p < 0.05$). Fe shows lower negative correlations with Ca and CO₃ ($r = 0.2$, $p < 0.05$) and similarly correlations of Fe with K and Si were not

significant ($r = 0.1$, $p < 0.05$). It suggests that a part of Fe present in clastic minerals was released and re-precipitated along with carbonate (e.g., Mason and Moore, 1982; Cohen, 2003).

4.5. Chronology

An age-depth model assigned chronology to sediments present at depths between 266 cm and 78 cm. Lower part of the sediment sequence (560–267 cm) was constrained by extrapolating an average sedimentation rate calculated between 266 and 78 cm depths (Fig. 4). The Bayesian age-depth model was constructed with 6 different calibrated ^{14}C ages (Reimer et al., 2013) and using P-sequence with $k = 0.3$ in OxCal version 4.2 (Bronk Ramsey, 2008, 2009, Table 1 and Fig. 4a). It assigns median ages between ~27.3 and 8.0 ka for sediments of 266–78 cm depths. The agreement index (A) between modeled age and calibrated ages varies between 77 and 100%. Sedimentation rates vary between 3.1 and 40.4 cm/ka in sediments deposited between 266 cm and 78 cm.

We extrapolate an average sedimentation rate of 17.6 cm/ka to assign ~66.2–27.3 ka to sediments deposited between 560 and

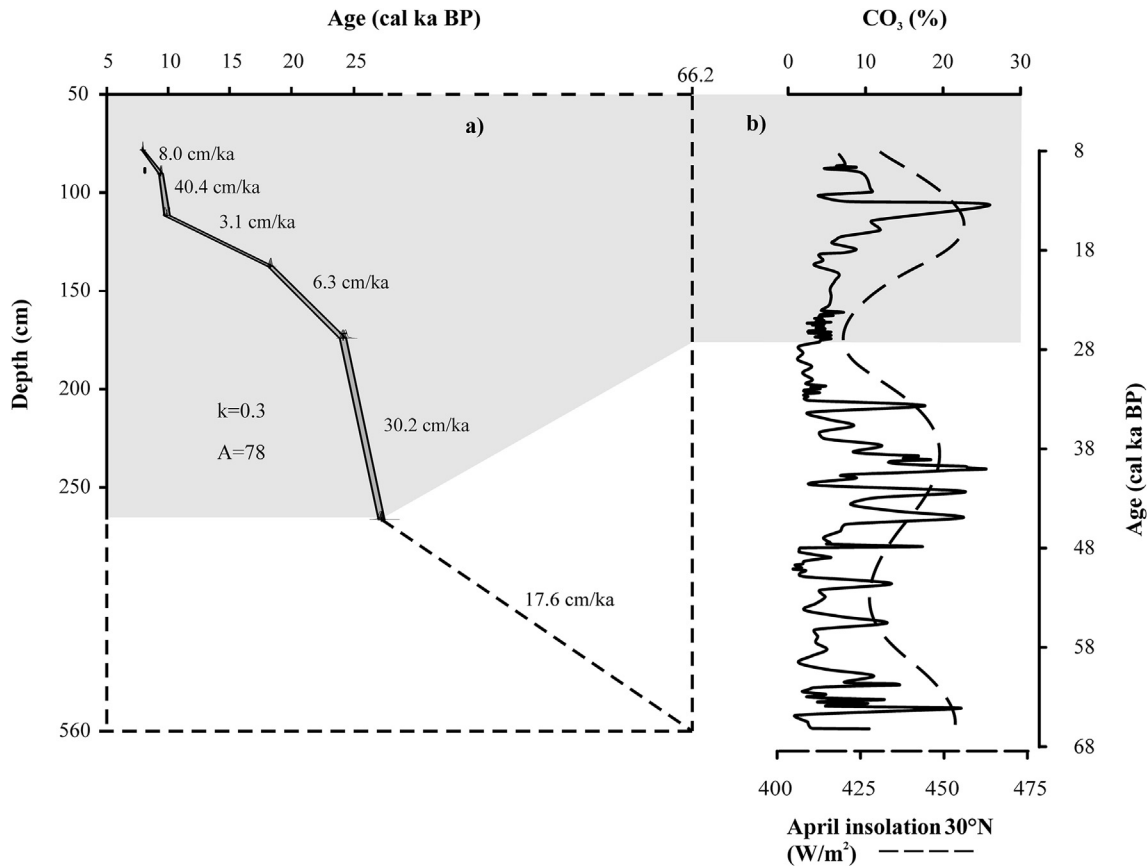


Fig. 4. (a) Age depth model for the sediment profile generated in online OxCal version 4.2. It has an Agreement Index (A) of 78% and extrapolates an average sedimentation rate of 17.6 cm/ka to assign chronology to sediments deposited between 560 and 267 cm. (b) Comparison between carbonate (CO_3) abundance in sediments of 66.2–8 ka and April insolation.

267 cm. In both the interpolated and extrapolated parts of the age model, chronological variation in abundance of CO_3 and spring (April) insolation show a first-order positive relationship (Fig. 4b). In the interpolated part (27.3–8.0 ka), higher deposition of CO_3 occurred during intervals of more spring insolation and abundance of CO_3 was lower during the intervals of less spring insolation. Tendencies of CO_3 and spring insolation also remained similar in the extrapolated part (~66.2–27.3 ka) of the age model. Based on this age model, we identify the six different Heinrich Stadials and consider that sediments of 536–514 cm depth represent H6 (~63.2–60.1 ka), 437–418 cm depth represent H5 (~50.0–47.0 ka), 365–349 cm depth represent H4 (~40.2–38.3 ka), 314–297 cm depth represent H3 (~32.7–31.2 ka), 242–176 cm depth represent H2 (~26.5–24.3 ka) and 135–128 cm depth were deposited during H1 (~18.0–15.6 ka). Chronology of the Heinrich Stadials is also supported by $\delta^{18}\text{O}$ composition of carbonates. Except for H2, carbonate deposited during all other Heinrich Stadials shows negative excursions in $\delta^{18}\text{O}$ (Fig. 3).

5. Discussion

5.1. Hydrological responses to Heinrich Stadial

Hydrological responses of the Chihuahua Desert of Mexico are reconstructed from the chemical and stable isotope composition of sediments deposited in the Santiagillo Basin (Fig. 5). This basin is topographically closed and receives sediments from the erosion of a volcanic catchment through ephemeral streams. Absence of limestone in the catchment and any microfossil remnants suggests that

calcite present in the sediments is dominantly authigenic and deposition of more Ca and CO_3 occurred during the intervals of higher water column salinity and enhanced evaporation. Deposition of more CO_3 represents intervals of higher lake water salinity and vice versa occurred during intervals of lower salinity. The clastic minerals present are sourced from the volcanic catchment geology and negative correlation of elements reflecting clastic mineral abundance with carbonate indicate that clastic mineral abundance was diluted during the intervals of more carbonate deposition. In order to reduce the noise factor associated with dilution effect of calcite, we followed Weltje and Tjallingii (2008) and used ratios of Si/Ca, Al/Ca, K/Ca and Ti/Ca to estimate runoff. However, distributions of all the elemental ratios are similar ($r = 0.5–0.6$, $p < 0.05$). Hence, we represent sediments with higher values of Al/Ca to intervals of more runoff and higher amounts of precipitation and sediments with lower Al/Ca were deposited during intervals of less runoff and lower amounts of precipitation.

In closed lakes without significant groundwater seepage, the oxygen isotope composition of lacustrine carbonate is dependent upon carbonate mineralogy (e.g., calcite, aragonite and dolomite), vital effects of different organisms (e.g., ostracod and mollusc), atmospheric temperature and evaporation/precipitation ratio (Dansgaard, 1964; Abell and Williams, 1989; Land, 1980; Holmes and Chivas, 2002; Leng and Marshall, 2004; Darling et al., 2006). As the lacustrine sediments contain only calcite and there is no visible skeletal remnants of ostracod and mollusc shells in macroscopic inspection and microscopic observations, we relate the swing of ~8‰ in $\delta^{18}\text{O}$ mainly to evaporation/precipitation controlled isotope composition of water column from which calcite

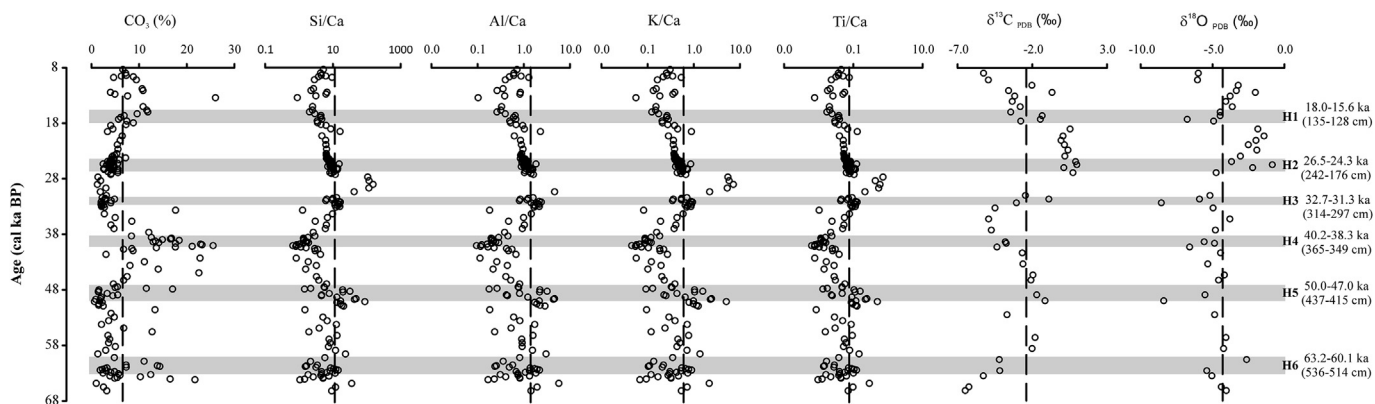


Fig. 5. Distributions of carbonate (CO_3), ratios of Si/Al, Al/Ca, K/Ca, Ti/Ca, and $\delta^{13}\text{C}$ and $\delta^{18}\text{O}$ in sediments deposited during six different Heinrich Stadials (H6 to H1).

precipitated. More evaporation in the water column and in soil zone of the basin catchment would lead to preferential evaporation of lighter ^{16}O and enrichment of the heavier isotope ^{18}O in the water column (i.e., higher $\delta^{18}\text{O}$) during the warmer intervals. Similarly, the cooler intervals would lead to less evaporation and hence lower $\delta^{18}\text{O}$ values.

Carbonate isotope composition ($\delta^{13}\text{C}$) of lacustrine carbonate is a tracer to identify the source of dissolved inorganic carbon (HCO_3^-) present in the water column (Leng and Marshall, 2004). Dissolved HCO_3^- could be sourced from terrestrial catchment vegetation, lacustrine phytoplankton, atmospheric CO_2 and interaction of inflow water with carbonate bearing rocks (Meyer and Teranes, 2001; Leng and Marshall, 2004). However, the basin catchment lack any carbonate bearing rock and chemical signature shows that organic carbon present in sediment was mainly sourced from lacustrine phytoplankton ($\text{C/N} < 10$; Talbot and Johannessen, 1992). During the intervals of more lacustrine productivity, aquatic plants preferentially uptake ^{12}C during photosynthesis and led to higher $\delta^{13}\text{C}$ in the water column from which calcite precipitates. We relate variation in $\delta^{13}\text{C}$ to intervals of HCO_3^- sourced dominantly from atmospheric CO_2 (i.e., lower $\delta^{13}\text{C}$) and intervals of more lacustrine productivity (i.e., higher $\delta^{13}\text{C}$). Temperature of the water column, and influences of lacustrine productivity and atmospheric CO_2 on dissolved HCO_3^- during the Heinrich Stadials are shown in Fig. 5.

Variations in the hydrological conditions (i.e., water column salinity and runoff) during the six different Heinrich Stadials are estimated by calculating minimum, maximum and average values of the proxies for each of the intervals (Fig. 6). We offered a semi-quantitative estimation of the hydrological responses by presenting the proxies with respect to average values calculated for the entire sediment sequence (i.e., 560–78 cm, ~66.2–8 ka) and difference between the maximum and minimum values in each interval. For example, sediments with CO_3 abundance higher than the entire sediment sequence average represent an interval of above average water column salinity. Similarly, the intervals with lowest difference between the maximum and minimum abundances of CO_3 experienced homogeneous water column salinity.

Heinrich Stadial 6 (H6; ~63.2–60.1 ka): It was characterized by millennial-scale variability in runoff, water column salinity and temperature. All the proxies fluctuate between below average and above average values. Average value of Al/Ca calculated for this interval remained below the average of entire sediment sequence. However, averages of both CO_3 and $\delta^{18}\text{O}$ for this interval were almost similar to the entire sediment sequence average. Overall conditions remained arid with below average runoff and almost average water column salinity. During this interval, dissolved HCO_3^- was dominantly sourced from the atmospheric CO_2 .

Heinrich Stadial 5 (H6; ~50.0–47.0 ka): This interval had the most heterogeneous hydrological variability among all the Heinrich Stadials. Proxies indicating runoff and water column salinity showed variability much higher than the variability observed during H6. However, the average values of Al/Ca and CO_3 for this interval remained above and below the overall average, respectively. Both suggest that the overall hydroclimate of this interval was humid. Oxygen and carbon isotope compositions suggest in general cooler conditions and more lacustrine productivity.

Heinrich Stadial 4 (H4; ~40.2–38.3 ka): It was characterized by the most homogeneous of all the Heinrich Stadials and below average runoff into the basin. This arid interval had variable but above average water column salinity. Oxygen and carbon isotope compositions suggest cooler conditions and dissolved HCO_3^- was dominantly sourced from the atmospheric CO_2 .

Heinrich Stadial 3 (H3; ~32.7–31.3 ka): Runoff into the basin was variable but overall runoff was slightly above the average of entire sediment sequence. During this humid interval, water column salinity remained below average. Oxygen isotope suggests that conditions were cooler. Variable carbon isotope indicates influence of lake productivity on dissolved HCO_3^- during a part of this interval and HCO_3^- was dominantly sourced from the atmospheric CO_2 during the other part.

Heinrich Stadial 2 (H2; ~26.5–24.3 ka): Runoff was relatively homogeneous compared to H6 and H5 but overall remained below average. Above average $\delta^{18}\text{O}$ values suggests that water column during this interval was relatively warmer compared to the other Heinrich Stadials. Above average $\delta^{13}\text{C}$ values indicate dominant influence of lacustrine productivity on dissolved HCO_3^- of the water column. However, abundance of CO_3 remained below average during this warmer interval. Deposition of more organic carbon on the lake floor and its subsequent oxidation might have played an important role to generate acidic condition and hence deposition of below average carbonate.

Heinrich Stadial 1 (~18.0–15.6 ka): Overall runoff remained below average and it was even lower than H2. Water column salinity was variable but overall remained above average. Composition of stable isotopes of oxygen suggests cooler conditions. However, the isotopes of carbon indicate more lake productivity during a part of this interval and HCO_3^- was dominantly sourced from the atmospheric CO_2 during the other part of this fluctuating hydrological regime.

5.2. Comparison with other registers

Proxies suggest that hydroclimate of the Chihuahua Desert of Mexico responded differently to different Heinrich Stadials. The

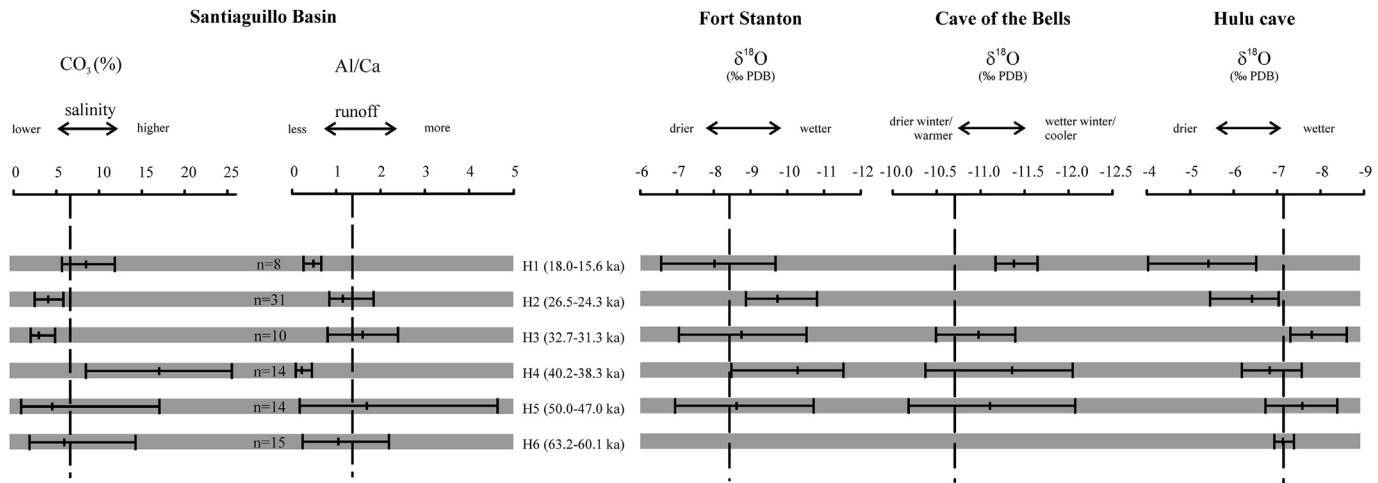


Fig. 6. Comparison of hydrological variation in the Santiaguillo Basin (lake water salinity and runoff) with hydroclimates of Fort Stanton and Cave of Bells in southwest US, and Hulu Cave in China.

overall runoff and hence precipitation remained below average during H6, H4, H2 and H1. Both of them were above average during H5 and H3. Similarly, runoff during H4 showed the least variability and it was the most variable during H5. The atmospheric response to interaction between North Hemisphere ice sheets and North Atlantic Ocean are also documented in oxygen isotope composition of independently dated stalagmite calcite collected from the Cave of Bells and Fort Stanton (Wagner et al., 2010; Asmerom et al., 2010). Both the records document dynamics of aridity in the southwest US and related those to varying strengths of the westerly winter storms. In general, both the records suggest increase in the amounts of winter precipitation during the Heinrich Stadials compared to their immediate previous intervals. However, we calculated the minimum, maximum and average of speleothem δ¹⁸O values and presented those with respect to the overall average in order to compare variable hydrology of the Santiaguillo Basin with hydroclimate of the southwest US during the Heinrich Stadials (Fig. 6).

Similar to the Chihuahua Desert of Mexico, both the speleothems showed that hydroclimate in the southwest US experienced millennial-scale variability and some intervals were more homogeneous compared to others. For example, hydroclimate of the Cave of Bells was relatively more homogeneous during H1 compared to H5. Similarly, hydroclimate of the Fort Stanton was relatively more homogeneous during H2 compared to H5 and H3. The Fort Stanton speleothem also responded differently to different Heinrich Stadials. Above average δ¹⁸O during H4 and H2 indicated more winter precipitation and below average δ¹⁸O during H1 suggested less winter precipitation compared to average value of the entire register. We did not observe concurrency in proxy records of the Chihuahua Desert of Mexico and southwest US. With millennial-scale fluctuations, hydroclimates of the Santiaguillo, Fort Stanton and Cave of Bells remained humid during H5 and H3. However, hydroclimates of the Santiaguillo and Fort Stanton remained arid and hydroclimate of the Cave of Bells was humid during H1.

In one of our previous research on sediments deposited in the Babicora Basin (Roy et al., 2013), we observed that influence of the westerly winter storms was minimal in the region located at south of 29°N latitude. Both Metcalfe et al. (2015) and Roy et al. (2015) reported that hydroclimate of the Chihuahua Desert of Mexico was controlled by summer as well as autumn precipitation during the Holocene as well as the last glacial period. Absence of synchronous reduction in runoff into the Santiaguillo Basin during all

the intervals of enhanced winter precipitation in southwest US was possibly indicative of lack of concurrency in the latitudinal displacement of Inter tropical convergence zone and sea surface temperature of the eastern Pacific Ocean controlling the summer as well as autumn precipitation and polar jet streams controlling strength of the westerly winter storms during all the Heinrich Stadials. Oxygen isotope composition of speleothems from the Hulu Cave of China provides proxy information about the East Asian summer monsoon (Wang et al., 2001). It identified existence of a hemispheric link between the North Atlantic climate and the East Asian summer monsoon. In the present study, we observe a possible hemispheric link between hydroclimate of the Chihuahua Desert of Mexico and the East Asian Monsoon. Tendencies between runoff into the Santiaguillo Basin and intensity of the East Asian monsoon during the six different Heinrich Stadials were similar (Fig. 6b). With millennial-scale variations, both the records show overall below average values during H4, H2 and H1, and above average values during H5 and H3.

6. Conclusions

A new proxy record was reconstructed by studying sediments deposited between depths of 560 and 78 cm (~66.2–8 ka) in the Santiaguillo Basin in order to infer hydrological responses of the Chihuahua Desert of Mexico to possible Heinrich Stadials. Al/Ca ratio provided information about runoff, carbonate abundance helped to register the varying water column salinity, oxygen isotope composition of carbonate was a proxy for water column temperature, and carbon isotope composition provided information about source of dissolved inorganic carbon present in water column. More specifically;

- Except for the H2, water column was generally cooler compared to the overall average during the Heinrich Stadials. However, the hydroclimate was different during different Heinrich Stadials. With millennial-scale fluctuations, the overall runoff remained below average during H6, H4, H2 and H1. Runoff was above average during H5 and H3. Similarly, H4 showed the least variability in runoff and H5 had the most variable runoff.
- In general, dissolved HCO₃⁻ was dominantly sourced from atmospheric CO₂ during the intervals of reduced runoff. Lake productivity and atmospheric CO₂ influenced inorganic

- carbon pool of the water column during intervals of fluctuating hydrological regimes.
- iii. H2 was characterized by relatively warmer water column compared to the other Heinrich Stadials. More lacustrine productivity and subsequent oxidation of deposited organic carbon on the lake floor possibly led to an acidic condition and deposition of less carbonate during this interval of overall below average runoff.
 - iv. Lack of synchronous regimes of runoff into the Santiaguillo Basin and enhanced winter precipitation in southwest US during the Heinrich Stadials was possibly indicative of lack of concurrency in forcings controlling the summer and autumn precipitation as well as westerly winter storms during the North Atlantic Stadials.
 - v. Similarity between proxy records from the Santiaguillo Basin and Hulu Cave suggest a possible hemispheric link between hydroclimate of the Chihuahua Desert of Mexico and the East Asian Monsoon.

Acknowledgements

Data produced in this paper are financed by Basic Science project from CONACYT (CB-237579). First author (JDQJ) was awarded a scholarship from CONACYT (235509) for the doctoral study and the revised version of this manuscript was developed during sabbatical of PDR with a scholarship from DGAPA-UNAM. Jose Luis Sánchez Zavala (IGL, UNAM) helped in fieldwork, Nayeli Lopez Balbiaux and Victor H. Lemus Neri (USAI, UNAM) provided laboratory assistance and Oscar Sandate (Ecoterra Servicios Ambientales, S.A. de C.V.) helped in the sediment core collection. Fire Brigade and Civil Protection of Durango provided accompanied the expedition members during several fieldworks. We acknowledge suggestions and comments from both the anonymous reviewers.

References

- Abell, P.I., Williams, M.A.J., 1989. Oxygen and carbon isotope ratios in gastropods shells as indicators of paleoenvironments in the Afar region of Ethiopia. *Palaeogeogr. Palaeolimnol. Palaeoecol.* 74, 265–278.
- Álvarez-Solas, J., Montoya, M., Ritz, C., Ramstein, G., Charbit, S., Dumas, C., Nisancioğlu, K., Dokken, T., Ganopolski, A., 2011. Heinrich event 1: an example of dynamical ice-sheet reaction to oceanic changes. *Clim. Past* 7, 1297–1306.
- Andrews, J.T., Tedesco, K., Jennings, A.E., 1993. Heinrich events: chronology and processes, east-central Laurentide ice sheet and NW Labrador sea. In: Peltier, W.R. (Ed.), *Ice in the Climate System*, vol. 12. NATO ASI Series, Springer-Verlag, New York, pp. 167–186.
- Asmerom, Y., Polyak, V.J., Burns, S.J., 2010. Variable winter moisture in the southwestern United States linked to rapid glacial climate shifts. *Nat. Geosci.* 3, 114–117.
- Bond, G., Heinrich, H., Broecker, W., Labeyrie, L., McManus, J., Andrews, J., Huon, S., Jantschik, R., Clasen, S., Simet, C., Tedesco, K., Klas, M., Bonani, G., Ivy, S., 1992. Evidence for massive discharges of icebergs into the North Atlantic ocean during the last glacial period. *Nature* 360, 245–249.
- Bronk Ramsey, C., 2008. Deposition models for chronological records. *Quat. Sci. Rev.* 27, 42–60.
- Bronk Ramsey, C., 2009. Bayesian analysis of radiocarbon dates. *Radiocarbon* 51, 337–360.
- Calov, R., Ganopolski, A., Petoukhov, V., Claussen, M., Greve, R., 2002. Large-scale instabilities of the Laurentide ice sheet simulated in a fully coupled climate-system model. *Geophys. Res. Lett.* 29, 2216.
- Castro, C.L., McKee, T.B., Pielke Sr., R.A., 2001. The relationship of the North American Monsoon to tropical and North Pacific sea surface temperatures as revealed by observational analysis. *J. Clim.* 14, 4449–4473.
- Cohen, A.S., 2003. *Palaeolimnology: The History and Evolution of Lake Systems*. Oxford University Press, New York.
- Dansgaard, W., 1964. Stable isotopes in precipitation. *Tellus* 16, 436–468.
- Dansgaard, W., Clausen, H.B., Gundestrup, N., Hammer, C.U., Johnsen, S.F., Kristindottir, P.M., Reeh, N., 1982. A new Greenland deep ice core. *Science* 218, 1273–1277.
- Dansgaard, W., Johnsen, S.J., Clausen, H.B., Dahl-Jensen, D., Gundestrup, N.S., Hammer, C.U., Hvilstedt, C.S., Steffensen, J.P., Sveinbjörnsdóttir, A.E., Jouzel, J., Bond, G., 1993. Evidence for general instability of past climate from a 250-kyr ice-core record. *Nature* 364, 218–220.
- Darling, W.G., Bath, A.H., Gibson, J.J., Rozanski, 2006. Isotopes in water. In: Leng, M.J. (Ed.), *Isotopes in Palaeoenvironmental Research*. Springer, Dordrecht, The Netherlands.
- Donders, T.H., Jan de Boer, H., Finsinger, W., Grimm, E.C., Dekker, S.C., Reichart, G.J., Wagner-Cremer, F., 2011. Impact of the Atlantic warm pool on precipitation and temperature in Florida during North Atlantic cold spells. *Clim. Dyn.* 36, 109–118.
- Flower, B.P., Hastings, D.W., Hill, H.W., Quinn, T.M., 2004. Phasing of deglacial warming and Laurentide ice sheet meltwater in the Gulf of Mexico. *Geology* 32, 597–600.
- Grimm, E.C., Watts, W.A., Jacobson Jr., G.L., Hansen, B.C.S., Almquist, H.R., Dieffenbacher-Krall, A.C., 2006. Evidence for warm wet Heinrich events in Florida. *Quat. Sci. Rev.* 25, 2197–2211.
- Hall, I.R., Moran, S.B., Zahn, R., Knutz, P.C., Shen, C.C., Edwards, R.L., 2006. Accelerated drawdown of meridional overturning in the late-glacial Atlantic triggered by transient pre-H event freshwater perturbation. *Geophys. Res. Lett.* 33, L16616.
- Heinrich, H., 1988. Origin and consequences of cyclic ice rafting in the northeast Atlantic Ocean during the past 130,000 years. *Quat. Res.* 29, 142–152.
- Hendy, I.L., Kennet, J.P., 2000. Dansgaard-oescher cycles and the California current system: planktonic foraminiferal response to rapid climate change in Santa Barbara basin, ocean drilling program hole 893A. *Paleoceanography* 15, 30–42.
- Holmes, J.A., Chivas, A.R., 2002. Ostracod shell chemistry-overview. In: Holmes, J.A., Chivas, A.R. (Eds.), *The Ostracoda: Applications in Quaternary Research*. Geophysical Monograph 131, American Geophysical Union, Washington D.C., pp. 185–204.
- Hulbe, C., MacAyeal, D., Denton, G., Kleman, J., Lowell, T., 2004. Catastrophic ice shelf breakup as the source of Heinrich event icebergs. *Paleoceanography* 19, PA1004.
- Jennerjahn, T.C., Ittekkot, V., Arz, H.W., Behling, H., Pätzold, J., Wefer, G., 2004. Asynchronous terrestrial and marine signals of climate change during Heinrich events. *Science* 306, 2236–2239.
- Jonkers, L., Moros, M., Prins, M., Dokken, T., Dahl, C., Dijkstra, N., Perner, K., Brummer, G., 2010. A reconstruction of sea surface warming in the northern North Atlantic during MIS 3 ice-raftering events. *Quat. Sci. Rev.* 29, 1791–1800.
- Kirby, M.E., Andrews, J.T., 1999. Mid-Wisconsin Laurentide ice sheet growth and decay: implications for Heinrich events 3 and 4. *Paleoceanography* 14, 211–223.
- Lachnit, M.S., Asmerom, Y., Bernal, J.P., Polyak, V.J., Vazquez-Sellem, L., 2013. Orbital pacing and ocean circulation-induced collapses of the Mesoamerican monsoon over the past 22,000 y. *Proc. Natl. Acad. Sci.* 110, 9255–9260.
- Land, L.S., 1980. The isotopic and trace element geochemistry of dolomite: the state of the art. In: Zenger, D.H., Dunham, J.B., Ethington, R.L. (Eds.), *Concepts and Models of Dolomitisation*. Society of Economic Paleontologist and Mineralogists, Special Publication, vol. 28, pp. 87–110.
- Leduc, G., Vidal, L., Tachikawa, K., Rostek, F., Sonzogni, C., Beaufort, L., Bard, E., 2007. Moisture transport across Central America as a positive feedback on abrupt climatic change. *Nature* 445, 908–911.
- Leng, M.J., Marshall, J.D., 2004. Palaeoclimate interpretation of stable isotope data from lake sediment archives. *Quat. Sci. Rev.* 23, 811–831.
- Lozano-García, S., Ortega, B., Roy, P.D., Beramendi-Orosco, L., Caballero, M., 2015. Climatic variability in the northern sector of the American tropics since the latest MIS 3. *Quat. Res.* 84, 262–271.
- Magaña, V.O., Vazquez, J.L., Perez, J.L., Perez, J.B., 2003. Impact of El Niño on precipitation in Mexico. *Geofís. Int.* 42, 313–330.
- Mason, B., Moore, C.B., 1982. *Principles of Geochemistry*. John Wiley & Sons, New York.
- McClintock, E.L., Ganeshram, R.S., Pichevin, L.E., Talbot, H.M., van Dongen, B.E., Thunell, R.C., Haywood, A.M., Singarayer, J.S., Valdes, P.J., 2012. Sea-surface temperature records of Termination 1 in the Gulf of California: challenges for seasonal and interannual analogues of tropical Pacific climate change. *Paleoceanography* 27, PA2202.
- McCrea, J.M., 1950. On the isotopic chemistry of carbonates and palaeo-temperature scale. *J. Chem. Phys.* 18, 849–857.
- Metcalfe, S.E., Barron, J.A., Davies, S.J., 2015. The Holocene history of the North American Monsoon: 'known knowns' and 'known unknowns' in understanding its spatial and temporal complexity. *Quat. Sci. Rev.* 120, 1–27.
- Meyer, P.A., Teranes, J.L., 2001. Sediment organic matter. In: Last, W.M., Smol, J.P. (Eds.), *Tracking Environmental Change Using Lake Sediments*. Vol. 2: Physical and Geochemical Techniques. Kluwer Academic Publishers, Dordrecht, The Netherlands, pp. 239–269.
- Munguía-Rojas, P., García-Padilla, J.L., Armenta-Román, R., Cruz-Pérez, R., Camacho, J.M., Céspedes, J.S., 1998. *Carta Geológico-Minera Durango G13-11, escala 1:250000 con texto explicativo*: Secretaría de Comercio y Fomento Industrial, Servicio Geológico Mexicano.
- Nieto-Samaniego, A.F., Barajas-Gea, C.I., Gómez-González, J.M., Rojas, A., Alaniz-Álvarez, S.A., Xu, S., 2012. Geología, evolución estructural (Eoceno al actual) y eventos sísmicos del Graben de Santiaguillo, Durango, México. *Rev. Mex. Ciencias Geol.* 29, 115–130.
- Prasad, S., Vos, H., Negendank, J.F.W., Waldmann, N., Goldstein, S.L., Stein, M., 2004. Evidence from Lake Lisan of solar influence on decadal to centennial-scale climatic variability during marine oxygen isotope stage 2. *Geology* 32, 581–584.
- Reimer, P.J., Bard, E., Bayliss, A., Beck, J.W., Blackwell, P.G., Ramsey, C.B., Grootes, P.M., Guilderson, T.P., Hajdas, I., Hatté, C., Heaton, T.J., Hoffmann, D.L., Hogg, A.G., Hughen, K.A., Kaiser, K.F., Kromer, B., Manning, S.W., Niu, M., Reimer, R.W., Richards, D.A., Scott, E.M., Southon, J.R., Staff, R.A., Turney, C.S.M., van der Plicht, J., 2013. *IntCal13 and MARINE13 radiocarbon age*

- calibration curves 0–50000 years cal BP. *Radiocarbon* 55, 1869–1887.
- Roche, D., Paillard, D., Cortijo, E., 2004. Constraints on the duration and freshwater release of Heinrich event 4 through isotope modelling. *Nature* 432, 379–382.
- Roy, P.D., Chávez-Lara, C.M., Beramendi-Orosco, L.E., Sánchez-Zavala, J.L., Muthu-Sankar, G., Lozano-Santacruz, R., Quiroz-Jimenez, J.D., López-Balbiaux, N., 2015. Pleohydrology of the Santiaguillo Basin (Mexico) since late last glacial and climate variation in southern part of western subtropical North America. *Quat. Res.* 84, 335–347.
- Roy, P.D., Jonathan, M.P., Pérez-Cruz, L.L., Sánchez-Córdova, M.M., Quiroz-Jiménez, J.D., Romero, F.M., 2012. A millennial-scale late Pleistocene–Holocene palaeoclimatic record from the western Chihuahua Desert, Mexico. *Boreas* 41, 707–717.
- Roy, P.D., Quiroz-Jiménez, J.D., Pérez-Cruz, L.L., Lozano-García, S., Metcalfe, S.E., Lozano-Santacruz, R., López-Balbiaux, N., Sánchez-Zavala, J.L., Romero, F.M., 2013. Late Quaternary paleohydrological conditions in the dryland of northern Mexico: a summer precipitation proxy record of the last 80 cal ka BP. *Quat. Sci. Rev.* 78, 342–354.
- Roy, P.D., Rivero-Navarrete, A., Sánchez-Zavala, J.L., Beramendi-Orosco, L.E., Muthu-Sankar, G., Lozano-Santacruz, R., 2016. Atlantic Ocean modulated hydroclimate of the subtropical northeastern Mexico since the last glacial maximum and comparison with the southern US. *Earth Planet. Sci. Lett.* 434, 141–150.
- Ruehlemann, C., Mulitz, S., Mueller, P.J., Wefer, G., Zahn, R., 1999. Warming of the tropical Atlantic Ocean and slowdown of thermohaline circulation during the last deglaciation. *Nature* 402, 511–514.
- Sanchez-Goni, M.F., Harrison, S.P., 2010. Millennial-scale climate variability and vegetation changes during the Last Glacial: concepts and terminology. *Quat. Sci. Rev.* 29, 2823–2827.
- Schnurrenberger, D., Russell, J., Kelts, K., 2003. Classification of lacustrine sediments based on sedimentary components. *J. Paleolimnol.* 29, 141–154.
- Talbot, M.R., Johannessen, T., 1992. A high-resolution palaeoclimatic record for the last 27,500 years in tropical West Africa from carbon and nitrogen isotope composition of lacustrine organic matter. *Earth Planet. Sci. Lett.* 110, 23–37.
- Wagner, J.D.M., Cole, J.E., Beck, J.W., Patchett, P.J., Henderson, G.M., Barnett, H.R., 2010. Moisture variability in the southwestern United States linked to abrupt glacial climate change. *Nat. Geosci.* 3, 110–113.
- Wang, Y.J., Cheng, H., Edwards, R.L., An, Z.S., Wu, J.Y., Shen, C.C., Dorale, J.A., 2001. A high-resolution absolute-dated late Pleistocene Monsoon record from Hulu Cave, China. *Science* 294, 2345–2348.
- Weltje, G.J., Tjallingii, R., 2008. Calibration of XRF core scanners for quantitative geochemical logging of sediment cores: theory and application. *Earth Planet. Sci. Lett.* 274, 423–438.
- Zic, M., Negrini, R., Wigand, P., 2002. Evidence of synchronous climate change across the Northern Hemisphere between the North Atlantic and northwestern Great Basin, United States. *Geology* 30, 635–638.

CONCLUSIONES



Conclusiones

La caracterización estratigráfica, geoquímica, mineralógica y magnética de los sedimentos depositados en la cuenca del lago Santiaguillo, ubicado en el centro-norte de México, proporciona información acerca de la respuesta que tuvo el Desierto de Chihuahua la variabilidad climática de escala orbital y milenaria durante el último ciclo interglacial-glacial-interglacial. La comparación de los datos generados con otros registros paleoambientales aporta un panorama regional de estos cambios y permite identificar los posibles forzamientos climáticos que afectaron la región tropical y subtropical de Norteamérica. A continuación se resumen las conclusiones generales de los tres artículos que comprenden este trabajo de tesis.

- Con excepción del Estadio Isotópico Marino (MIS) 2, se presentaron intervalos de sequía en los últimos cinco Estadios Isotópicos Marinos. Además, el registro de sequías exhibe una relación positiva de primer orden con la insolación de primavera.
- Durante el MIS 2 no se presentaron sequías en el centro-norte de México, en cambio el MIS 1 se caracterizó por dos eventos de aridez a los c. 13.5 y 7 ka. Las sequías de c.13.5 ka ocurrieron durante un intervalo de temperaturas globales cálidas (aunque fluctuantes) y mayor actividad de El Niño Oscilación del Sur (ENOS). Este intervalo fue sincrónico con lapsos de sequía documentados en otros registros provenientes del trópico y subtrópico de México. Esto sugiere que la combinación de forzamientos orbitales (Milankovitch) junto con temperaturas cálidas globales y la variabilidad de ENOS pudieron propiciar la expansión de las condiciones áridas en la región.
- Se reconstruyó la variabilidad climática de escala milenaria durante los seis diferentes intervalos estadiales Heinrich (H). En general, la escorrentía permaneció inferior al promedio durante H6, H4, H2 y H1 y fue superior al promedio en H5 y H3. El estadal Heinrich H4 presentó la menor variabilidad de escorrentía y H5 fue el intervalo más variable.

- El H2 se caracterizó por una columna de agua relativamente cálida en comparación con los demás estadios Heinrich. La mayor productividad lacustre y la subsecuente oxidación del carbono orgánico depositado en el piso del lago pudieron generar condiciones ácidas y por lo tanto, menor deposición de carbonato durante este intervalo de escorrentía inferior a la media.
- La ausencia de regímenes sincrónicos de escorrentía en la cuenca del lago Santiaguillo y el aumento de la precipitación invernal en el suroeste de EUA durante los estadios Heinrich, son posibles indicadores de la ausencia de concurrencia entre los forzamientos que controlaron la precipitación de verano-otoño y las tormentas invernales durante los estadios del Noratlántico.
- La similitud entre los registros de Santiaguillo y la cueva Hulu (China) sugieren un posible vínculo hemisférico entre el hidroclima del desierto de Chihuahua en su parte mexicana y el Monzón del Este Asiático.
- El Monzón de Norteamérica (NAM) tuvo una influencia mínima en la parte terminal del Último Periodo Glacial; en cambio, la frecuente formación de ciclones tropicales en el este del Norpacífico, en franjas restringidas de lluvia, llevaron mayor precipitación a la región centro norte de México. Sin embargo, en la parte norte-noroeste de México, la presencia (o ausencia) de un NAM debilitado propició condiciones áridas.
- Durante el Holoceno temprano, un NAM fortalecido y la expansión de la franja de ciclones tropicales llevaron mayor cantidad de humedad procedente del Golfo de California y el este del Pacífico a una amplia región que se extendió desde el centro-norte de México hasta el interior del suroeste de EUA.